


1985

Elemental tests for the seismic resistance of composite floor diaphragms

Mike Dean Prins
Iowa State University

Follow this and additional works at: <https://lib.dr.iastate.edu/rtd>

 Part of the [Civil Engineering Commons](#), and the [Structural Engineering Commons](#)

Recommended Citation

Prins, Mike Dean, "Elemental tests for the seismic resistance of composite floor diaphragms" (1985). *Retrospective Theses and Dissertations*. 17272.
<https://lib.dr.iastate.edu/rtd/17272>

This Thesis is brought to you for free and open access by the Iowa State University Capstones, Theses and Dissertations at Iowa State University Digital Repository. It has been accepted for inclusion in Retrospective Theses and Dissertations by an authorized administrator of Iowa State University Digital Repository. For more information, please contact digirep@iastate.edu.

Elemental tests for the seismic resistance
of composite floor diaphragms

by

Mike Dean Prins

A Thesis Submitted to the
Graduate Faculty in Partial Fulfillment of the
Requirements for the Degree of
MASTER OF SCIENCE

Department: Civil Engineering
Major: Structural Engineering

Approved:

Signatures redacted for privacy.

Iowa State University
Ames, Iowa

1985

TABLE OF CONTENTS

	Page
LIST OF SYMBOLS	v
1. INTRODUCTION	1
1.1. General	1
1.2. Objective of Overall Research Project	3
1.3. Objective and Scope of This Study	4
2. PREVIOUS RESEARCH AND BACKGROUND	6
2.1. Previous Full-scale Testing	6
2.2. Failure Modes	9
2.2.1. Composite slab failure	14
2.2.2. Deck-concrete shear transfer mechanism failure	16
2.2.3. Diaphragm-edge member connection failure	18
2.3. Previous Elemental Tests	21
3. EXPERIMENTAL TESTING AND RESULTS	31
3.1. Full-scale Tests	31
3.1.1. Test facility	31
3.1.2. Load program	33
3.1.3. Instrumentation	35
3.1.4. General behavior and failure modes	39
3.1.4.1. Slab 5	39
3.1.4.2. Slab 6	40
3.1.4.3. Slab 9	40
3.1.4.4. Slab 10	40
3.1.4.5. Slab 11	42
3.1.4.6. Slab 15	44
3.1.4.7. Slab 19	44
3.1.4.8. Slab 20	47
3.1.5. Measured results	47
3.1.6. Summary of testing parameters and results	53

	Page
3.2. Cantilever Elemental Test	53
3.3. Elemental Friction Test	58
3.3.1. Test set-up	58
3.3.2. Experimental results	60
3.4. Elemental Shear Test	62
3.4.1. Test set-up	62
3.4.2. Experimental results	64
3.5. Elemental Push-off Test	67
3.5.1. Test set-up	67
3.5.2. Summary of testing parameters	70
3.5.3. Behavior and failure modes	70
3.5.3.1. Deck Type 5	75
3.5.3.2. Deck Type 5B	84
3.5.3.3. Deck Type 6	86
3.5.3.4. Deck Type 7	89
3.5.3.5. Deck Type 8	91
3.5.3.6. Deck Type 9	93
3.5.3.7. Deck Type 2	95
3.5.3.8. Deck Type 4	97
3.5.3.9. Weld tests	100
3.5.4. Summary of test results	104
4. ANALYTICAL INVESTIGATION	108
4.1. Background and Previous Techniques	108
4.2. Interpretation and Application of Elemental Push-off Tests	109
4.2.1. Failure modes	113
4.2.2. Parametric investigation	113
4.2.3. Relationship to full-scale slab	115
4.2.3.1. Finite element analysis	115
4.2.3.2. Stiffness	119
4.2.3.3. Ultimate load	121
4.3. Proposed Predictive Method	124

	Page
4.3.1. Edge zone distance	124
4.3.1.1. Theoretical solution	124
4.3.1.2. Experimental evidence	128
4.3.1.3. Finite element model	129
4.3.2. Stiffness	132
4.3.3. Ultimate load	146
4.3.3.1. Composite slab: diagonal tension failure	147
4.3.3.2. Shear transfer mechanism failure: edge zone distance method	148
4.3.3.3. Shear transfer mechanism failure: beam on elastic foundation method	150
4.3.3.4. Edge connection failure	156
4.4. Comparison of Experimental and Analytical Results	158
4.4.1. Initial stiffness	158
4.4.2. Ultimate load	160
5. SUMMARY AND CONCLUSIONS	166
5.1. Summary	166
5.2. Conclusions	167
5.3. Recommendations for Continued Study	169
6. REFERENCES	171
7. ACKNOWLEDGMENTS	174

LIST OF SYMBOLS

A	= cross-sectional area
A_b	= effective area of edge beams
A_f	= area under load-displacement curve at failure
A_s	= steel deck cross-sectional area
A_{Δ}	= area under the load-displacement curve up to displacement Δ
a	= length of diaphragm perpendicular to applied load
a'	= effective edge zone width at failure, perpendicular to corrugations
a''	= initial effective edge zone width, perpendicular to corrugations
B	= $\sqrt{fk/GA}$
b	= length of diaphragm parallel to applied load
b'	= effective edge zone width at failure, parallel to corrugations
b''	= initial effective edge zone width, parallel to corrugations
C_{po}	= push-off test correction factor
D	= apparent diameter of spot weld
d	= corrugation spacing
d_a	= diameter of spot weld at mid-thickness of sheeting
d_e	= effective fused diameter of arc spot weld
E_b	= edge beam modulus of elasticity
E_c	= concrete modulus of elasticity
E_s	= steel deck modulus of elasticity
F_u	= deck steel minimum ultimate tensile strength

- F_{xx} = AWS electrode classification
 F_y = steel deck yield strength
 F_1 = one of two perpendicular forces on corner connection
 F_2 = one of two perpendicular forces on corner connection
 f = shear flexibility shape factor
 f_c' = concrete compressive strength
 G_c = shear modulus of concrete
 G_s = shear modulus of steel deck = 11300 ksi
 g_p = $\sqrt{K_p/E_b A_b}$
 g_t = $\sqrt{K_t/E_b A_b}$
 I = horizontal moment of inertia of edge beam
 I_b = moment of inertia of edge beams about girder neutral axis
 I_c = moment of inertia of composite web (slab)
 K = edge zone elastic foundation stiffness
 K_b = bending stiffness of composite system
 K_{eq} = energy equivalent linear elastic stiffness
 K_f = frame-abutment connection stiffness
 K_p = basic edge zone stiffness parallel to corrugations
 K_s = shear stiffness of composite system
 K_t = basic edge zone stiffness transverse to corrugations
 K_{tot} = total composite diaphragm stiffness
 K_z = edge zone stiffness
 ℓ_p = $(b^2 + 3bb' - 2b'^2)/6a$
 ℓ_p' = $(b^2 + 4bb' - 4b'^2)/4a$
 ℓ_p'' = $(r_1 b^2 + r_2 3bb'' - r_2 2b''^2)/6a$

- $l_t = a'(3a - 2a')/3a$
 $l_t' = 2a' - 2a'^2/a$
 $l_t'' = a''[r_3(3a - a'') - a''r_4]/3a$
 $n =$ elasticity modulus ratio of steel deck to concrete
 $n_a =$ number of connections in length a
 $n_b =$ number of connections in length b
 $n_s =$ shear modulus ratio of steel deck to concrete
 $Q =$ slab edge zone capacity
 $Q_p =$ slab edge zone capacity parallel to corrugations
 $Q_{po} =$ push-off test edge zone capacity
 $Q_{ppo} =$ push-off test capacity parallel to corrugations
 $Q_t =$ slab edge zone capacity transverse to corrugations
 $Q_{tpo} =$ push-off test capacity transverse to corrugations
 $Q_u =$ ultimate connection capacity
 $Q_w =$ spot weld ultimate shear strength
 $Q_{wd} =$ design shear strength of spot weld
 $q_p =$ edge force parallel to corrugations on parallel edge member
 $q_p' =$ edge force parallel to corrugations on transverse edge member
 $q_{pav} =$ average edge force on side beam (parallel to corrugations)
 $q_{p1} =$ edge force at fixed end of side beam (parallel to corrugations)
 $q_{p2} =$ edge force at free end of side beam (parallel to corrugations)
 $q_t =$ edge force transverse to corrugations on transverse edge member
 $q_t' =$ edge force transverse to corrugations on parallel edge member
 $q_{tb} =$ edge force along abutment (transverse to corrugations)
 $q_{tf} =$ edge force along length of front beam (transverse to corrugations)

- q_{tfav} = average edge force on front beam (transverse to corrugations)
 q_{tf0} = edge force at center of front beam (transverse to corrugations)
 q_{tfl} = edge force at end of front beam (transverse to corrugations)
 r_1 = Δ_{p1}/Δ_{pav}
 r_2 = Δ_{p2}/Δ_{pav}
 r_3 = $\Delta_{tfl}/\Delta_{tfav}$
 r_4 = $\Delta_{tb}/\Delta_{tfav}$
 s = total length of steel sheeting (perimeter) per corrugation
 t = thickness of steel sheeting
 t_c = average thickness of concrete
 t_e = $t_c + n_s t_s d/s$
 t_s = thickness of steel deck sheeting
 V = total shear load applied to diaphragm
 V_1 = shear force in the steel deck
 W_p = perpendicular force at end of front beam
 W_{ppo} = W_p before being corrected for push-off test factors
 W_t = perpendicular force at end of side beam
 W_{tpo} = W_t before being corrected for push-off test factors
 Δ = specified displacement
 Δ_b = bending deflection of composite system
 Δ_c = shear deflection of composite system
 Δ_f = diaphragm deflection due to axial flexibility of edge beam framing connections
 Δ_{pav} = average slab to edge beam relative displacement (parallel to corrugations)

- Δ_{p1} = slab to edge beam relative displacement at fixed end of side beam (parallel to corrugations)
- Δ_{p2} = slab to edge beam relative displacement at free end of side beam (parallel to corrugations)
- Δ_s = shear deflection of composite system
- Δ_{tb} = slab to abutment relative displacement
- Δ_{tfav} = average slab to edge beam relative displacement (transverse to corrugations)
- Δ_{tf0} = slab to edge beam relative displacement at center of front beam (transverse to corrugations)
- Δ_{tf1} = slab to edge beam relative displacement at end of front beam (transverse to corrugations)
- Δ_{tot} = total diaphragm deflection
- Δ_z = diaphragm deflection due to edge zone deformation
- μ = coefficient of friction
- σ = axial stress in side beam

1. INTRODUCTION

1.1. General

In the past 20 years, cold-formed metal deck, composite slabs have become a popular flooring system for multistory building construction. Steel deck reinforced floor slabs have several advantages which have accounted for their increased popularity. The steel deck, which is placed first, acts as the form for the cast-in-place concrete and eliminates the need for most formwork and shoring. After being cast and cured, the concrete acts compositely with the steel deck. The steel deck then serves as positive bending moment reinforcement for the slab, and only negative bending moment and temperature steel must be added. Also, because of its location, the steel is more effective than in a conventional reinforced concrete slab, thus less concrete and steel material can be used to obtain the same structural strength. Other advantages of steel deck reinforced floor slabs are the safe working platform provided by the steel deck and the built-in raceways for placing utility lines. Figure 1 shows a typical composite floor system.

Since the steel deck is to act as the positive moment reinforcing for the composite slab, some type of interlocking device between the steel and concrete must be provided. These interlocking devices are typically embossments, indentations, holes, or transverse wires attached to the steel deck. Chemical bond and friction between the two materials also help to provide the necessary interlocking force.

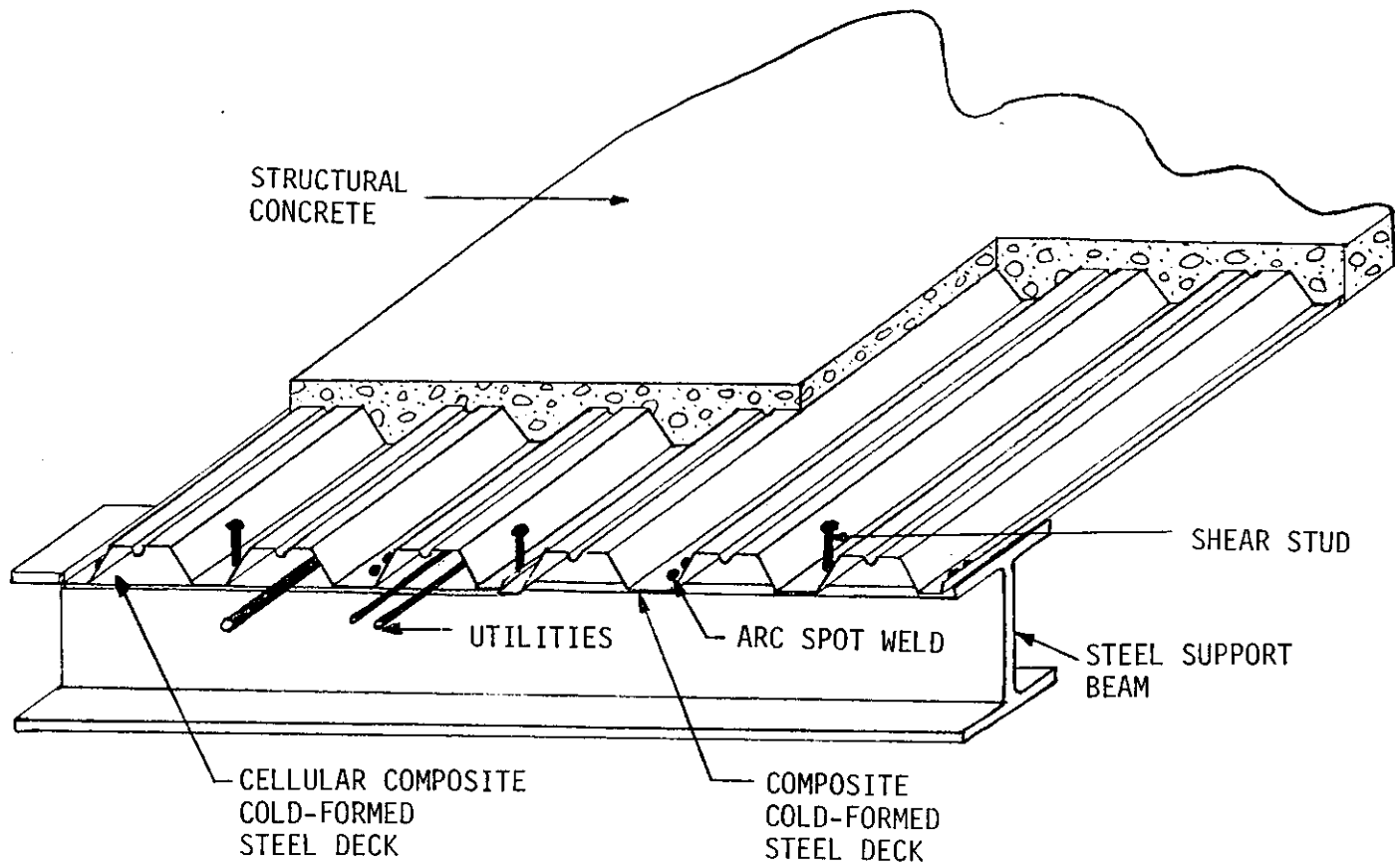


Figure 1. Typical composite floor system

The composite slab is typically connected to the surrounding support beams by means of arc spot welds, or shear connectors, such as studs. If stud connections are used, the slab will act compositely with the support beams. If arc spot weld connections are used, the slab may act compositely with the edge beams, but more research is needed in this area.

1.2. Objective of Overall Research Project

The floor system in many multistory buildings is designed to resist in-plane loads, as well as the vertical gravity loads; the slab portion of this type of system is referred to as a diaphragm. In-plane horizontal loads are typically produced by earthquakes and/or wind. The function of the floor system with diaphragms is to transfer any horizontal forces produced into the vertical lateral load resisting system (shear walls, for example) of the building. The way in which these horizontal forces will be distributed to the shear walls or other system depends on the properties of the diaphragm slab. Thus, knowledge of diaphragm slab properties is necessary to perform a lateral load (wind or seismic) analysis of the multistory building.

The objective of the overall research project is to support this type of analysis by providing basic behavioral and strength properties of composite steel deck diaphragms. Basic properties to be investigated include maximum load, hysteretic behavior, ductility, stiffness, and failure mode. Each of these characteristics is to be studied both experimentally and analytically.

Experimental testing, including both full-scale tests and supporting elemental tests, will be used to examine the effects of various parameters on the above listed properties. Parameters to be investigated include:

- thickness, geometry, and shear transfer device of the steel deck
- thickness and strength of concrete
- number, type, and spacing of edge connections
- in-plane loading with and without superimposed vertical loads.

The objective of the analytical work is to develop predictive equations for various diaphragm properties (i.e., maximum load, stiffness), so that expensive full-scale tests are not required for every possible combination of parameters. Any force distribution used in the development of these equations is to be verified using finite element analysis.

1.3. Objective and Scope of This Study

The research reported on in this document was conducted as part of the second of two research projects on composite floor diaphragms which have been conducted at Iowa State University. The particular concern of this study was elemental (as opposed to full-scale) slab testing. The purpose of the elemental tests was to provide basic in-plane properties of the steel deck to concrete composite system. Elemental tests were necessary to provide these properties since each

manufacturer of steel deck has its own "style" of corrugation geometry and shear transfer devices, which change the composite system's behavior.

The purposes of this study included the following:

- 1) Design, build, and experiment with several different elemental testing apparatus, of much smaller scale and budget than the full-scale slab tests.
- 2) Evaluate testing apparatus, and use one to experimentally determine effects of certain parameters (i.e., deck type, concrete strength) on basic in-plane composite system behavior.
- 3) Analytically relate results of elemental test to full-scale slabs. Verify using finite element analysis.
- 4) Use basic values obtained from elemental tests to predict characteristics of full-scale slabs, using modified existing and/or newly developed predictive equations.
- 5) Compare predicted behavior and values to actual full-scale testing results.

2. PREVIOUS RESEARCH AND BACKGROUND

2.1. Previous Full-scale Testing

A review of past research on diaphragms showed that many tests had been conducted on diaphragms constructed of wood and corrugated steel deck (alone), but very few on composite steel deck concrete systems. A summary of previously tested composite diaphragms and a brief summary of steel deck diaphragms is included.

The earliest tests on steel deck (alone) diaphragms performed in the United States were done by Johnson and Converse (cited in [1]) in 1947, and by S. B. Barnes and Associates in 1949-50. Data from the latter set of tests were used in developing design equations for the Tri-Service design manual entitled Seismic Design of Buildings [2].

In 1955, a more comprehensive study of bare steel deck diaphragms, involving over 50 full-scale tests, was initiated at Cornell University under Winter and Nilson [1, 3]. The effects of end closures, marginal beams, span length, and corrugation profile were investigated. Methods for separating the total deflection into components due to flexural stress, shear stress, seam slip, and edge connector slip were also developed.

A later series of steel deck diaphragm tests at Cornell University, under the direction of Luttrell [4] and Apparo [5], was used to investigate the effects of panel configuration, material properties, and fastening methods. This work was used for the basis of design recommendations in the Design of Light Gage Steel Diaphragms,

published by the American Iron and Steel Institute (AISI) in 1967 [6].

Steel deck diaphragm testing at the University of Kansas, under the direction of Easley [7], was used to determine general buckling strength equations.

A series of over 160 full-scale steel deck diaphragm tests was conducted by Luttrell, at West Virginia University, beginning in 1968. These tests were conducted for the Steel Deck Institute (SDI). The strength and stiffness characteristics obtained were used as a basis for the Steel Deck Institute's Diaphragm Design Manual published in 1981 [8].

Additional steel deck diaphragm tests have been conducted in England, under the direction of Bryan and El-Dakhakni [9] and Davies and Lawson [10]. This work resulted in the design procedures outlined in the book Manual of Stressed Skin Diaphragm Design [11].

In each of the above experimental investigations, the most predominant type of failure was connection (weld, screw, or rivet) failure, at either sheet to sheet connection or sheet to edge beam connection.

As stated, experimental research on concrete steel deck composite diaphragms has been much less extensive. This type of system is constructed by fastening the corrugated sheets to each other (by weld or mechanical clinch), and to the edge beams (by puddle welds, screws, or welded studs), and then placing a structural concrete cover of 2 to 6 inches.

The earliest tests of composite steel deck concrete diaphragms, conducted in the United States, were those used as the basis for the general design equations which were published in the Tri-Service design manual, Seismic Design of Buildings [2]. The actual testing was performed by Pinkham of S. B. Barnes and Associates of Los Angeles, California. The equations developed were based on empirical relationships and basic statics, and were restricted to diaphragms composed of galvanized steel deck, having at least 1.5-in. concrete cover, having additional temperature reinforcement, and using only the steel deck (as opposed to studs) for transferring shear forces between the edge beams and the concrete slab. A guided cantilever concept was used for the development of the predictive equations (see Reference [12]). Several failure modes were determined including deck to edge beam weld failure, diagonal cracking of the concrete, concrete cracking parallel to corrugations, and vertical separation of concrete from the steel deck.

Four full-scale composite diaphragms were tested at the University of Salford, England, under the direction of Davies and Fisher [13]. Each diaphragm was constructed by attaching the steel deck to the edge beams with self-tapping screws, and casting a 2- to 3-inch concrete cover. The ultimate capacity in each case was controlled by failure of the deck to edge beam connections.

Nine full-scale composite diaphragms were tested as part of a previous project at Iowa State University. This testing, under the direction of Porter and Greimann, was performed between 1977 and 1980.

For the remainder of this report, these slabs shall be referred to as Slab 1 through Slab 9. Each diaphragm was 15 ft. x 15 ft., and was tested on the same facility as described in Section 3.1. Four different types of steel deck were tested. Figures 2a and 2b show typical views of Deck Types 1 and 2. Deck Type 3 was similar to Deck Type 1, except the steel thickness was 16 gage rather than 20 gage. Deck Type 4 was similar to Deck Type 3, except that it was cellular deck, i.e., it was as pictured in Figure 2 with a 16 gage flat sheet spot welded to the bottom. Both arc spot welds and studs were used as edge beam connections. Concrete cover varied from 2 to 6 inches. Table 1 gives a summary of parameters for Slabs 1 through 9; Table 2 gives a summary of experimental results. Complete discussion and description of these diaphragm tests can be found in References [12], [14], and [15]. Also, behavior and results as compared with present tests may be found in the subsequent sections of this report.

2.2. Failure Modes

Table 3 lists potential failure modes for steel deck concrete composite diaphragms. This list was based on the previously described research, as well as test results of this project.

The basic function of a floor diaphragm is to transfer horizontal force to the vertical shear resisting system of the building. In a typical building, this means force must be transferred from a steel beam into the corrugated steel deck through the edge connections. The steel deck must then transfer the force into the concrete through its

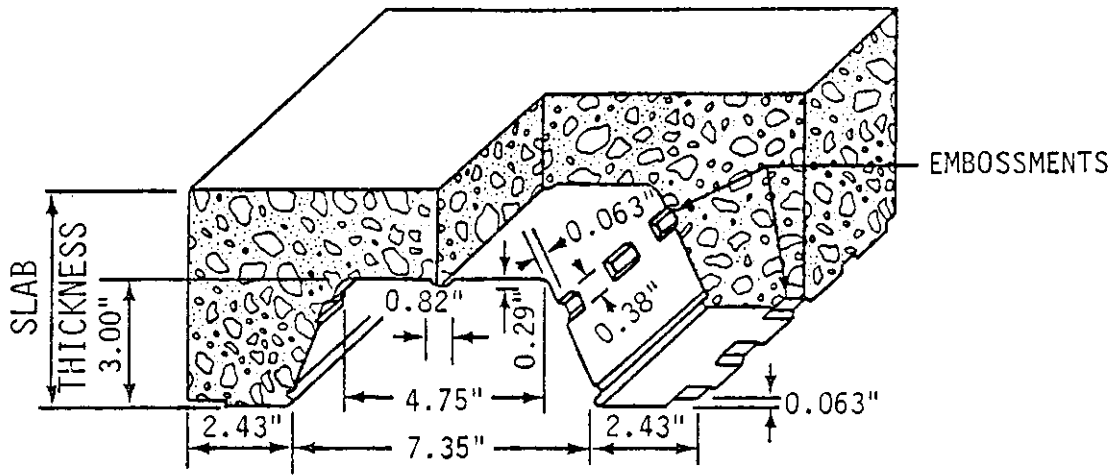


Figure 2a. Typical view of Deck Type 1 [15]

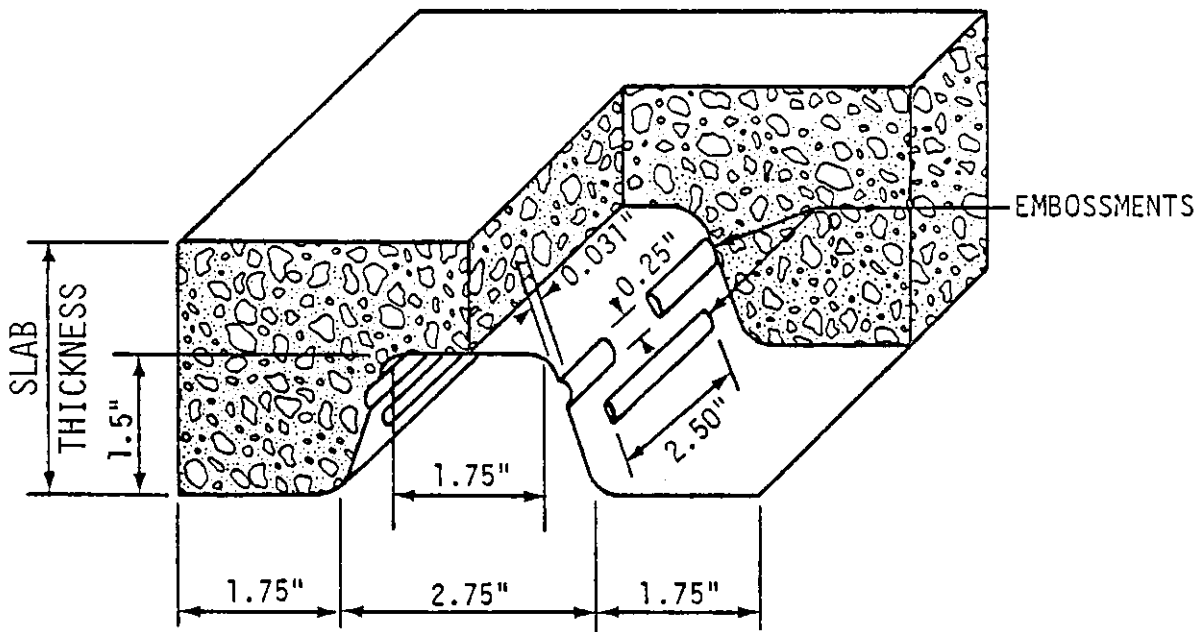


Figure 2b. Typical view of Deck Type 2 [15]

Table 1. Summary of parameters for slab specimens (Slabs 1-9) [15]

Slab number	Concrete parameters			Steel deck parameters				Connections per side
	Nominal thickness (in.)	Actual thickness ^a (in.)	f'_c (psi)	Deck type ^b	Thickness (in.)	Yield strength (ksi)	Ultimate strength (ksi)	
1	5 1/2	5.38	5634	1	0.034	41.7	53.4	30 studs
2	5 1/2	5.50	5250	1	0.034	41.7	53.4	30 studs
3	5 1/2	5.65	4068	1	0.034	41.7	53.4	60 welds
4	5 1/2	5.28	3849	1	0.034	41.7	53.4	60 welds
5	3 1/2	3.53	2966	2	0.062	48.2	60.7	30 welds
6	7 1/2	7.44	4549	2	0.062	48.2	60.7	60 welds
7	5 1/2	5.40	5435	3	0.058	49.7	61.1	60 welds
8	5 1/2	5.47	3345	1	0.035	41.7	53.4	4 studs (each N-S side) 6 studs (each E-W side)
9	5 1/2	5.48	5412	4 (pan) 4	0.058 0.057	51.8 52.4	63.2 64.9	60 welds

^aOut-to-out thickness.

^bSee Section 2.1.

Table 2. Summary of experimental results (Slabs 1-9) [15]

Slab number	Initial stiffness (KIPS/in.)	V_u (KIPS)	Failure mode
1	1800	168	diagonal tension
2	2000	186	diagonal tension
3	1600	97.8	shear transfer mechanism-transverse
4	1300	87.7	shear transfer mechanism-transverse
5	1700	116	diagonal tension
6	2600	147	shear transfer mechanism-parallel
7	1500	137	shear transfer mechanism-transverse
8	1100	54.4	diagonal tension/ shear connector
9	1900	220	diagonal tension

Table 3. Failure modes for composite diaphragms

-
1. Composite slab
 - a. Concrete shear strength
 1. Diagonal tension
 2. Parallel to deck corrugations
 - b. Localized failure
 - c. Stability failure
 2. Deck-concrete shear transfer mechanism
 - a. Parallel to corrugations
 1. Interfacial slip (shear bond)
 2. Concrete shear
 - b. Transverse to corrugations
 1. Interfacial slip (overriding and foldover)
 2. Concrete shear
 3. Corbel/rib
 3. Diaphragm-edge member connections
 - a. Arc spot weld
 1. Weld shear
 2. Sheet tear
 3. Sheet tear and buckling
 - b. Studs
 1. Shearing of stud
 2. Shear failure of concrete around stud
 3. Corbel or edge strip
-

shear transfer (interlocking) devices. The reverse order of force transfer will occur at the far end of the diaphragm, where the force is ultimately transmitted into a shear wall or other vertical shear carrying system. If studs are used, the force may be transmitted directly from the steel frame into the concrete. If any of these components (edge connectors, deck shear transfer devices, concrete slab) fails, then the diaphragm will have lost its capacity to transfer horizontal load.

2.2.1. Composite slab failure

Composite slab failure will occur if the shear load transferred to it is greater than its material strength. Diagonal tension failure (Failure Mode 1.a.1) occurs when the maximum principal tensile stress in the concrete exceeds the concrete's tensile strength. This failure mode is characterized by a diagonal crack at approximately 45 degrees across the slab (see Figure 3). After this crack forms, the steel deck transfers some force across the crack, but does not function as completely effective shear reinforcement because of its flexibility transverse to the corrugations.

Another type of composite slab failure is direct shearing of the concrete along a line parallel to the deck corrugations (Failure Mode 1.a.2). This type of failure will most likely occur when concrete cover is thin and/or weak, and will result in cracking above a deck top flange (see Figure 3).

A third type of composite slab failure, localized failure, occurs when there is a nonuniform shear distribution in the diaphragm, and

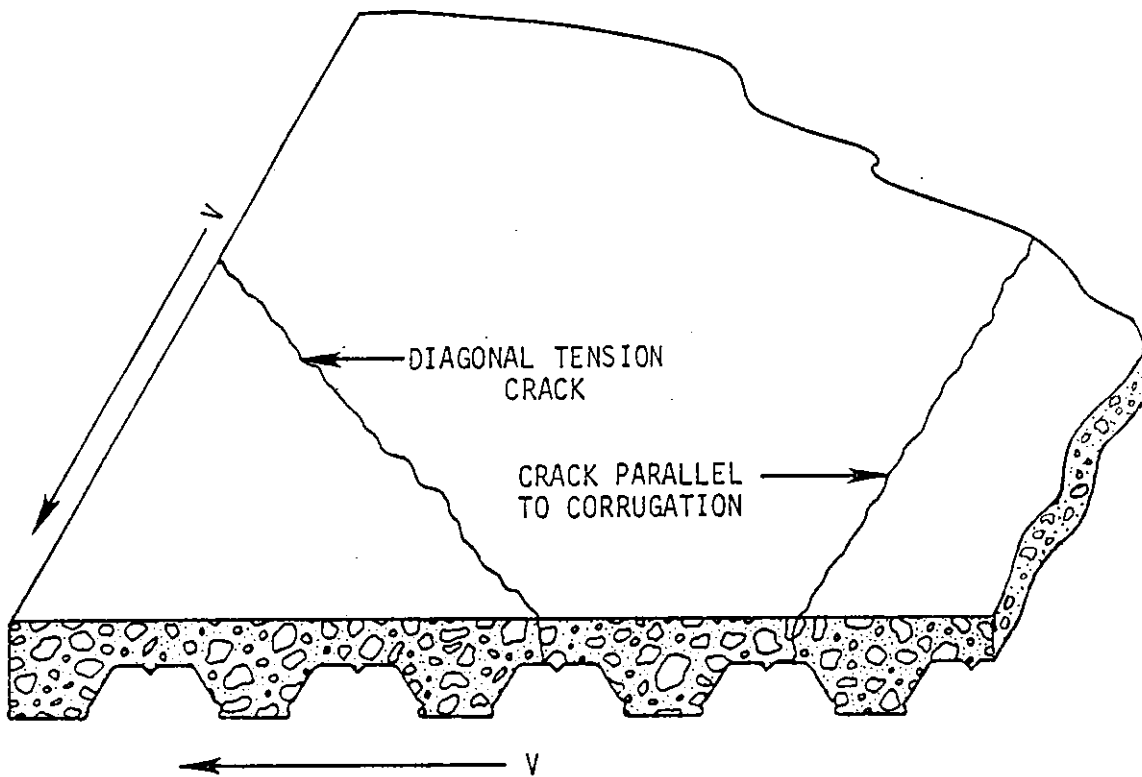


Figure 3. Composite slab failure. a) diagonal tension (Failure Mode 1.a.1); b) crack parallel to corrugations (Failure Mode 1.a.2) [15]

consequently, a small region of high stress. This type of situation will most likely occur due to concentrated loads, unsymmetrical loading, openings in the slab, or changing geometry of the slab.

A fourth type of composite slab failure, stability failure, would involve out-of-plane buckling of the composite slab. Stability failure is not likely to be a primary failure mode under usual loading conditions.

2.2.2. Deck-concrete shear transfer mechanism failure

If the composite system does not use a direct shear transfer device such as studs, then all of the shear force transferred from the edge beams to the concrete must be carried by the deck's shear transfer mechanism or interlocking devices. All deck types tested for this project used embossments for this purpose, along with corrugation geometry, friction, and chemical bonding.

Two types of failure, or a combination of the two, were determined for shear transfer parallel to the corrugations. Interfacial slip parallel to the corrugations (Failure Mode 2.a.1) occurs when a large relative displacement between the concrete and steel deck is allowed due to the capacity of the shear transfer devices (embossments) being overcome (see Figure 4a). This failure mode is similar to the shear-bond failure experienced in vertically loaded specimens [16, 17]. Concrete shear (Failure Mode 2.a.2) occurs when the shear strength of concrete in the down corrugations is overcome (see Figure 4b). This failure mode is likely only to occur if the

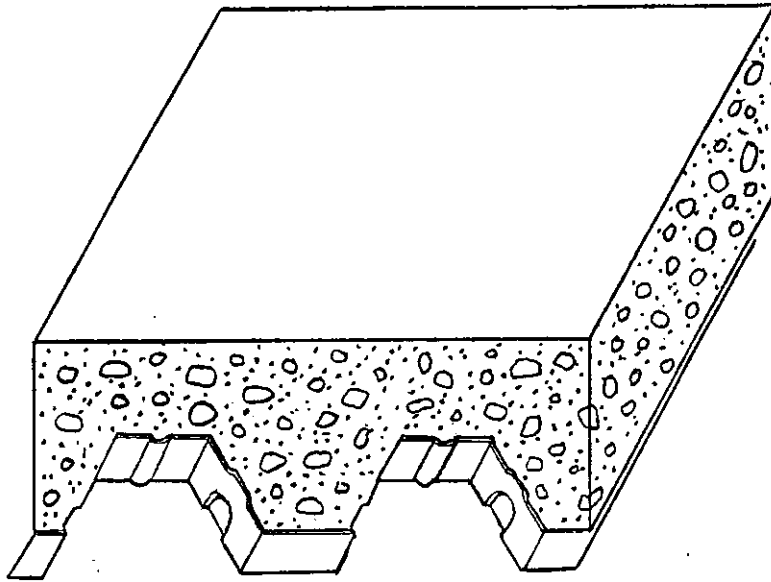


Figure 4a. Interfacial slip parallel failure
(Failure Mode 2.a.1)

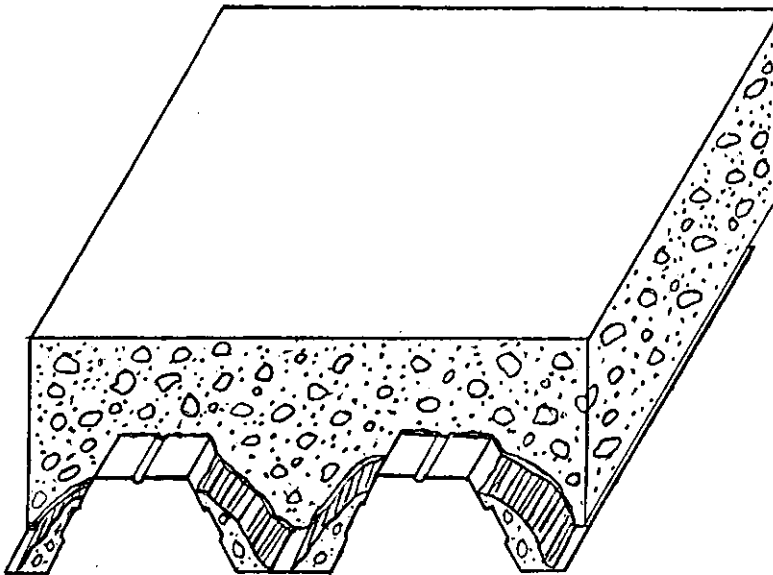


Figure 4b. Concrete shear parallel failure
(Failure Mode 2.a.2)

embossments or other shear transfer devices are very effective. That is, the capacity of the interlocking devices is high enough so that a shear plane through the concrete is weaker than the deck-concrete interface.

Three types of shear transfer mechanism failures are possible transverse to the corrugations. Interfacial slip (Failure Mode 2.b.1) occurs when the concrete overrides and/or folds over the steel deck top corrugations. Concrete shearing (Failure Mode 2.b.2) is very similar to Failure Mode 2.a.2, except that relative movement between concrete and steel deck is in the transverse rather than parallel direction (see Figure 5a). Corbel or rib failure (Failure Mode 2.b.3) occurs when concrete in the down corrugation shears off at the level of the top flange of the steel deck (see Figure 5b). After corbel failure has occurred, both longitudinal and transverse movement may occur across the sheared interface. This failure mode is likely to occur with narrow down corrugations.

2.2.3. Diaphragm-edge member connection failure

In the United States, edge connections are usually arc spot welds or studs. Three different failure modes have been defined for arc spot welds in shear [18]. Which of the three modes, weld shear, sheet tear, or sheet tear and buckling (see Figure 6), will control depends on weld size, sheet thickness, and sheet strength. Predictive equations for each mode are given in Section 2.3.

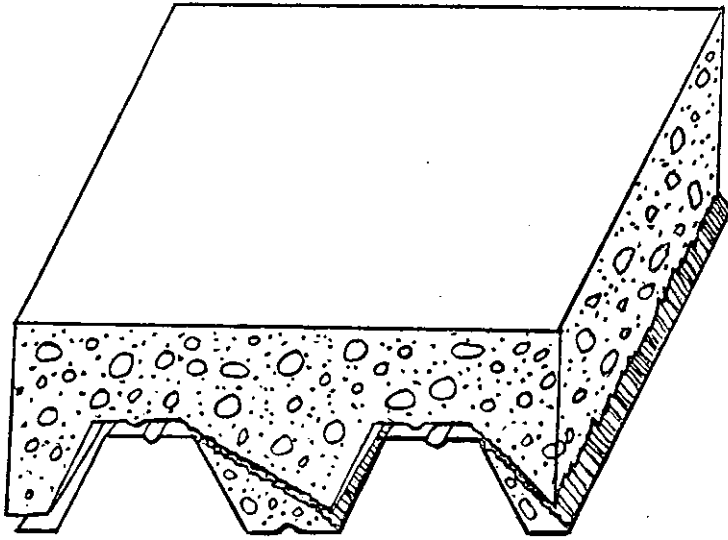


Figure 5a. Concrete shear transverse failure (Failure Mode 2.b.2)

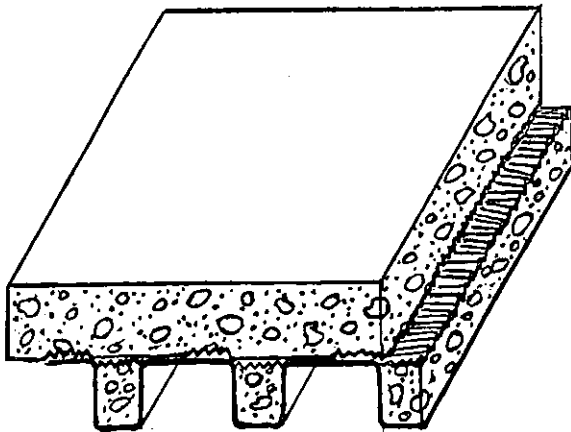


Figure 5b. Corbel or rib failure (Failure Mode 2.b.3)

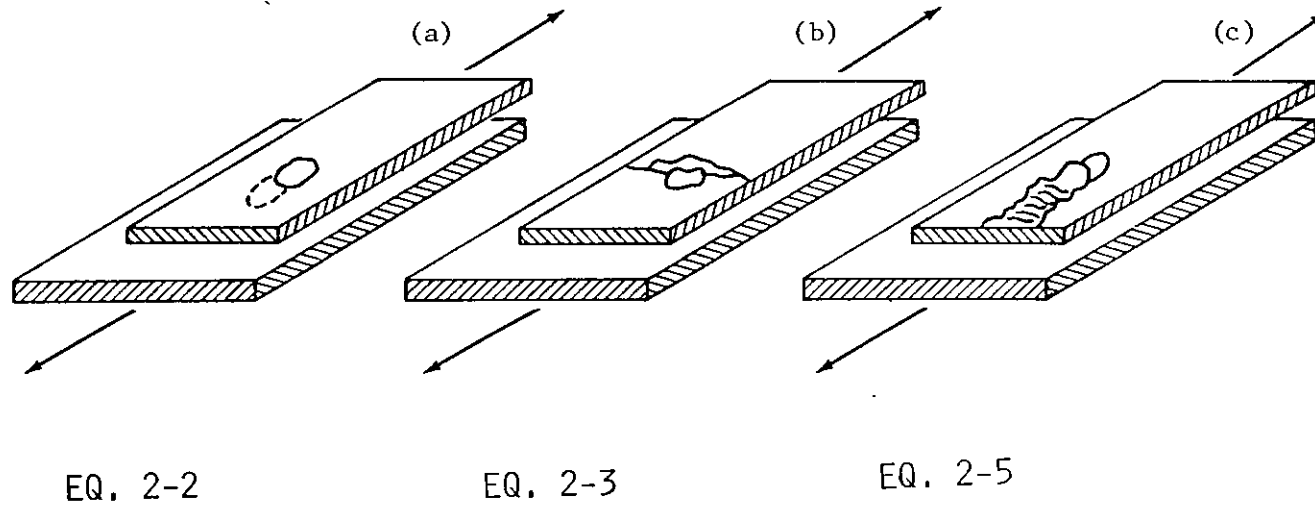


Figure 6. Arc spot weld failure modes. a) weld metal shear; b) sheet tear; c) sheet tear and buckling [18]

Three types of failure are also possible with stud shear connectors. Failure may occur by direct shearing of the studs, by localized failure of the concrete around the studs, or by corbel or edge strip failure of the concrete in which the studs are embedded. For corbel failure, the concrete will shear on a horizontal plane, similar to Failure Mode 2.b.3. For edge strip failure, the concrete will fail in tension on a vertical plane above the deck top flange which is nearest the edge. Corbel failure is likely to occur if the studs do not extend above the top flange of the deck. Edge strip failure is likely to occur if the concrete cover over the steel top flange is thin.

2.3. Previous Elemental Tests

Elemental tests are those used to obtain information on one or more of the components of the composite diaphragm system. Elemental tests discussed do not include basic material property tests, such as concrete compression (ASTM C39-81) and steel tension (ASTM A370-77), since these are standard laboratory tests. Previous elemental tests can be placed into four basic categories: 1) those testing shear studs, 2) those testing arc spot welds, 3) those testing corrugated steel deck equivalent properties, and 4) those testing the deck-concrete shear transfer mechanism.

Numerous elemental tests have been performed to determine the properties of stud shear connectors. Since no studs were used for any of the diaphragms tested in this project, details are not reproduced here. However, testing methods did give some guidance in the

development of other elemental tests. Details of stud testing methods and results can be found in References [19] and [20].

Numerous elemental tests have also been performed on arc spot welds. A series of over 60 simple tension tests at West Virginia University resulted in the specifications now included in the Steel Deck Institute's Diaphragm Design Manual [8]. An empirical relationship for the ultimate strength of a spot weld, Q_w , (sheet to structure) was given as

$$Q_w = (5.46t + 0.52)\pi Dt F_y \quad (2-1)$$

where

t = thickness of connected sheeting

D = apparent weld diameter

F_y = sheeting yield strength.

The initial flexibility (of 0.625 inch diameter spot welds) was also determined, and plotted as a function of the connected sheeting thickness.

An extensive series of arc spot weld tests has also been conducted at Cornell University. These tests led to the specifications which are included in the AISI Specification for the Design of Cold-Formed Steel Members [21]. The ultimate design strength of a spot weld, Q_{wd} , was given as the smaller of

$$Q_{wd} = \frac{d_e^2 F_{xx}}{4} \quad (2-2)$$

or one of the following:

$$Q_{wd} = 0.88 t d_a F_u \quad (2-3)$$

$$\text{for } \frac{d_a}{t} \leq \frac{140}{\sqrt{F_u}}$$

$$Q_{wd} = 0.112 \left[1 + \frac{960 t}{d_a \sqrt{F_u}} \right] t d_a F_u \quad (2-4)$$

$$\text{for } \frac{140}{\sqrt{F_u}} < \frac{d_a}{t} < \frac{240}{\sqrt{F_u}}$$

$$Q_{wd} = 0.56 t d_a F_u \quad (2-5)$$

$$\text{for } \frac{d_a}{t} \leq \frac{240}{\sqrt{F_u}}$$

where

d = apparent weld diameter

d_a = weld diameter of spot weld at mid-thickness

= $(d-t)$ for single sheets, $(d-2t)$ for multiple sheets

d_e = effective fused diameter

= $0.7d - 1.5t < 0.55d$

t = thickness of sheeting

F_{xx} = AWS electrode classification

F_y = specified minimum yield point of steel

F_u = specified minimum tensile strength of steel.

The design strength (Q_{wd}) must be multiplied by a factor of safety of 2.5 to find the predicted ultimate strength. Equation (2-2) is for weld metal shear failure; Eq. (2-3) for sheet tear failure; Eq. (2-5) for sheet tear and buckling; and Eq. (2-4) for a combination of the second and third failure modes.

Note that both References [8] and [21] warn that weld properties vary widely depending on exact process and quality control techniques used. Also note that none of the previous elemental tests performed include the effects (if any) of a cast-in-place concrete topping directly covering the welds.

The third category of elemental tests is those to determine equivalent flat plate properties of corrugated steel deck. Equivalent properties which must be determined, are the effective modulus of elasticity in the corrugated direction, and the effective shear modulus. The effective elastic modulus is usually determined through some type of tension test, although no standard procedure has been put forward. The shear modulus has been deduced both from full-scale tests [8] and from elemental tests, such as those performed by Hussain and Libove at Syracuse University [22]. The Syracuse testing apparatus consisted of a "hinged picture frame", varying in size from 2.0 ft. x 7.5 ft. to 2.0 ft x 1.5 ft. The results were used to verify theoretical equations for determining the

shear stiffness of a corrugated plate.

Elemental tests to determine the in-plane properties of the deck-concrete interface or shear transfer mechanism have been much fewer in number than those of other categories. Since these properties are very important to composite diaphragm behavior, their determination became the major objective of this study. Previous elemental tests in this area, all conducted at Iowa State University, are summarized below.

In 1967-68, a series of vertical and horizontal pushout specimens (see Figure 7) was tested by Porter [23]. Although the results of these tests were intended for use with gravity loads rather than in-plane loading, the types of stress produced in the elemental test were similar. Results showed that the bond stress developed was inversely related to the interface length. These tests were found not to correlate well with the actual vertically loaded specimens. The reason for the discrepancy was thought to be the difference in curvature.

Another series of vertical pushout tests was performed in conjunction with the previous diaphragm research project [15]. These tests were determined not to model the actual behavior of the full-scale slabs because of a lack of constraint in the direction normal to the interface. Once initial cohesion was lost, large displacements and deck pull-away made further testing meaningless.

Two more series of pushout tests were also conducted [13]. For these tests, the slabs were placed horizontally, and the load applied

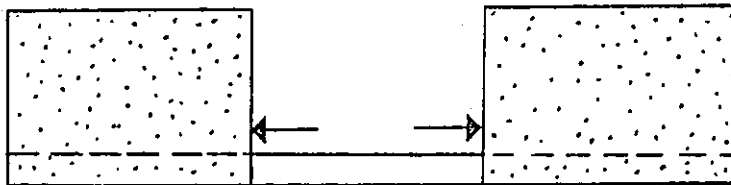
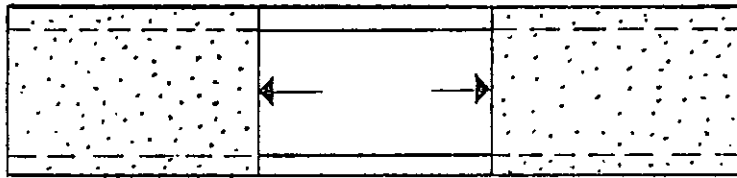
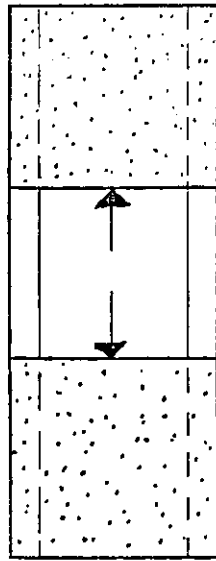


Figure 7. Vertical and horizontal pushout tests [23]

at one edge. Figure 8 shows a schematic view of the testing apparatus. Pushout strengths were determined both parallel and transverse to the deck corrugations. Table 4 shows parameters and test results of the two series tabulated on a per inch of specimen length basis. Stiffness values shown were obtained by doing a linear regression through a displacement of 0.005 in. General behavior of these tests seemed to match that occurring in the diaphragm, however, some practical testing problems were encountered. These included:

- 1) localized failure of the first corrugation on the transverse specimens, 2) the concrete overriding the deck rather than deforming deck geometry on the transverse specimens, 3) out-of-plane twisting occurring at large displacements. Results were somewhat erratic (especially the stiffness), but judged reasonable. Not including those specimens with localized failures, the values shown in Table 5 were determined and used for the strength and stiffness of the deck-concrete interface for the various deck types tested, for both the parallel and transverse directions.

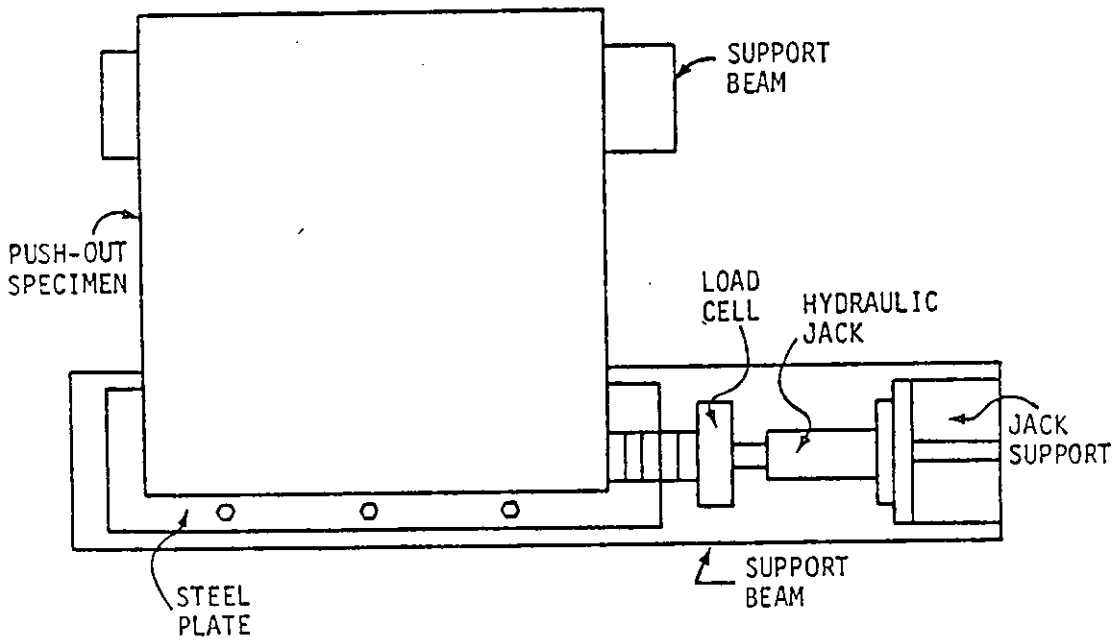
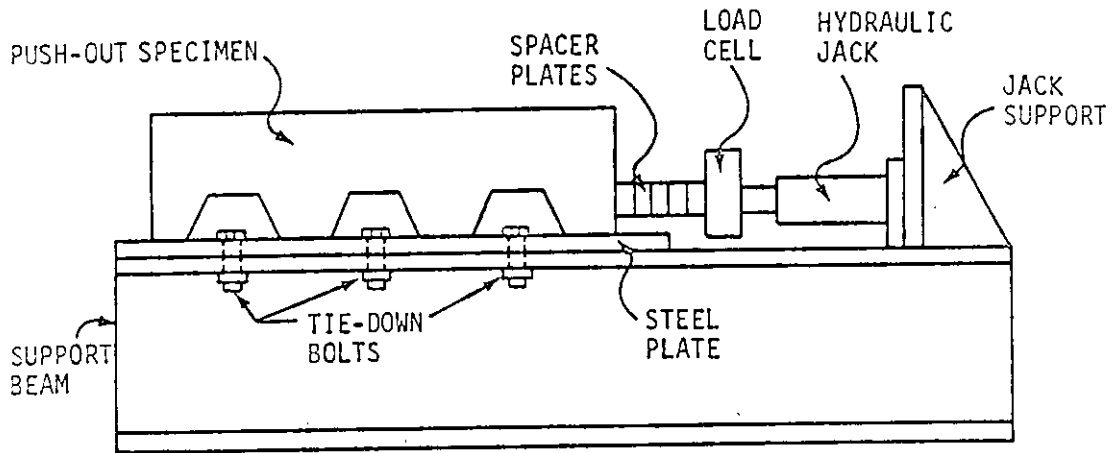


Figure 8. Schematic of pushout test [15]

Table 4. Testing parameters and results of pushout specimens [15]

Specimen number	Deck type	Dimensions (in.)		Load direction	Thickness (in.)	f'_c	K KIPS/in./in.	P_u (KIPS/in.)
		Parallel	Perpendicular					
2-1	1	36	36	parallel	5 1/2	2950	168	.406
2-2	2	30	30	parallel	7	2950	∞	.447
2-3	1	36	36	perpendicular	5 1/2	2950	- ^a	.216 ^b
2-4	1	36	36	parallel	5 1/2	2950	33	.531
2-5	2	30	30	parallel	7	2950	21	.383
2-6	2	15	30	parallel	7	2950	45	.460 ^b
2-7	1	18	36	perpendicular	5 1/2	3197	26	.264 ^b
2-8	1	36	36	perpendicular	5 1/2	3197	36	.383 ^b
2-9	2	30	30	perpendicular	7	3197	65	.963
3-1	1	36	36	perpendicular	7 1/4	6250	53	.458
3-2	1	36	36	perpendicular	7 1/4	6250	43	.450
3-3	4	36	36	parallel	7 1/4	6250	35	.597
3-4	4	36	36	parallel	7 1/4	6250	39	.911
3-5	4	36	36	perpendicular	7 1/4	6250	60	.708
3-6	4	36	36	perpendicular	7 1/4	6250	66	.792

^aNo value calculated.

^bNot included in calculations.

Table 5. Pushout test results by deck type [15]

Deck type	Q_{tpo} (lbs./in.)	Q_{ppo} (lbs./in.)	K_t (KIPS/in./in.)	K_p (KIPS/in./in.)
1	454	468	47	55
2	967	415	65	42
3	_a	_a	_a	_a
4	750	754	63	37

^aNo pushout tests conducted with Deck Type 3.

3. EXPERIMENTAL TESTING AND RESULTS

3.1. Full-scale Tests

At the time of writing this report, 11 full-scale composite slabs (Slabs 10-20) had been tested in conjunction with this project. Although the main focus of this study was the elemental testing, a short summary of full-scale tests is given, since performance of the elemental tests was judged by how closely they modeled the full-scale slabs.

A summary of testing parameters and results for Slabs 10-20 are given in Section 3.1.6. However, only Slabs 5, 6, and 9 (from the previous project) and Slabs 10, 11, 15, 19, and 20 are used for detailed comparison, since they used the same deck types tested in the elemental tests and did not include a superimposed vertical load (see Reference [24] for the effects of vertical load on diaphragm behavior).

3.1.1. Test facility

A cantilever diaphragm test frame, which had been built for use with Slabs 1 to 9 was also used for Slabs 10 to 20. The fixed edge of the diaphragm models attachment to an adjacent slab or shear wall; the free edge models attachment to a structural steel frame.

Figure 9 shows a schematic view of the 15 ft. x 15 ft. diaphragm test frame. The fixed edge was provided by three large concrete reaction blocks, anchored to the laboratory floor with 2 in. diameter high strength bolts. An embedded steel plate was used to connect the

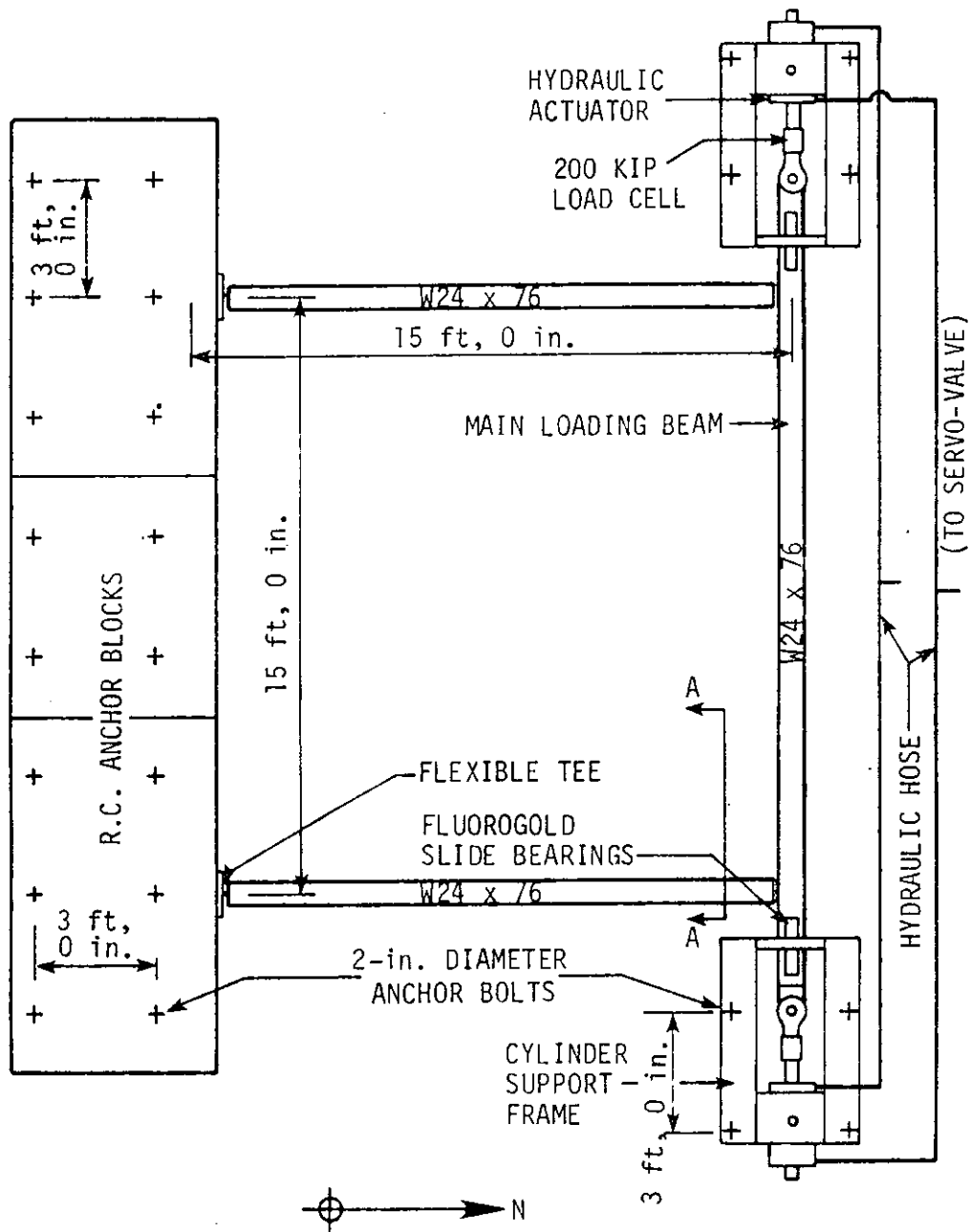


Figure 9. Schematic view of diaphragm test frame [15]

steel deck to the reaction blocks. The frame was composed of three W24 x 76 wide flange sections, connected by flexible tee-shaped elements. Two hydraulic double-acting cylinders, one at each end of the front moving beam, were used to apply the force. The system was designed for a working load of ± 400 KIPS and a maximum displacement of ± 6.0 in. Details on the diaphragm testing facility can be found in Reference [12].

3.1.2. Load program

A reversed cyclic loading program, with displacement control, was used for each of the slabs tested. The displacement of the front moving beam was held constant while load point readings were taken. For Slabs 10 through 20, the basic displacement cycling pattern was: $\pm .025$ in., $\pm .05$ in., $\pm .10$ in., $\pm .20$ in., $\pm .40$ in., ± 1.0 in. Cycling at each displacement continued until at least three complete cycles had been performed and the load loss between cycles was less than 5.0 percent.

Although complete data readings were taken only at load points, the load-displacement curve was plotted continuously. Figure 10 shows a typical load-displacement plot. Note how the stiffness degrades and energy dissipated (area within one load-displacement loop) increases as the cyclic displacement limit is increased.

After cycling at ± 1.0 in. was completed, many gages were removed, and several cycles at ± 5.0 in. were performed. These cycles were useful for obtaining post-ultimate ductility information as

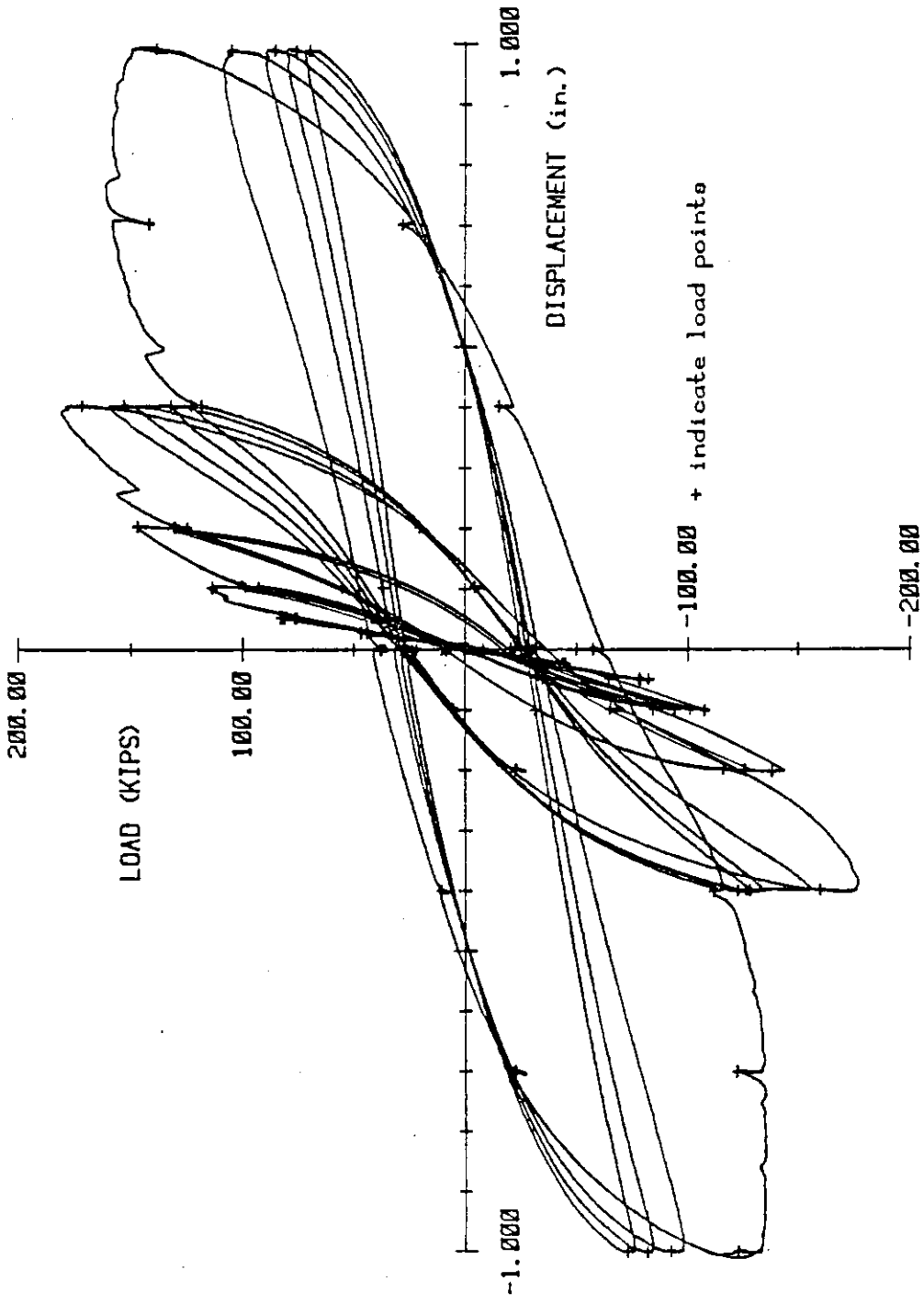


Figure 10. Typical load-displacement plot [24]

well as examining exaggerated behavior.

3.1.3. Instrumentation

Instrumentation for each slab was designed to aid in the analysis of slab behavior. Instrumentation was used to determine applied loads, in-plane displacements, out-of-plane displacements, concrete strains, steel deck strains, strains in framing beams, relative slip between concrete and steel deck, and relative slip between steel deck and framing beams.

A pair of 200-KIP axial load cells was used to measure the load applied to the front moving beam. The load cells were connected in series and the total load found from adding the two values.

Displacements were measured using electric direct current differential transducers (DCDTs) and mechanical dial gages. Locations of in-plane displacements (horizontal) and out-of-plane displacements (vertical) which were typically recorded are shown in Figure 11. The signal from the DCDT in the northeast corner was sent to a digital readout, from which the specified displacement was obtained by manual adjustment of the MTS servo-controller unit. Locations of horizontal slip measurements between the concrete and steel deck, between the steel deck and frame, and between the concrete and frame are shown in Figure 12. On Slabs 18, 19, and 20, special horizontal measurements were recorded at the southwest corner of the slab, to determine the flexibility of the frame-to-abutment connection. The locations of these measurements are not shown on Figure 12.

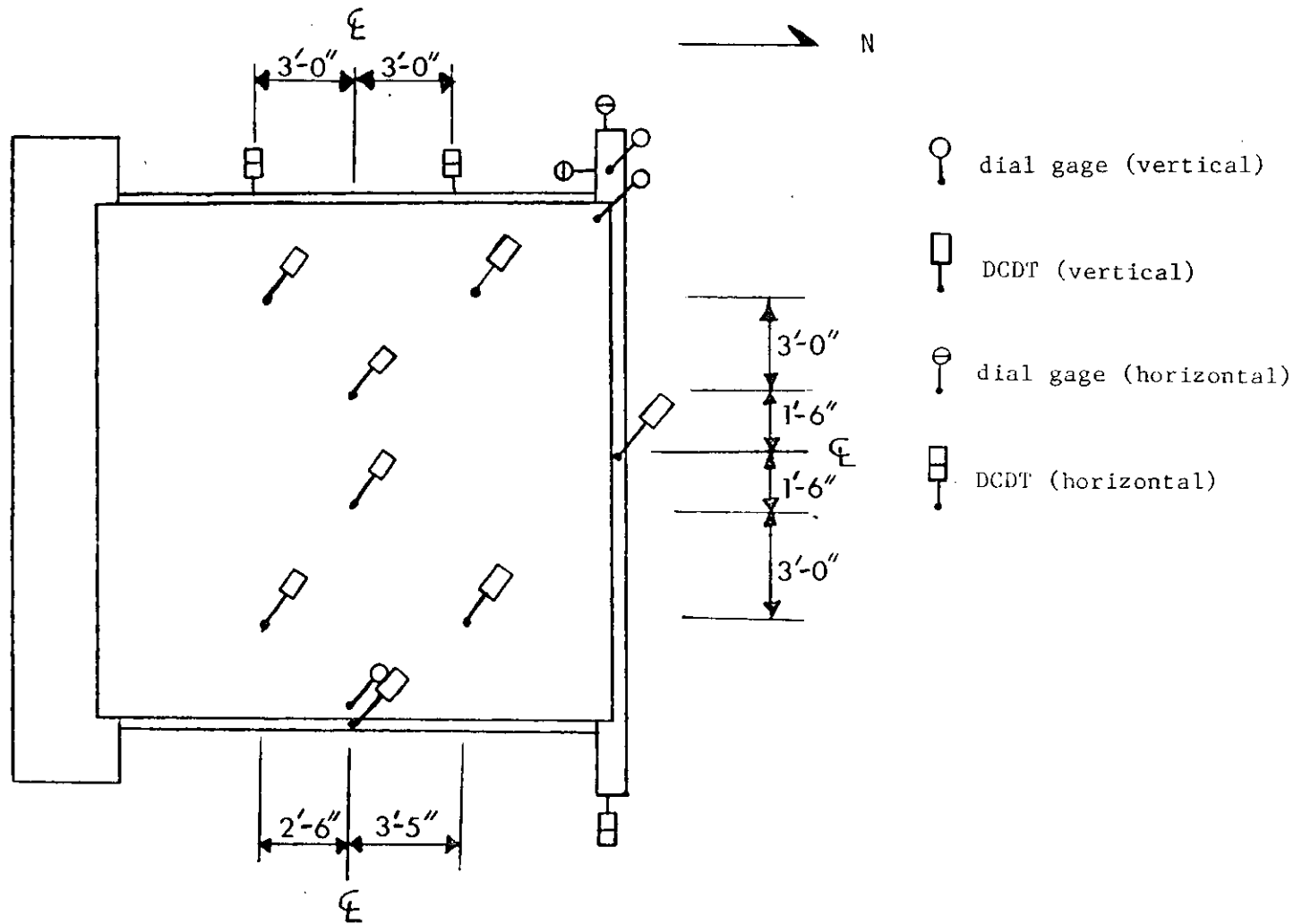


Figure 11. Locations of vertical and horizontal measurements

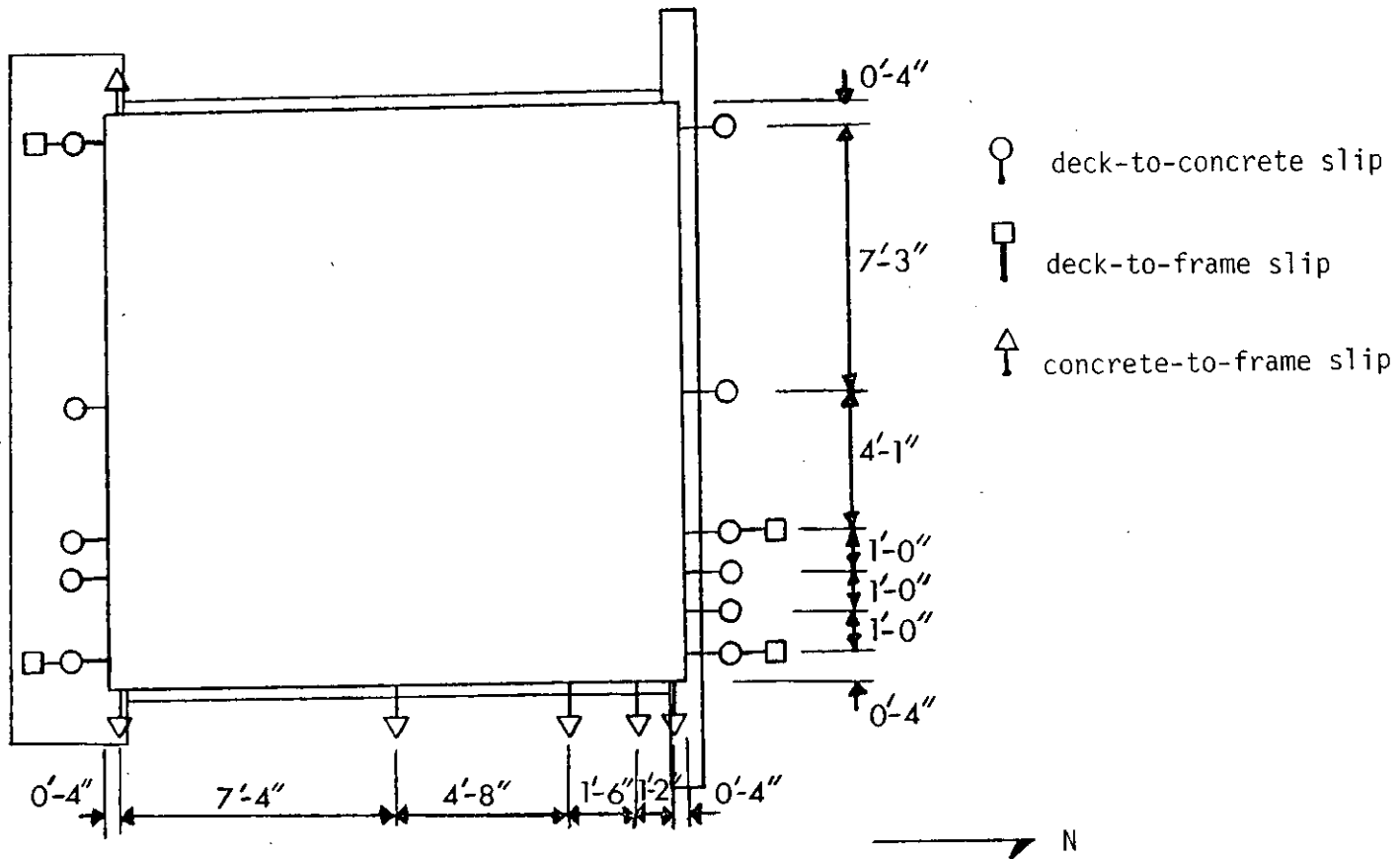


Figure 12. Locations of slip measurements

On several of the slabs, the extent of separation between the steel deck and the concrete was determined by a dip-stick measurement. This measuring device consisted of a 0.022-in. thick piece of banding steel inserted at the edge of the slab, and pushed inward as far as possible. The actual separated distance was assumed to extend 12 in. or less beyond the measured distance. Although somewhat approximate, the measurement did give a good indication of the amount of separation.

A varying number of strain gages was used to measure strains on the top surface of the concrete, as well as the bottom surface of the steel deck. Gages on steel deck and concrete were all placed in corresponding pairs. Both uniaxial and three-gage rosettes were used.

Strain gages already located at various sections on the framing beams were also read and recorded at each load point. Other test recording devices included photographs of the crack patterns and visible behavior, and a hand-held tape recorder on which test observers could describe behavior. Video tapes of testing in progress were also made for several of the diaphragm slab tests.

All electrical instrumentation (DCDTs, strain gages, and load cells) were read and recorded by a 150-channel Data Acquisition System (DAS). The DAS was composed of a 150-channel voltmeter, five independent power supply units, a digital plotter, a microcomputer, and a dual disk drive.

3.1.4. General behavior and failure modes

Slabs 1 through 20 were all 15 ft. x 15 ft. in size and tested on the previously described test facility. All deck types used had a galvanized surface coating. Arc spot weld connections were a nominal 0.75 in. diameter, and were made with a submerged arc "MIG" welder, with the amperage varied according to the deck thickness. All slabs, except Slab 4, had the deck corrugations oriented in the north-south direction. Following is a description of slab tests relevant to this study.

3.1.4.1. Slab 5 Slab 5 was constructed from Deck Type 2 (Figure 2b). Thirty arc spot welds per side connected the deck to the edge beams. Total slab thickness was 3.5 in. A maximum load of 115.6 KIPS occurred during the first cycle at 0.1 in. displacement. During the second cycle, a diagonal crack occurred in the southwest corner. The previous maximum load of 115.6 KIPS had not been reached when this crack formed. Cycling at larger displacements caused many of the welds to fail along the east edge of the slab. These weld failures were probably premature, due to poor weld penetration into the base metal.

Diagonal tension was chosen as the ultimate failure mode because it was the formation of the diagonal tension crack which limited the slab from taking a higher load at a higher displacement. Post-ultimate behavior included extensive diagonal cracking as well as slip parallel to the corrugations.

3.1.4.2. Slab 6 Slab 6 was similar to Slab 5, except that the slab thickness was increased to 7 in. The maximum load for Slab 6 was 146.8 KIPS, and occurred at a 0.1 in. displacement. The failure mode for this slab was interfacial slip parallel to the corrugations. No drastic loss in load occurred following the maximum load; in fact, a load of approximately 75 percent of ultimate was maintained out to displacements of 1 in. This was due to the fact that the shear transfer mechanism still had considerable strength, even though displaced past its maximum capacity. No cracks ever formed on the top surface of the slab.

3.1.4.3. Slab 9 Slab 9 was constructed of Deck Type 4, the cellular deck. Sixty arc spot welds per side were used to connect the deck to the edge beams. Total slab thickness was 5.5 in. A maximum load of 220 KIPS was reached while moving to a 0.2 in. displacement. While cycling at lower displacements, diagonal cracks had occurred on three corners of the slab; however, the slab continued to carry an increasing amount of load until formation of the diagonal crack, which occurred at the 0.2 in. displacement. This crack was accompanied by a loss in load of nearly 50 KIPS; thus, the ultimate failure mode was determined to be diagonal tension. Extensive diagonal cracks continued to form while cycling at higher displacements.

3.1.4.4. Slab 10 Deck Type 5 (Figure 13) was used for Slab 10. The deck was 16-gage and connected to the framing beams by 60 arc spot welds per side. Nominal slab thickness was 5.5 in. A maximum load of 161 KIPS was reached at a displacement of 0.4 in. The

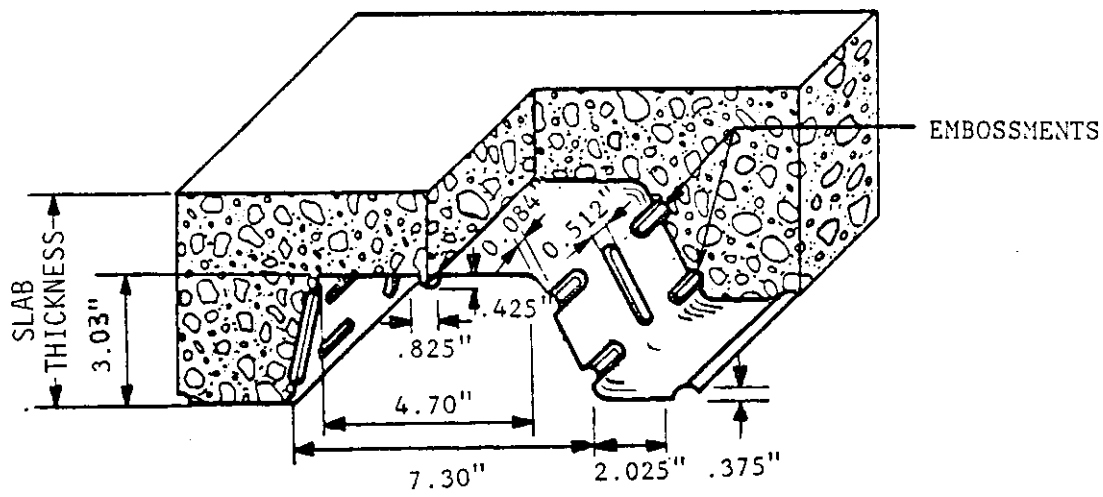


Figure 13. Typical view of Deck Type 5 [24]

primary failure mode was diagonal tension, with each of the four corners cracking off either a half cycle previous to or at the maximum load. Even though the failure mode was diagonal tension, significant interfacial slip had occurred both parallel (.038 in.) and transverse (.058 in.) to the corrugations prior to the maximum load cycle. This indicates that an increasing amount of load may be transferred from the deck to the concrete, even after substantial slip. Cycling at larger displacements caused increases in slip both parallel and transverse to the corrugations, and two cracks (parallel to corrugations) roughly dividing the slab into thirds.

3.1.4.5. Slab 11 Deck Type 6 (Figure 14) was used in constructing Slab 11. Deck Type 6 had a geometry similar to Deck Type 5, but was 18 gage, and had a different embossment pattern. Sixty arc spot welds per side connected the deck to the edge beams. Slab thickness was 5.5 in. A maximum load of 95 KIPS was reached while moving to a 0.4 in. displacement. Although a diagonal crack did begin to form at the maximum load, it did not propagate completely across the southwest corner until two full cycles later. The average interfacial slip (parallel to the corrugations) at the corners before ultimate was 0.095 in. Cycling after ultimate caused continuing increase in slip parallel to the corrugations. No other surface cracking occurred until cycling at ± 5.0 in. Thus, the primary failure mode at ultimate was slip parallel to the corrugations. Cycling at large displacements caused concrete cracking parallel to the corrugations, some weld failure, and out-of-plane buckling of the

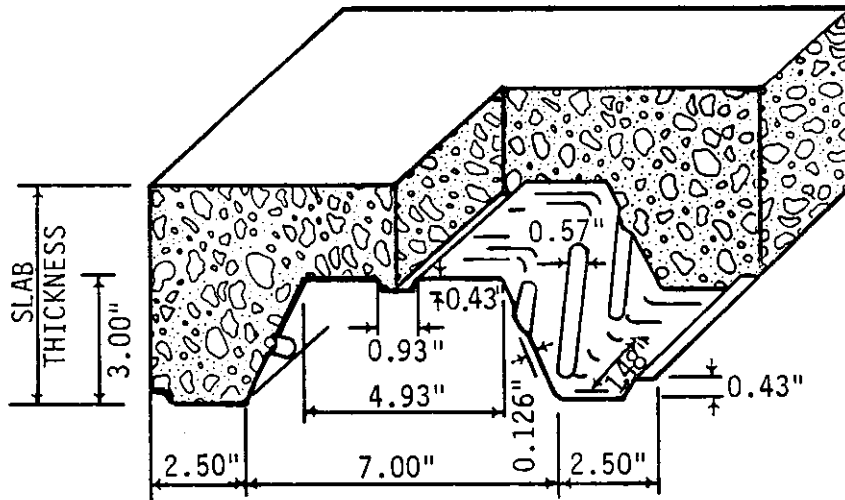


Figure 14. Typical view of Deck Type 6

deck on the southwest corner.

3.1.4.6. Slab 15 Deck Type 7 (Figure 15) was used for Slab 15. This deck was 18 gage, 1.5 in. deep, and had down corrugations which were one-half the width of the up corrugations. Sixty arc spot welds per side connected the deck to the edge beams. Nominal slab thickness was 4 in. Slab 15 reached an ultimate load of 103 KIPS while moving to a displacement of 0.4 in. for the first time. Prior to this, most of the down corrugations on both the north and south faces had sheared off from the main body of the slab (corbel or rib failure). Significant interfacial slip had also occurred, with an average parallel slip at the corners of the slab of 0.058 in., and an average transverse relative displacement at the corners of 0.060 in. The transverse relative displacement was due to a combination of corbel failure and interfacial slip. No surface cracking occurred until the third cycle at ± 1.0 in. Behavior indicated the failure mode to be corbel failure. Cycling at higher displacements caused increased slip both parallel and transverse to the corrugations.

3.1.4.7. Slab 19 Slab 19 was constructed using Deck Type 8 (Figure 16). Deck Type 8 was very similar to Deck Type 5, except the embossment pattern was different. Sixty arc spot welds per side connected the deck to the edge beams. Nominal slab thickness was 5.5 in. A maximum load of 147 KIPS was reached when moving to a 0.4 in. displacement for the first time. Interfacial slip both parallel and transverse to the corrugations began early in the test at the

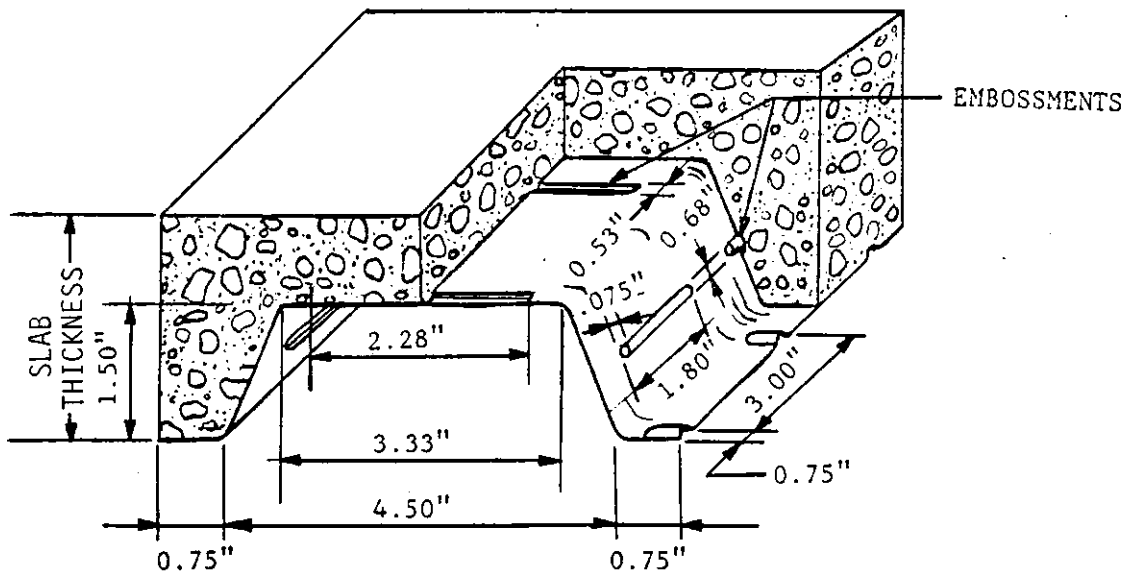


Figure 15. Typical view of Deck Type 7 [24]

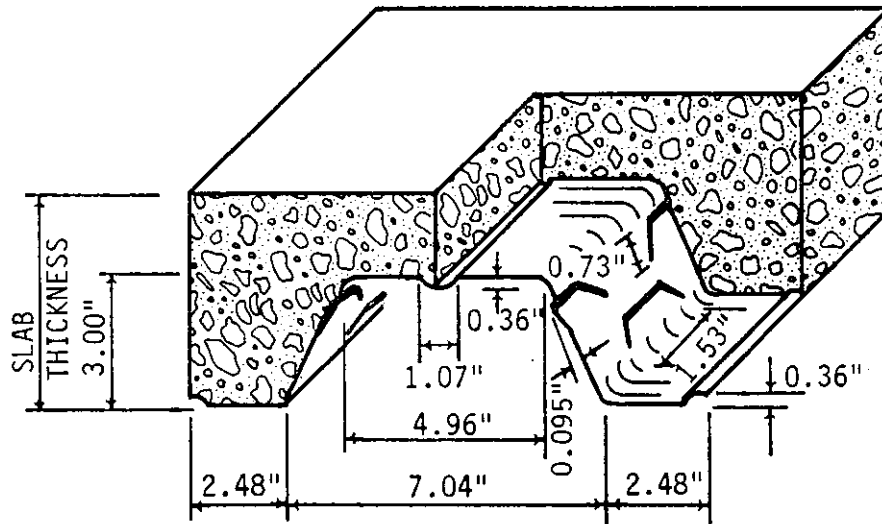


Figure 16. Typical view of Deck Type 8

0.025 in. cycles and increased with each displacement increment. On the way up to the maximum load, intermediate points were taken at 0.2 in. and 0.3 in. At the 0.2 in. displacement, a diagonal crack formed across the southwest corner. Even though higher loads were taken at the 0.3 in. and 0.4 in. displacements, the capacity was limited by the diagonal crack across the corner. Thus, the primary failure mode was diagonal tension. Cycling at large displacements caused cracking parallel to the corrugations, and some weld failure.

3.1.4.8. Slab 20 Slab 20 was constructed using Deck Type 9 (Figure 17). This deck type was 20 gage, 2.5 in. deep, and had an embossment pattern with alternating inward and outward embossments directly adjacent to each other. Forty arc spot welds per side connected the steel deck to the framing beams. Nominal slab thickness was 5.5 in. A maximum load of 94.6 KIPS was reached while moving to a 0.4 in. displacement for the first time. The primary failure mode was interfacial slip transverse to the corrugations, with obvious deck foldover occurring, especially along the south edge. Stiffness degraded rapidly as welds along the north and south edges failed due to sheet tear around the weld. Cycling at large displacements caused the first corrugation on both the east and west edges to crack off from the rest of the slab.

3.1.5. Measured results

As stated in Section 3.1.3, many strains and displacements were recorded throughout each test. However, only a few typical results indicative of general behavior are presented here.

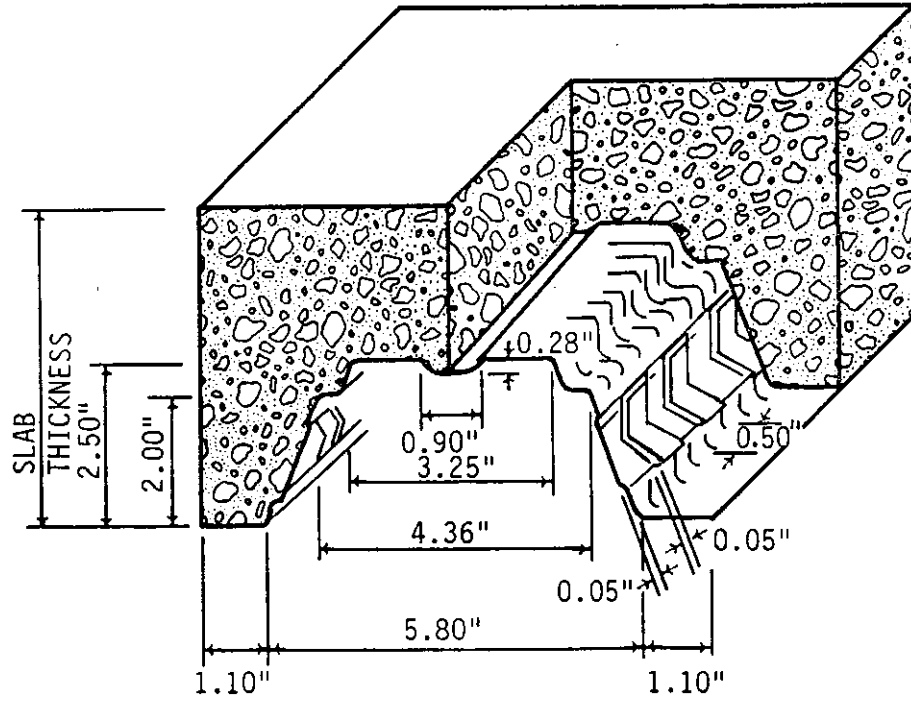


Figure 17. Typical view of Deck Type 9

The relative slip between deck and concrete para corrugations at several locations along the north ed shown on Figure 18. The slip, measured by mechanic shown for several different displacements of the front moving. This plot shows that interfacial slip is much greater near the edge of the slab, and also progresses inward as cyclic displacements are increased. Each of the slabs exhibited a similar behavior, although some had a more linear variation of slip along the length, especially at large displacements.

Typical steel deck strains (from Slab 10) are shown on Figure 19. Both of the indicated gages were located 7.67 ft. from both the north and south edges of the slab, and both were measuring strain in the north-south direction. Gage 3 was located 13 in. from the east edge; Gage 12 was located 49 in. from the east edge. The large increases in strain indicate that the steel deck at the location of Gage 3 was no longer acting compositely with the concrete beyond Load Point 26, the first displacement to 0.1 in. However, the steel deck at the location of Gage 12 acted compositely with the concrete through the ± 1.0 in. displacements. Note that no diagonal tension cracks occurred on Slab 10 until Load Point 47. Steel deck strains for each of the slabs exhibited a similar behavior, even though having different ultimate failure modes.

Another measurement which gave an indication of general behavior was the previously described dip-stick measurement. A typical result is shown in Figure 20. This particular set of measurements was taken

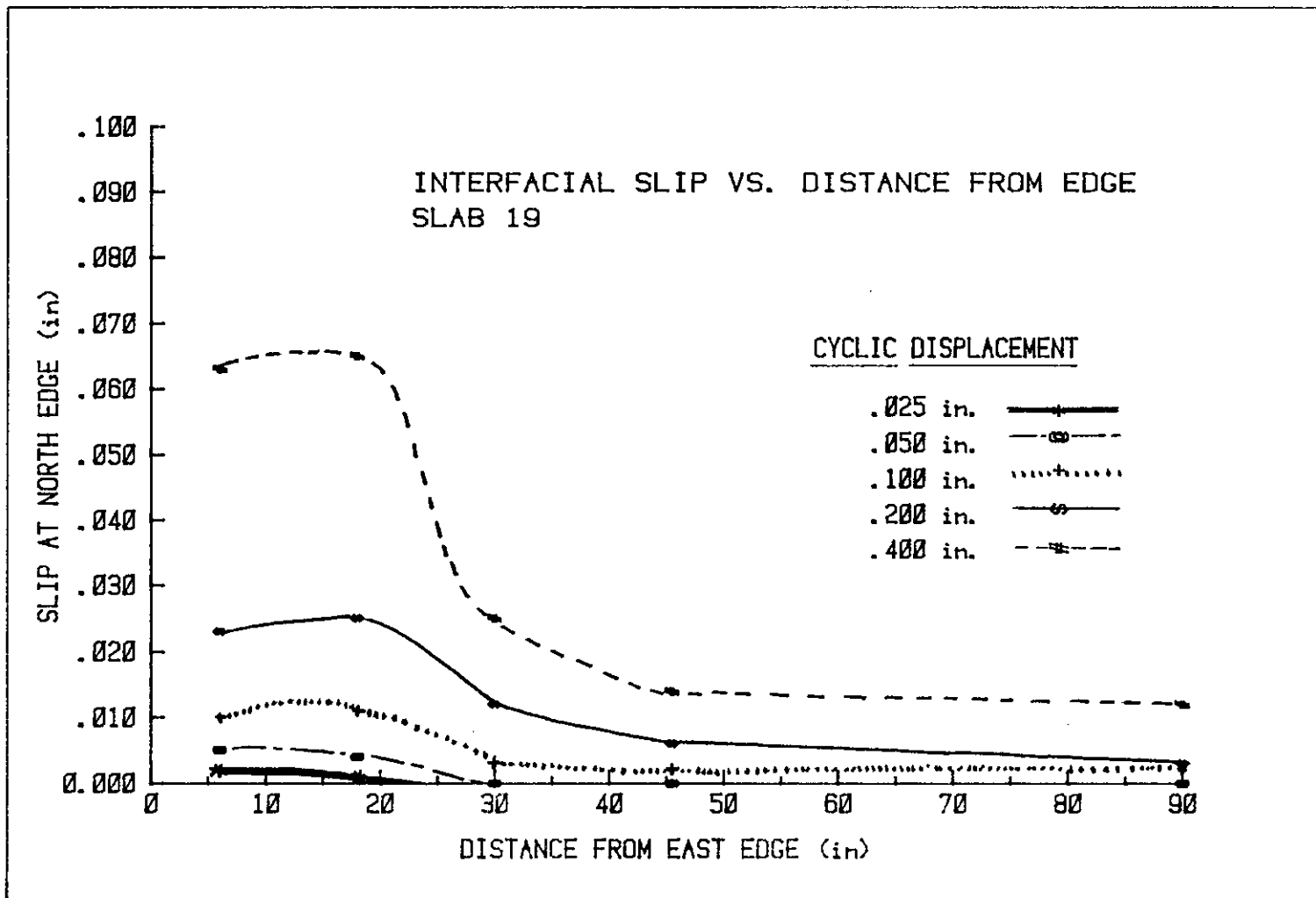


Figure 18. Interfacial slip parallel to the corrugations (Slab 19)

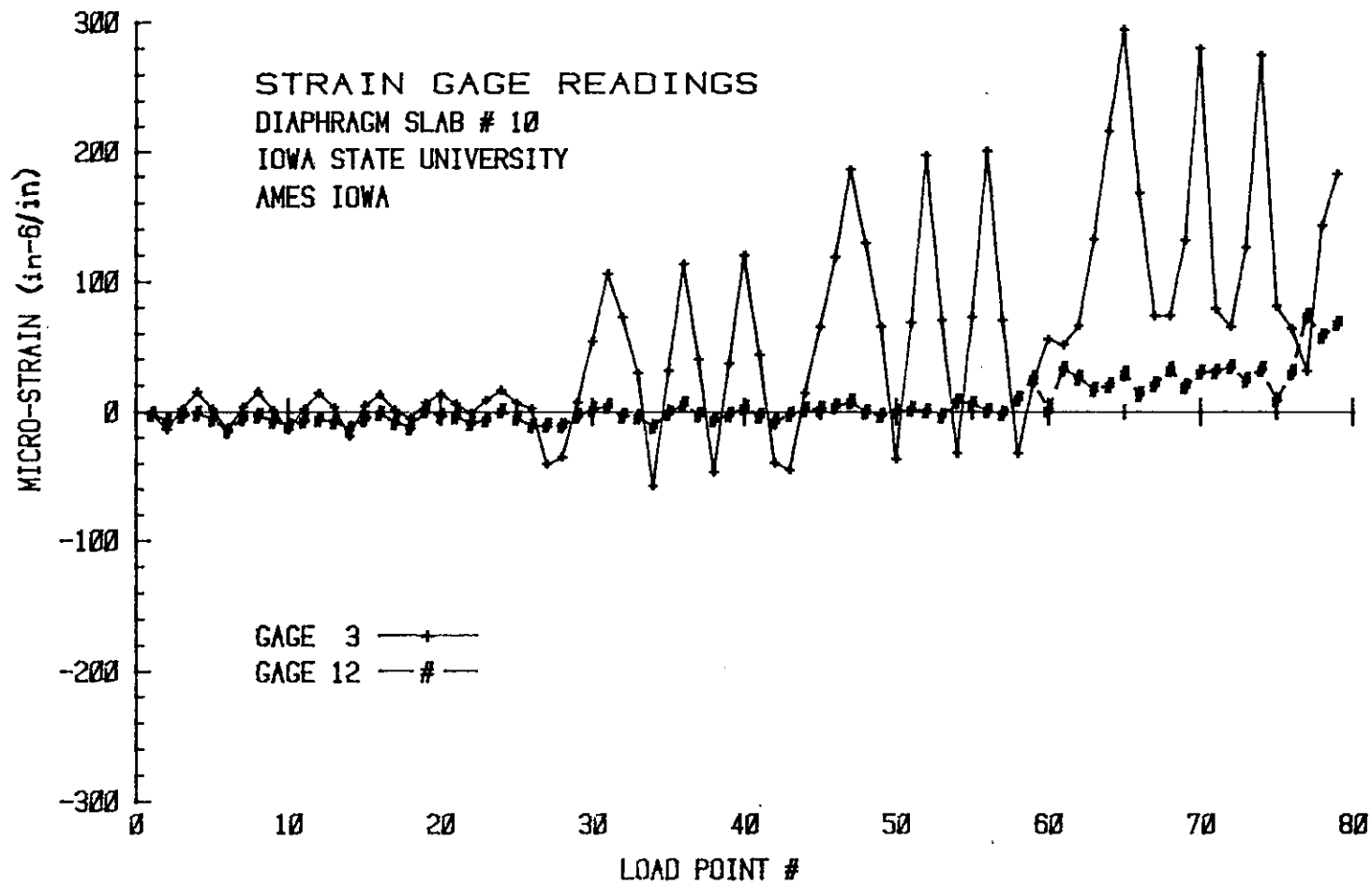
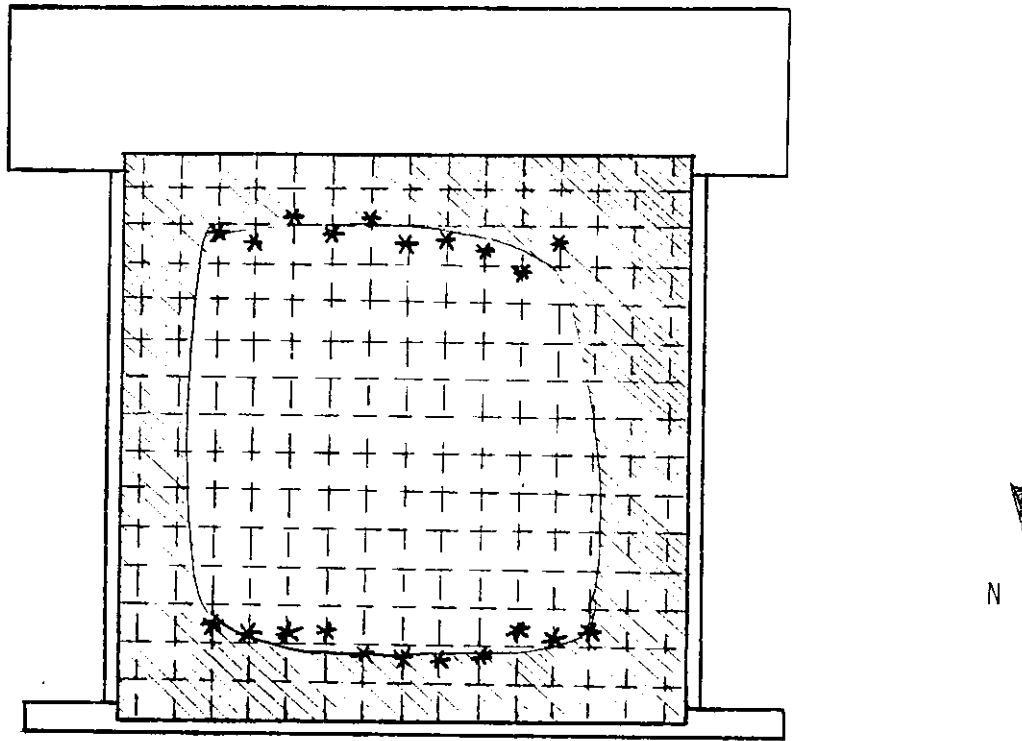


Figure 19. Typical steel deck strains (Slab 10)



- * "dip-stick" measurement location
- ▨ measurably separated area

Figure 20. Dip-stick measurement results

on Slab 19 at Load Point 94 (a 1.0 in. displacement). The shaded portion is an approximation of the amount of area over which the concrete and the deck were measurably separated. A 1 ft. x 1 ft. grid has been laid out on the diagram to help show distances.

3.1.6. Summary of testing parameters and results

A summary of testing parameters for Slabs 10 to 20 is shown in Table 6. All slabs tested to date were 15 ft. x 15 ft. Deck types, concrete thicknesses, concrete strengths, and superimposed vertical loads were varied as presented in Table 6.

The ultimate load, initial stiffness, and ultimate failure mode of each slab are shown in Table 7. The ultimate load shown was the maximum between load points as read by the data acquisition system, which continuously monitored the load between load points at the rate of 0.8 seconds per reading. The initial stiffness was determined as the load divided by the actual displacement to a nominal 0.025 in. displacement.

3.2. Cantilever Elemental Test

The cantilever elemental diaphragm test was designed to closely approximate the force transfer which takes place at the edge of a full-scale diaphragm. Each cantilever slab was 36 in. x 36 in. and tested as an in-plane cantilever beam (see Figure 21). The free end of the specimen modeled the framing beam on the edge of a slab; the fixed end modeled the slab interior.

Table 6. Summary of parameters for slab specimens (Slabs 10-20)

Slab number	Concrete parameters			Steel deck parameters			Connections per side	
	Nominal thickness (in.)	Actual thickness ^a (in.)	f'_c (psi)	Deck type ^b	Thickness	Yield strength (ksi)		Ultimate strength (ksi)
10	5 1/2	5.53	3311	5	.062	40.4	53.4	60 welds
11	5 1/2	5.72	3533	6	.047	89.7	93.6	60 welds
12	5 1/2	5.59	3412	5	.062	40.4	53.4	60 welds
13	5 1/2	5.53	6187	4 (pan)	.058 .057	51.8 52.4	63.2 64.9	60 welds
14	8	8.20	3699	5	.062	40.4	53.4	60 welds
15	4	4.21	2844	7	.047	89.7	93.6	60 welds
16	4	4.18	2952	7	.047	89.7	93.6	60 welds
17	7 1/2	7.44	4261	2	.062	46.0	54.4	60 welds
18	5 1/2	5.55	3052	5	.062	40.4	53.4	60 welds
19	5 1/2	5.75	2681	8	.062	49.4	55.5	60 welds
20	5 1/2	5.55	3973	9	.034	48.6	56.2	40 welds

^aOut-to-out thickness.

^bSee Section 3.1.4.

Table 7. Summary of experimental results (Slabs 10-20)

Slab number	Superimposed vertical load (psf)	Initial stiffness (KIPS/in.)	V_u (KIPS)	Failure mode
10	0	1700	161	diagonal tension
11	0	1600	95	shear transfer mechanism-parallel
12	65	1800	180	diagonal tension
13	200	1900	250	diagonal tension
14	135	1900	208	shear transfer mechanism-transverse
15	0	1300	103	shear transfer mechanism-transverse
16	35	1300	124	diagonal tension
17	100	2200	146	shear transfer mechanism-parallel
18	135	1700	161	diagonal tension
19	0	1300	147	diagonal tension
20	0	1300	95	shear transfer mechanism-transverse

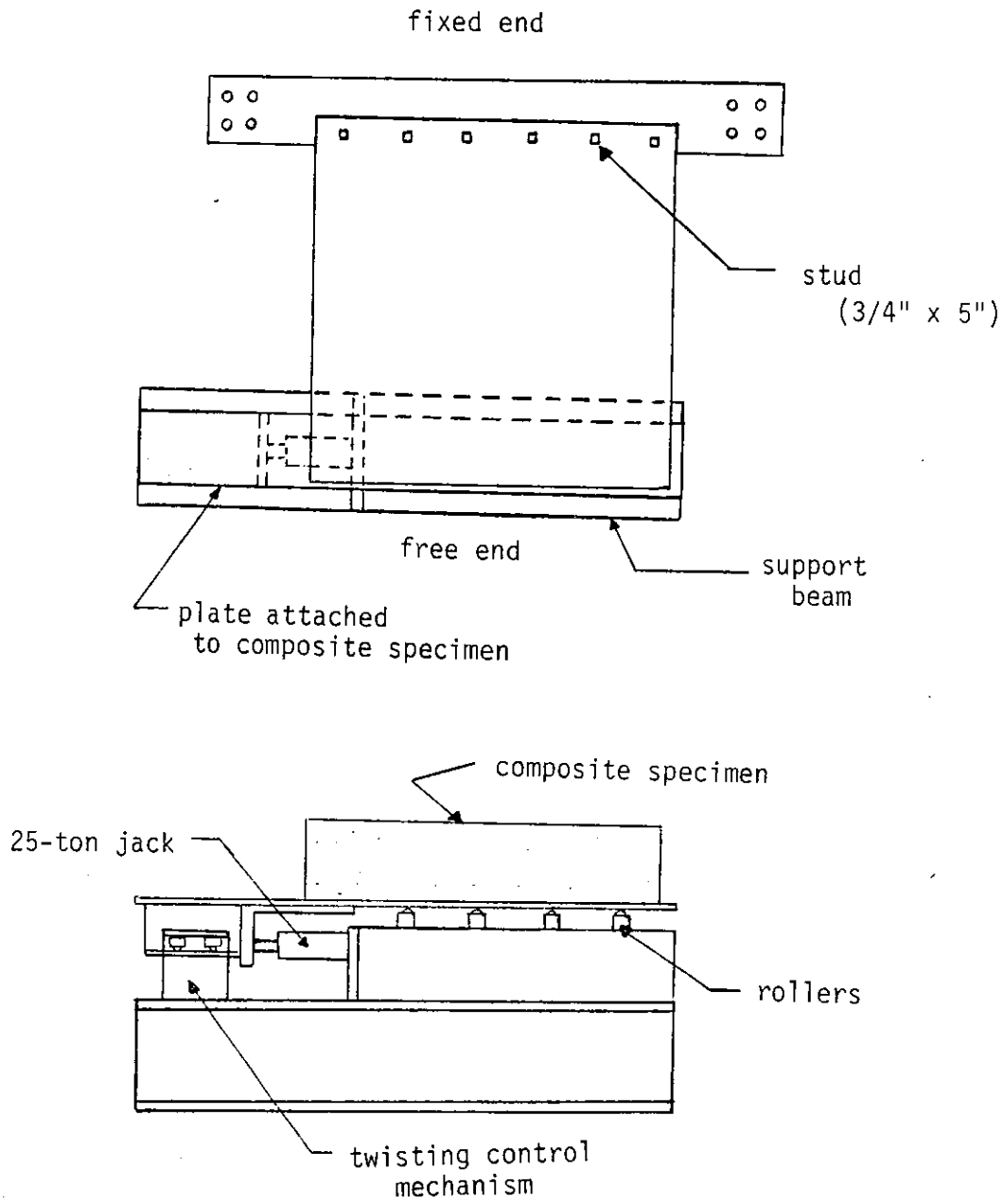


Figure 21. Schematic view of cantilever elemental test

The cantilever elemental diaphragm test was useful for observing flexural failure of composite slabs subjected to in-plane loads. The most important observation was the negligible strength of open geometry steel deck as tensile reinforcement in a direction transverse to the corrugations. Each of the specimens oriented in this direction failed in flexure, with a cracking of the concrete and deck deformation at the first up corrugation near the fixed end. The failure load was approximately that of an unreinforced concrete section. This failure mode shows the importance of the diaphragm slab being connected to the framing members along all four edges, so that the framing beams will carry the majority of the flexural load in the diaphragm slab system.

Although interesting behavioral characteristics of composite slabs were obtained, the cantilever model was abandoned as an elemental diaphragm test for two reasons:

- 1) Flexural failure and flexural stresses seemed to dominate in each specimen. However, in the full-scale diaphragm segment being modeled, shear transfer forces were the most critical. For this reason, an elemental test from which shear transfer properties could be obtained was necessary.

- 2) A completely "fixed" tie down, which is necessary as part of the testing apparatus, is difficult to construct in the lab.

3.3. Elemental Friction Test

3.3.1. Test set-up

The elemental friction test was designed to determine basic properties of the steel deck concrete interface, and its capacity for transferring shear force. The elemental friction test, which involved a forced interfacial failure, was similar in concept to the previously described vertical push-out test. Each specimen was approximately 1 ft. x 1 ft. x 1 ft. in size, with a 1 ft. square section of steel deck on two opposite faces. Each steel deck section was welded to a 12 in. x 6 in. x 0.5 in. steel plate before placing of the concrete. Figure 22 shows a schematic view of the testing apparatus. The vertical downward force on the concrete was provided by the 400 KIP Satec Testing Machine in the lab. The specimen was supported in the testing apparatus by the steel plates which were attached to the steel deck. A lateral force was provided by a system of four springs which had been previously calibrated. The springs were calibrated and the desired lateral force achieved by turning each nut a certain number of revolutions from a specified initial position, and thereby tensioning the springs to the desired force. Rather flexible springs were used so that a small lateral displacement (such as that due to overriding the embossments) would not significantly affect the applied lateral load. The spring system was capable of applying a load of up to 300 psf. It was hoped that by varying the lateral load, an effective coefficient of friction for the deck-concrete interface could be determined. At each load point, the load, two lateral displacements,

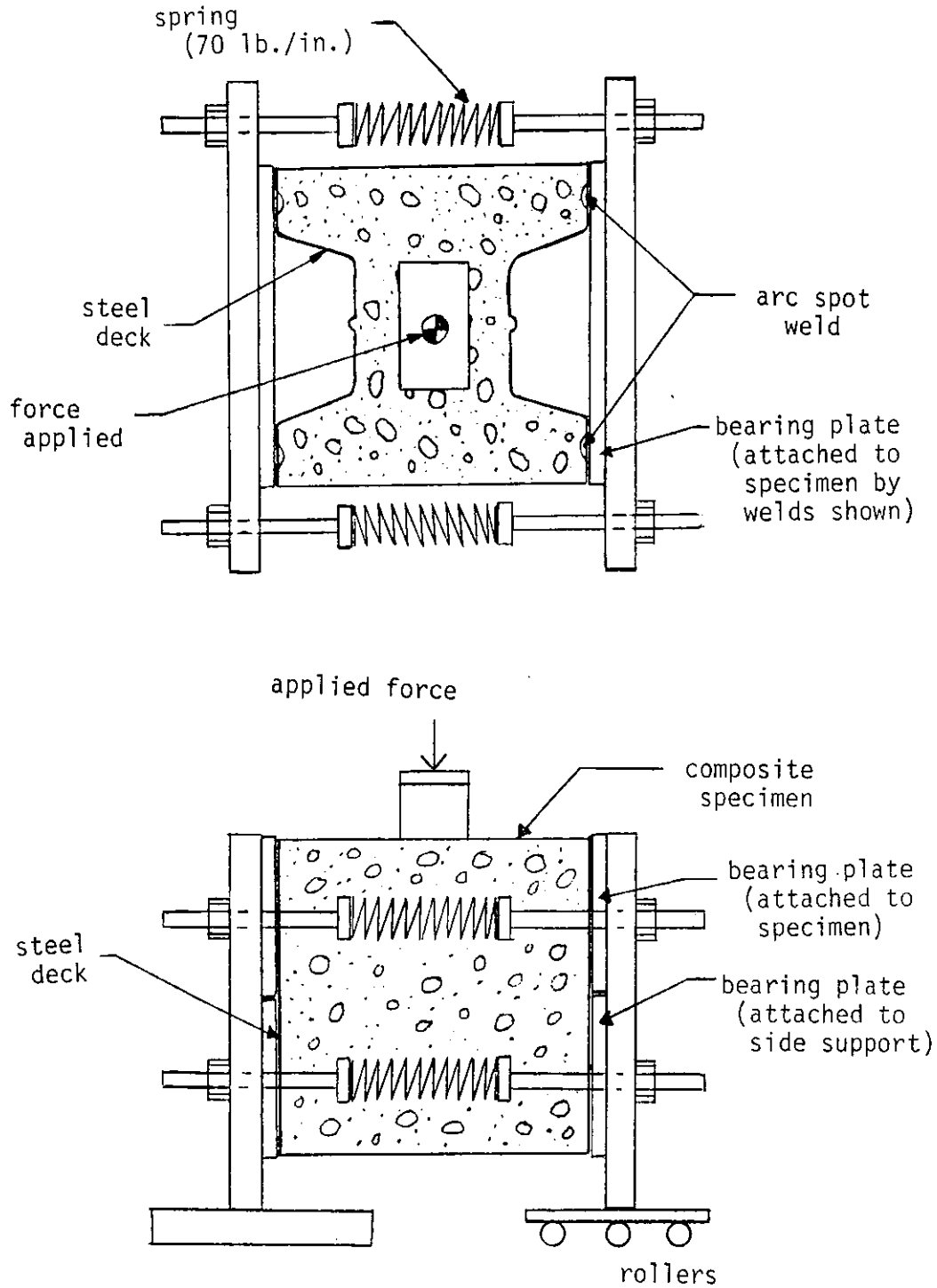


Figure 22. Schematic view of elemental friction test

and two vertical displacements were recorded. The maximum load between load points was also determined.

3.3.2. Experimental results

A total of eight elemental friction tests were performed, four with Deck Type 7 (EFT 1-1 to 1-4), and four with Deck Type 5 (EFT 2-1 to 2-4). In all eight tests, the primary force was applied parallel to the corrugations. Table 8 shows a summary of testing parameters and results. The lateral load shown was that applied at the beginning of the test, in no case did the lateral load increase by more than 5 psf prior to ultimate. The stiffness and ultimate load are given in a per square inch of projected deck area ($2 \times 144 = 288$ sq. in.) basis. The stiffness was found by doing a linear regression through the load points up to maximum load; the first few load points were not included in this analysis because some initial settlement was occurring in the test apparatus. The correlation coefficient for each stiffness linear regression was 0.99 or higher.

Each specimen failed by interfacial shear along one of its two interfaces. Failure seemed to occur as soon as the chemical bond was broken. No additional strength existed because the frictional and mechanical interference components of interfacial strength were not completely effective (due to the method of load application). Testing after this loss of initial adhesion became meaningless, as the specimen simply started to twist within the testing apparatus.

Examination of test results showed that similar tests did not always yield as consistent of results as might be desired. This was

Table 8. Testing parameters and results of elemental friction tests

Test number	Deck type	f_c' (psi)	Lateral load (psf)	K (lbs./in. ² /in.)	Maximum load (lbs./in. ²)
F-1-1	7	4019	159	1126	26
F-1-2	7	4019	285	1219	27
F-1-3 ^a	7	4261	159	468	17
F-1-4	7	4261	285	1392	29
F-2-1	5	4202	184	2132	50
F-2-2	5	4202	184	1771	59
F-2-3	5	4202	295	1568	52
F-2-4	5	4202	295	829	42

^aConcrete not properly compacted, some honeycombing.

thought to be due to the fact that chemical adhesion (which was important in this test) is such a widely varying property.

Also note that varying the lateral force, at least within the range tested, did not appreciably affect results.

The elemental friction test did not appropriately model the behavior of the full-scale slab, because the interface on the full-scale slab will carry a greater load after loss of initial adhesion. This is true because of deck profile warpage against the concrete, which causes an increasing amount of friction and mechanical interference between the steel deck and concrete. Deck profile warpage does not occur (due to the method of loading) on the elemental friction test.

3.4. Elemental Shear Test

3.4.1. Test set-up

The elemental shear test was designed to determine the basic in-plane shear properties of the deck-concrete interface. The basis for this test was ASTM Standard E519-81 [25], which is the standard test for the shear strength of masonry assemblages. The difference between the elemental shear test and the masonry shear test was that on the elemental shear test, interfacial shear failure would occur rather than diagonal tension failure, unless the interface was extraordinarily strong.

A schematic view of the elemental shear test is shown on Figure 23. Each specimen was constructed by welding a 2.0 ft. x 2.0 ft. section of steel deck to a 6 in. steel tube, with one diagonal of

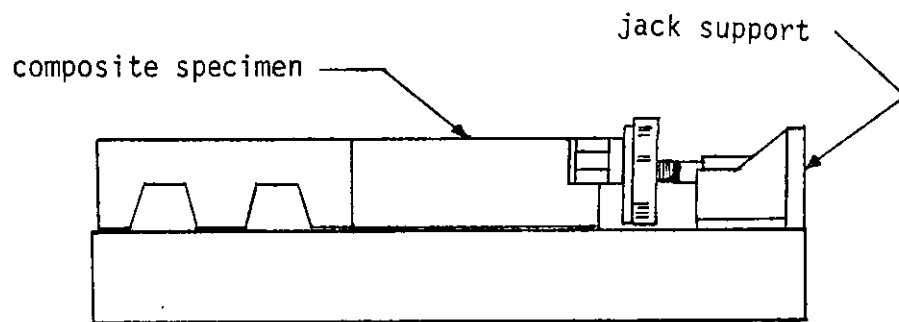
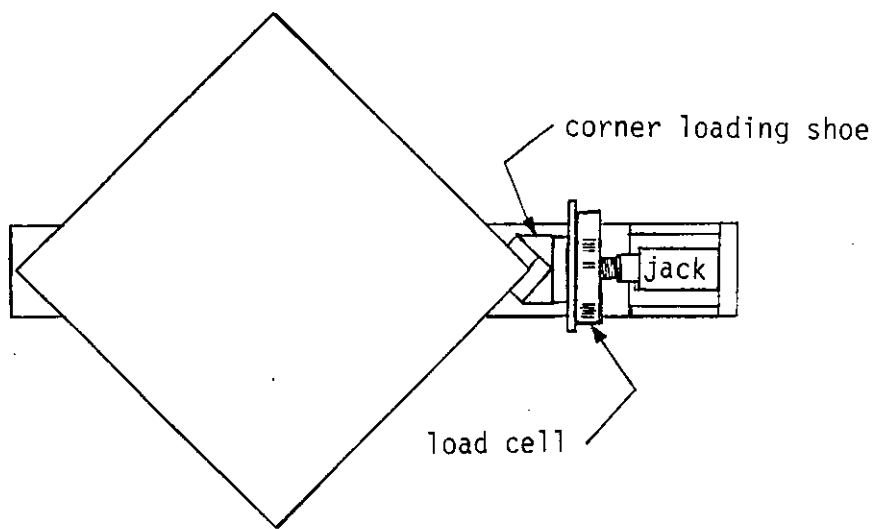


Figure 23. Schematic view of elemental shear test

the deck aligned along the tube's length. A 6 in. concrete slab was cast on each specimen. After curing of the concrete, a 25-ton hydraulic jack was attached to the tube, and a load applied on the corner of the concrete slab using a corner shoe. Each leg of the corner loading shoe was 2 in. long and 3 in. deep. The center of the jack was located 3.75 in. above the surface of the tube. Loads were measured using a load cell. Displacements recorded at each load point included slip parallel to the corrugations at two locations, slip transverse to the corrugations at two locations, and the vertical displacement of the deck at each of the corners.

3.4.2. Experimental results

Six elemental shear tests were conducted for this project, three with Deck Type 8, two with Deck Type 5, and one with Deck Type 4. Table 9 gives a summary of testing parameters and results. The direction of initial slip (given in Table 9) was the direction in which the first significant slip (greater than 0.001 in.) occurred. The direction of slip at failure was the principal direction of interfacial movement immediately following the ultimate load. Figure 24 shows a typical load-displacement curve for the elemental shear test. These curves (from Test S-1-1) show that the initial slip was transverse to the corrugations, slip at failure both parallel and transverse to the corrugations, and post-ultimate slip primarily parallel to the corrugations.

Table 9. Testing parameters and results of elemental shear tests

Specimen number	Deck type	f'_c (psi)	Connections	Slab depth (in.)	Maximum load (KIPS)	Direction of initial slip ^a	Direction of slip at failure ^a
S-1-1	8	2352	8 welds	6	8.13	T	P and T
S-1-2	4	2352	8 welds	6	10.05	P and T	P and T
S-2-1	5	3504	4 welds	6	5.64	T	T
S-2-2	8	3504	4 welds	6	8.20	T	P and T
S-3-1	5	4240	4 welds	6	6.49	T	T
S-3-2	8	4240	4 welds	6	8.10	T	P and T

^aP = parallel to corrugations; T = transverse to corrugations.

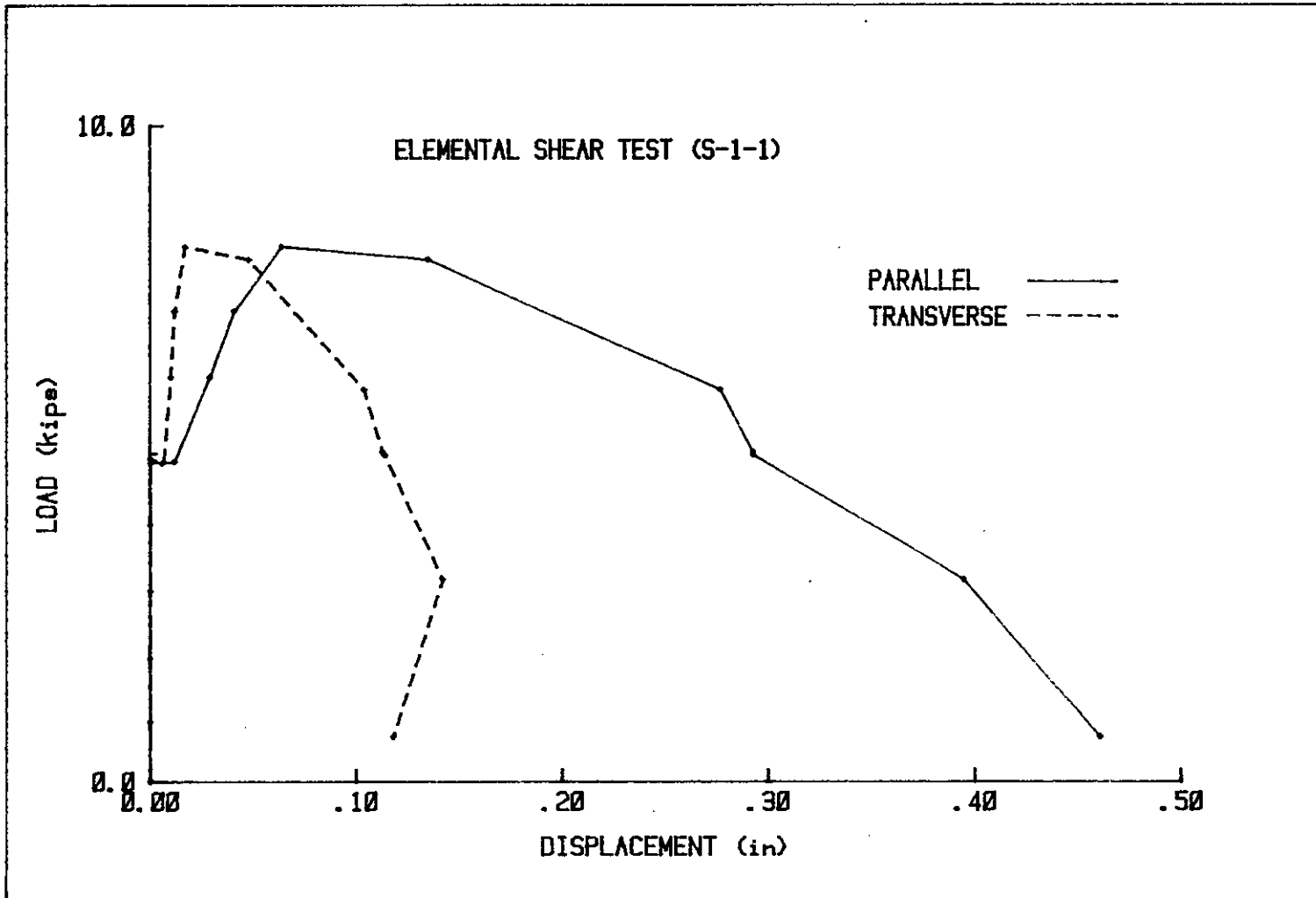


Figure 24. Typical results of elemental shear test

Ultimate capacity was controlled by failure of the shear transfer mechanism for all six tests. The measured failure load for each deck type was fairly consistent. Note the significant difference in strength between Deck Type 5 and Deck Type 8, even though the only major difference between the two was a differing embossment pattern. This result shows that the type of embossments has a significant effect on shear transfer mechanism capacity.

Although the elemental shear test seemed to be a good measure of interfacial strength, it was not readily adaptable to the present analytical technique, and therefore, results are not used in the proposed analysis.

3.5. Elemental Push-off Test

3.5.1. Test set-up

The elemental push-off test was designed to determine properties of the deck-concrete interface, and to determine the capacity of the shear transfer mechanism. It was similar in concept to the second series of push-out tests conducted with the previous diaphragm project.

Each specimen was constructed by welding one edge of a steel deck section to a 6 x 6 x 1/4 in. steel tube, using the same welding pattern and procedure as used for the full-scale slab. The opposite edge of the steel deck was connected to a plate. Steel deck sections were oriented with the corrugations both parallel and transverse to the tube. Some steel deck sections were formed from two separate pieces of deck welded at the seam, to include seam effects. Studs

(3/4 in. diameter by 5 in. tall) were placed on the plated end of each transverse specimen (except P-2-5), to keep the concrete from prematurely popping up rather than overriding the corrugations (see Section 2.3). A small roll (6 in. x 3 in. diameter) of welded wire fabric was placed at the corner of each transverse specimen where the load was to be applied, to prevent a localized bearing failure. Each specimen with corrugations parallel to the tube was shored at the midpoint during placement of the concrete. A concrete cover of 2.5 in. to 7 in. was cast on each specimen.

A schematic diagram of the testing apparatus is shown in Figure 25. For testing, each specimen was set on a frame consisting of a set of rollers and a support beam. The tube was set on the rollers and the plated end of the specimen set on, but not connected to, the support beam, so that the slab was horizontal. A 25-ton hydraulic jack was mounted on one end of the tube, and the load was applied to the concrete, to induce a shear transfer mechanism failure. The center of the jack was located 3 in. in from the edge of the slab, and 3.75 in. above the top of the tube, which was approximately at the vertical centroid of the concrete for most specimens. The location of the load placement was to model the actual diaphragm slab, in which the force is transferred from the edge beams, through the welds, to the centroid of the composite section. The load was measured using a load cell. Loading was by load control, with the typical increment being 1 KIP. Four displacements were recorded at each load point, three measuring relative movement between the concrete and the tube along

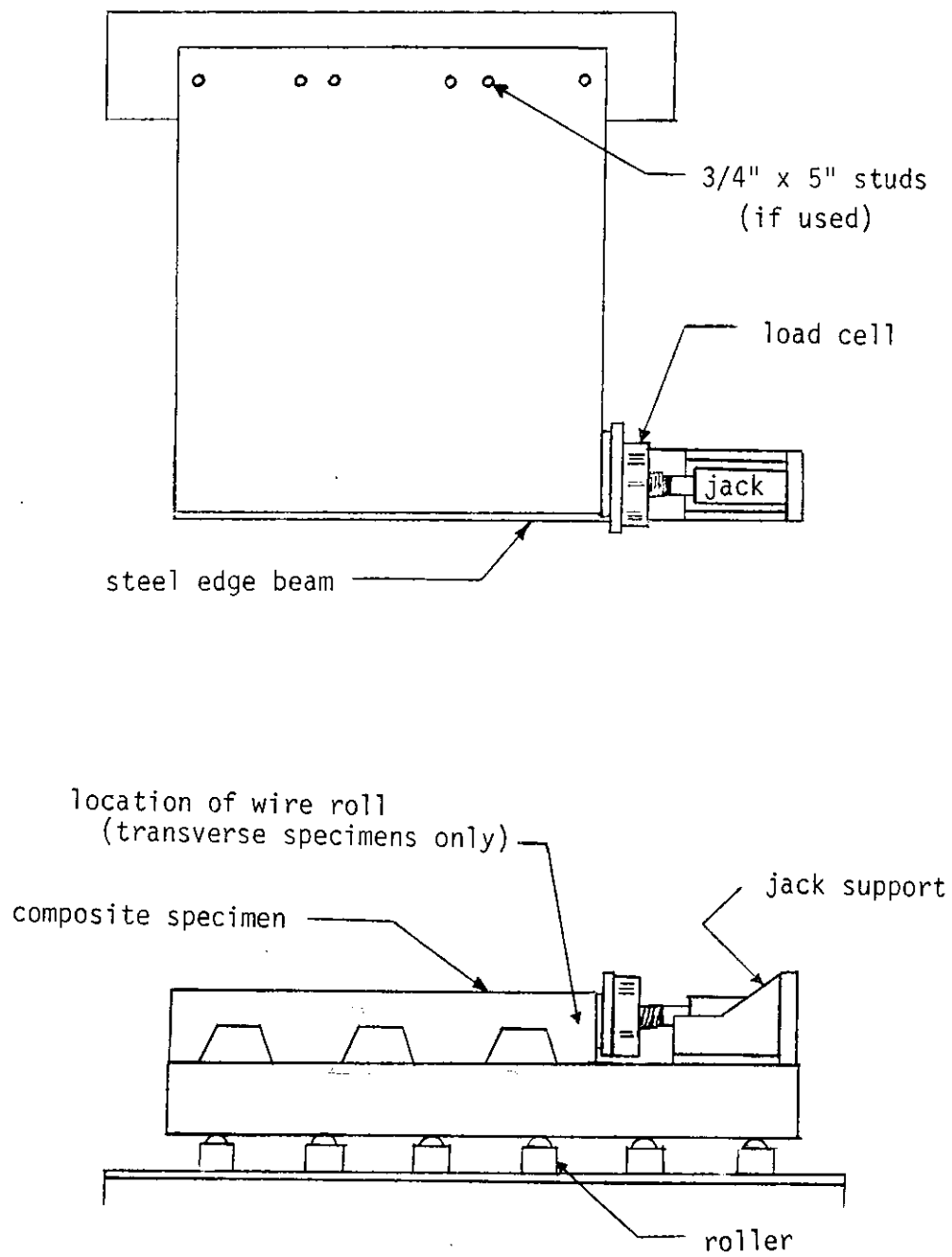


Figure 25. Schematic view of elemental push-off test

the "push" end of the specimen, and one measuring the deck-concrete slip 12 in. in from the edge. For plotting the load-displacement curve, the displacement was taken as the average of the relative movements (between the concrete and the steel tube) at each end of the slab. Strain gages were placed on the bottom of the steel deck on several specimens, to determine typical strains in the deck. The superimposed vertical load used on some of the specimens was provided by concrete blocks and steel plates, placed on a bed of sand to assure uniform distribution.

3.5.2. Summary of testing parameters

A total of 55 push-off tests were conducted for this project. Eight different deck types were tested both parallel and transverse to the corrugations. A series was also tested to determine the strength of the arc spot weld connections.

In addition to determining basic values for each deck type, parameters such as concrete strength, slab thickness, normal force, and location of seam were varied to determine what effects these variables had on the interfacial properties. Table 10 is a list of testing parameters for the 55 push-off tests. Note that Deck Type 5B is identical to Deck Type 5, except 22 gage rather than 16 gage.

3.5.3. Behavior and failure modes

The list of possible failure modes for each push-off test is identical to that for the full-scale slabs, which was described in Section 2.2. The only major difference from that description is that

P-4-5	4	parallel	36	36	5.5	2530		12 welds	6 studs	
P-4-6	4	transverse	36	36	5.5	2530	X	12 welds	6 studs	
P-4-7	5	parallel	36	36	7	2530		2 welds	12 welds	
P-5-1	6	parallel	36	36	7	2580	X	12 welds	12 welds	
P-5-2	6	parallel	36	36	7	2580	X	12 welds	12 welds	
P-5-3	6	transverse	36	36	6	2580	X	12 welds	6 studs	
P-5-4	6	transverse	36	36	6	2580	X	12 welds	6 studs	
P-5-5	6	parallel	36	36	7	2580	X	12 welds	12 welds	122
P-5-6	6	transverse	36	36	6	2580	X	12 welds	6 studs	122
P-5-7	6	parallel	36	36	7	2580	X	12 welds	6 studs	
P-6-1	7	parallel	36	31	7	4019		12 welds	6 studs	
P-6-2	7	parallel	36	31	4	4019		12 welds	12 welds	37
P-6-3	7	parallel	18	31	7	4019		6 welds	6 welds	
P-6-4	7	parallel	36	31	7	4019		12 welds	12 welds	
P-6-5	7	transverse	36	30	7	4019	X	12 welds	6 studs	
P-6-6	7	transverse	36	30	4	4019	X	12 welds	6 studs	37
P-6-7	7	transverse	36	18	7	4019	X	8 welds	6 studs	
P-7-1	2	parallel	36	30	7	2694		12 welds	12 welds	

P-9-1	8	parallel	36	36	7	3743	X	12 welds	12 welds	
P-9-2	8	parallel	36	36	7	2743	X	12 welds	12 welds	
P-9-3	8	transverse	36	36	6	3504	X	12 welds	6 studs	
P-9-4	8	transverse	72	24	6	3504		8 welds	4 studs	
P-9-5	8	transverse	72	24	6	3504		8 welds	4 studs	200
P-9-6	9	parallel	36	36	7	3743	X	9 welds	9 welds	
P-9-7	9	transverse	36	34	7	3743	X	10 welds	6 studs	
P-10-1	5	parallel	36	36	7	4240		2 welds	12 welds	
P-10-2	5	transverse	36	36	7	4240		4 welds	6 studs	
P-10-3	5B	parallel	36	36	7	4240		2 welds	12 welds	

diagonal tension was likely to occur simultaneously with failure of the shear transfer mechanism, due to the method of loading. A partial list of test results is given in Table 11. The values chosen for tabulation (ultimate load, failure mode, area under the load-displacement curve at 0.003 in. displacement, area under the load displacement curve at ultimate load, and the average relative displacement at ultimate load) are utilized in the proposed analysis presented in Chapter 4. All values are presented in a per inch of specimen length basis. For each deck type, an average visible post-test separation distance is reported. This distance was the average distance from the push end of the specimen, at which any relative movement between the concrete and steel deck could be visibly detected. This measurement was only possible on the parallel specimens, because on the transverse specimens, the outside lip of the deck would pull away from the concrete (along the entire width) early in the test.

The following is a short description of behavior and test results, categorized by deck type.

3.5.3.1. Deck Type 5 Nine tests parallel to the corrugations, and eight tests transverse to the corrugations were conducted on Deck Type 5. Load-displacement curves for all tests used in calculations are shown in Figures 26 (parallel) and 27 (transverse). Note the reasonable consistency in the shape of each set of curves, but some variability in the ultimate load, especially for the parallel specimens. Also note the obvious difference in behavior between the

P-4-5	473	3.9	.010	1.03	2.a.2/2.a.1/1.a.1
P-4-6	546	29.0	.057	0.98	2.b.2/2.b.1/1.a.1
P-4-7	456	32.5	.085	0.43	3.a.2
P-5-1	286	3.9	.014	0.77	2.a.1
P-5-2	310	2.6	.010	0.70	2.a.1
P-5-3	515	43.0	.091	1.05	2.b.1
P-5-4	509	71.6	.165	0.94	2.b.1
P-5-5	412	4.7	.014	0.74	2.a.1
P-5-6	539	67.2	.138	0.79	2.b.1/1.a.1
P-5-7	282	3.9	.018	0.48	2.a.1
P-6-1	497	18.0	.045	0.65	2.a.1
P-6-2	413	7.1	.021	0.85	2.a.1/1.a.1
P-6-3	585	23.4	.049	1.13	2.a.1
P-6-4	608	38.0	.085	0.87	2.a.1
P-6-5	561	58.0	.135	0.85	2.b.3
P-6-6	558	43.9	.109	0.73	2.b.3/1.a.1
P-6-7	474	92.9	.246	0.69	2.b.3
P-7-1	489	15.4	.041	0.57	2.a.1

P-9-2	543	60.9	.149	0.60	2.a.1
P-9-3	560	106	.212	0.66	localized
P-9-4	624	33.2	.082	0.59	2.b.1/1.a.1
P-9-5	786	109	.163	0.67	2.b.1
P-9-6	404	27.8	.090	0.50	2.a.1
P-9-7	437	69.0	.169	0.78	2.b.1
P-10-1	505	42.2	.098	0.69	3.a.2
P-10-2	574	48.1	.093	0.75	2.b.1
P-10-3	211	8.7	.048	0.48	2.a.1

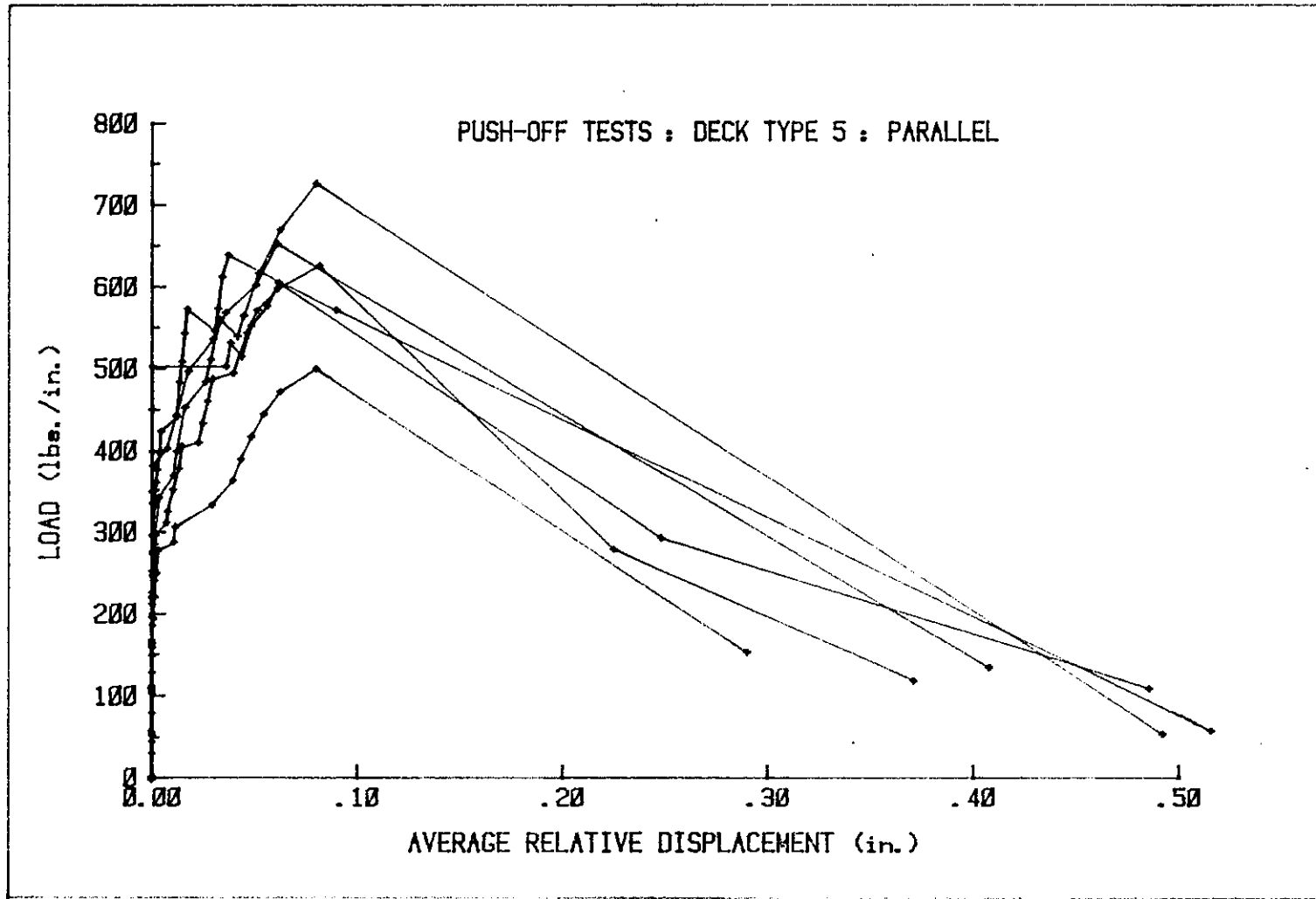


Figure 26. Push-off test results for Deck Type 5 (parallel to corrugations)

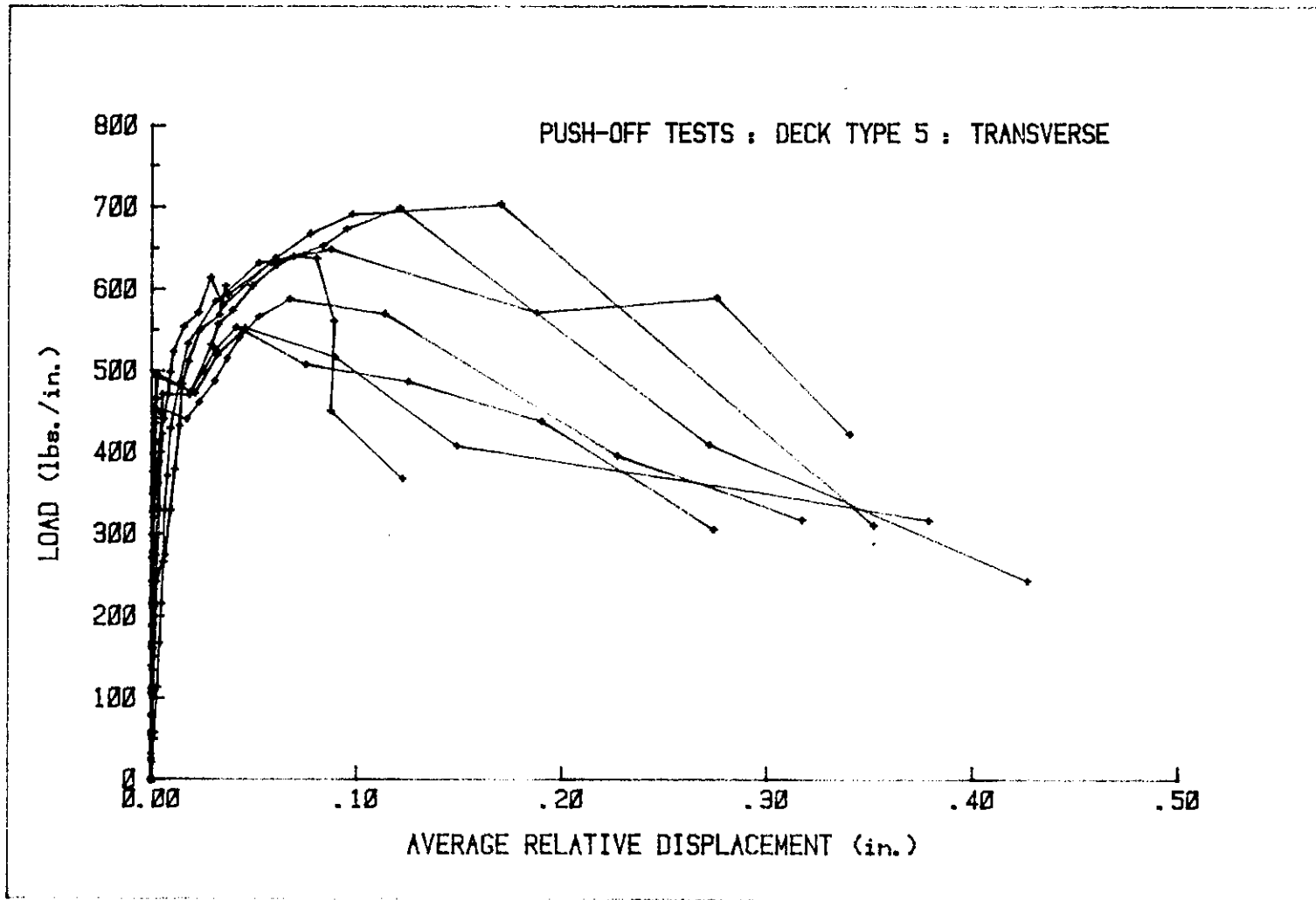


Figure 27. Push-off test results for Deck Type 5 (transverse to corrugations)

parallel and transverse specimens. Observed behavior, including interfacial slip, cell deformation, and diagonal cracks on the edges at the seams (see Figure 28a), seemed to match that occurring in the full-scale slabs. Failure of the shear transfer mechanism was by interfacial slip both parallel and transverse to the corrugations. Figure 28b shows a typical interfacial slip parallel failure for the push-off test.

Deck Type 5 was also used for several parametric comparisons. Comparison of Tests P-2-3, P-3-1, and P-4-1 and Tests P-2-2, P-3-2, and P-8-4 showed that interfacial slip strength was not highly dependent on the concrete strength (f_c'). Comparisons of Tests P-8-1 and P-8-2 and Tests P-8-4 and P-8-5 showed the effect of a superimposed vertical load of 122 psf. The superimposed vertical load caused a 15 percent increase in strength in the parallel direction, and a 7 percent decrease in transverse direction. Considering the variability, any change of less than 10 percent is probably not statistically significant. The vertical load did not seem to affect the stiffness in either direction.

Specimen P-8-3 was identical to P-8-1, except that the steel deck had been coated with oil (Mobil DTE-26) prior to placing of the concrete. The purpose of the oil was to eliminate chemical bonding. Post-test examination showed that the oil had been only partially effective in eliminating the chemical bond. Comparison of test results showed that the oiled specimen had a much lower initial stiffness, but the ultimate load was not affected.

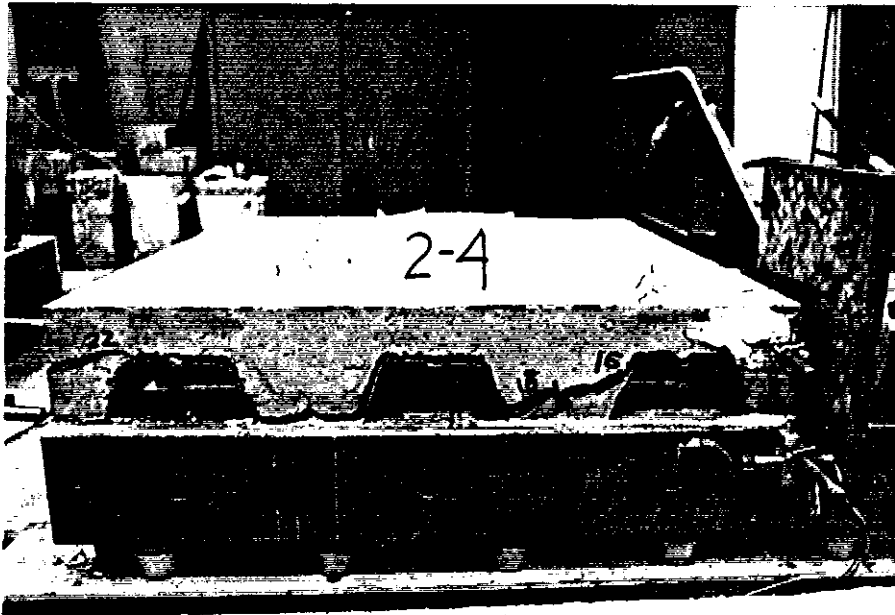


Figure 28a. Transverse interfacial slip for Deck Type 5

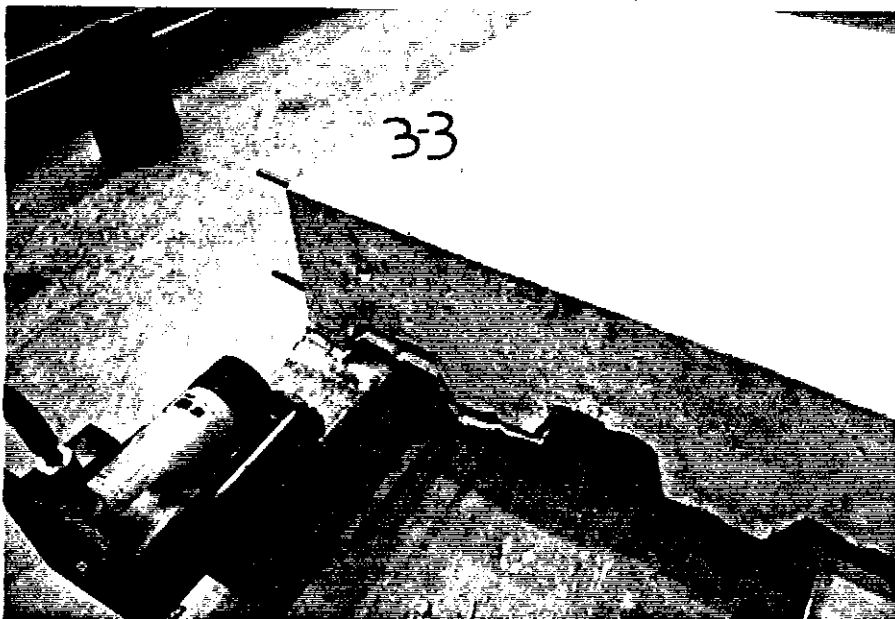


Figure 28b. Parallel interfacial slip for Deck Type 5

Strain readings on the steel deck, taken on Specimen P-8-4, were indicative of push-off test behavior, and are included as Figure 29. Both gages were located on the bottom of a down corrugation, and oriented parallel to the direction of the applied force. Gage 1 was 11 in. from the push end of the specimen; Gage 2 was 23 in. from the push end of the specimen. Microstrain readings are plotted against the average relative displacement at the push edge, to show that the distance over which the shear transfer was taking place increased as the relative displacement at the edge, and the corresponding applied load was increased. Post-test examination showed a visible separation between the concrete and the deck which averaged 23 in. in from the push edge.

All specimens except P-2-1 and P-8-3 were used for obtaining initial stiffness values. All specimens except P-2-1, P-8-2, P-8-3, and P-4-2 were used for obtaining ultimate load values. Specimen P-2-1 was not included because it had been cracked prior to testing. Specimen P-8-3 was not included because of the oiled deck. Specimen P-8-2 was not included because of the superimposed vertical load effect. Specimen P-4-2 was not included because of localized bearing failure at the point of load application.

3.5.3.2. Deck Type 5B Two specimens with Deck Type 5B (one parallel and one transverse) were tested, to determine what effects changing only the steel deck thickness would have on behavior as compared to Deck Type 5. Results showed (see Table 11) that the thinner deck had a much lower interfacial strength. Also, the post-test

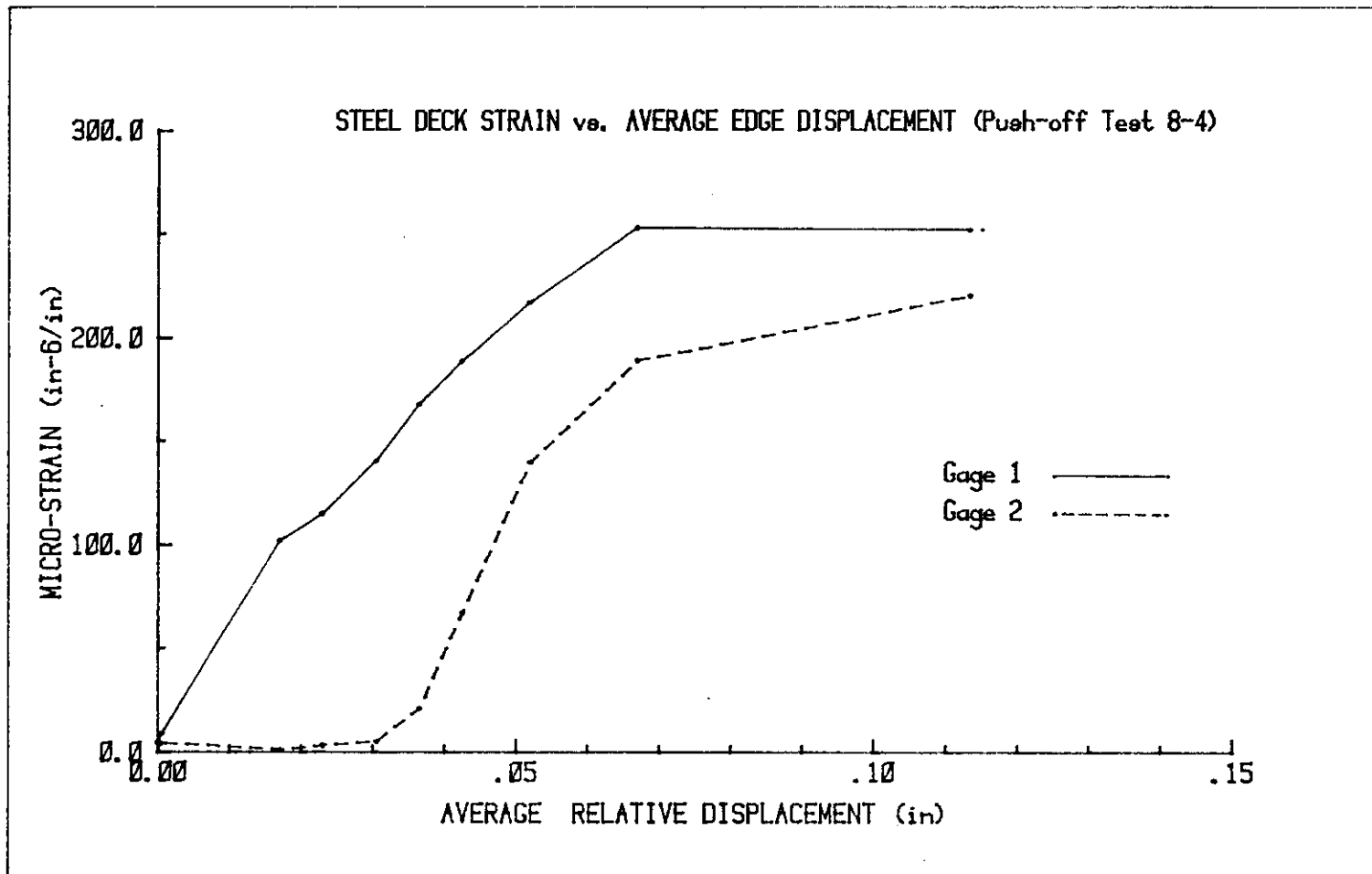


Figure 29. Typical push-off test steel deck strains

visible separation distance between the deck and concrete was 14 in. compared to 23 in. for Deck Type 5. Figure 30a shows the embossment interference which occurred during the testing of the parallel specimen.

3.5.3.3. Deck Type 6 Seven push-off tests were conducted with Deck Type 6 (four parallel and three transverse). Figure 31 shows load-displacement curves for Deck Type 6. Note again the similarity in the shapes of the curves. Failure of the shear transfer mechanism was by interfacial slip both parallel and transverse to the corrugations.

Deck Type 6 tests were also used to observe the effects of a superimposed vertical load, and the location of seam on a parallel specimen. In the transverse direction (compare Specimens P-5-4, P-5-5, and P-5-6), the superimposed vertical load seemed to have little effect, except that surface cracking occurred on the vertically loaded specimen and not on the others. In the parallel direction (compare Specimens P-5-1, P-5-2, and P-5-5), the superimposed vertical load of 122 psf increased the interfacial slip strength by approximately 38 percent. Specimen P-5-7 was constructed similarly to P-5-1 and P-5-2, except the steel deck seam was located 12 in. from the push end rather than 24 in. The ultimate load was not significantly changed; however, post-ultimate behavior included failure of the seam weld on Test P-5-7, and not on the other two tests. The visible separation between the deck and concrete at test completion averaged 21 in. in from the push end.



Figure 30a. Embossment interference for Deck Type 5B

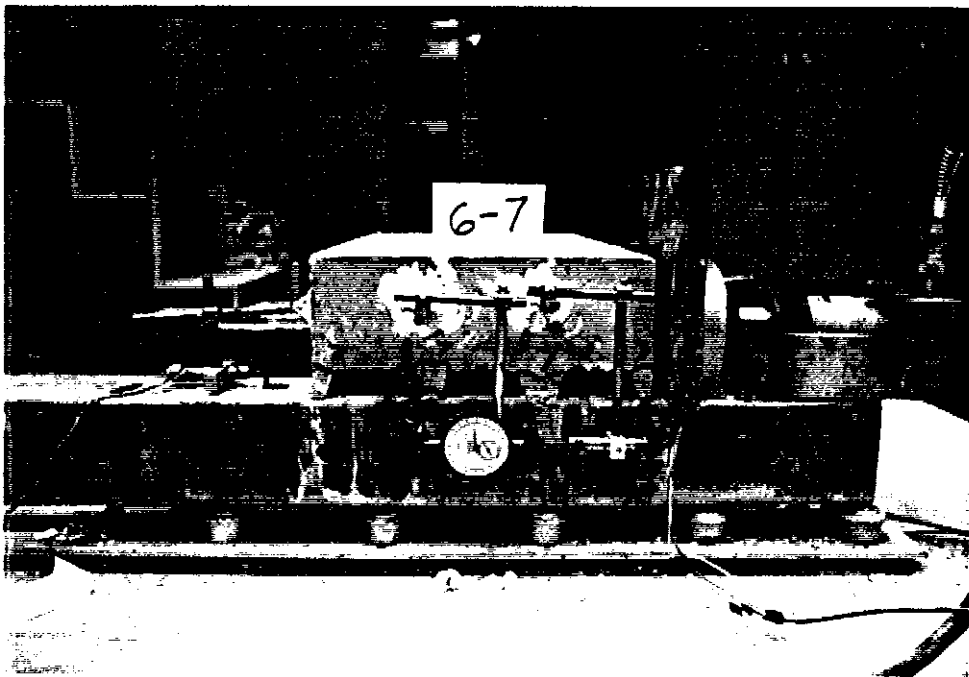


Figure 30b. Corbel failure for Deck Type 7

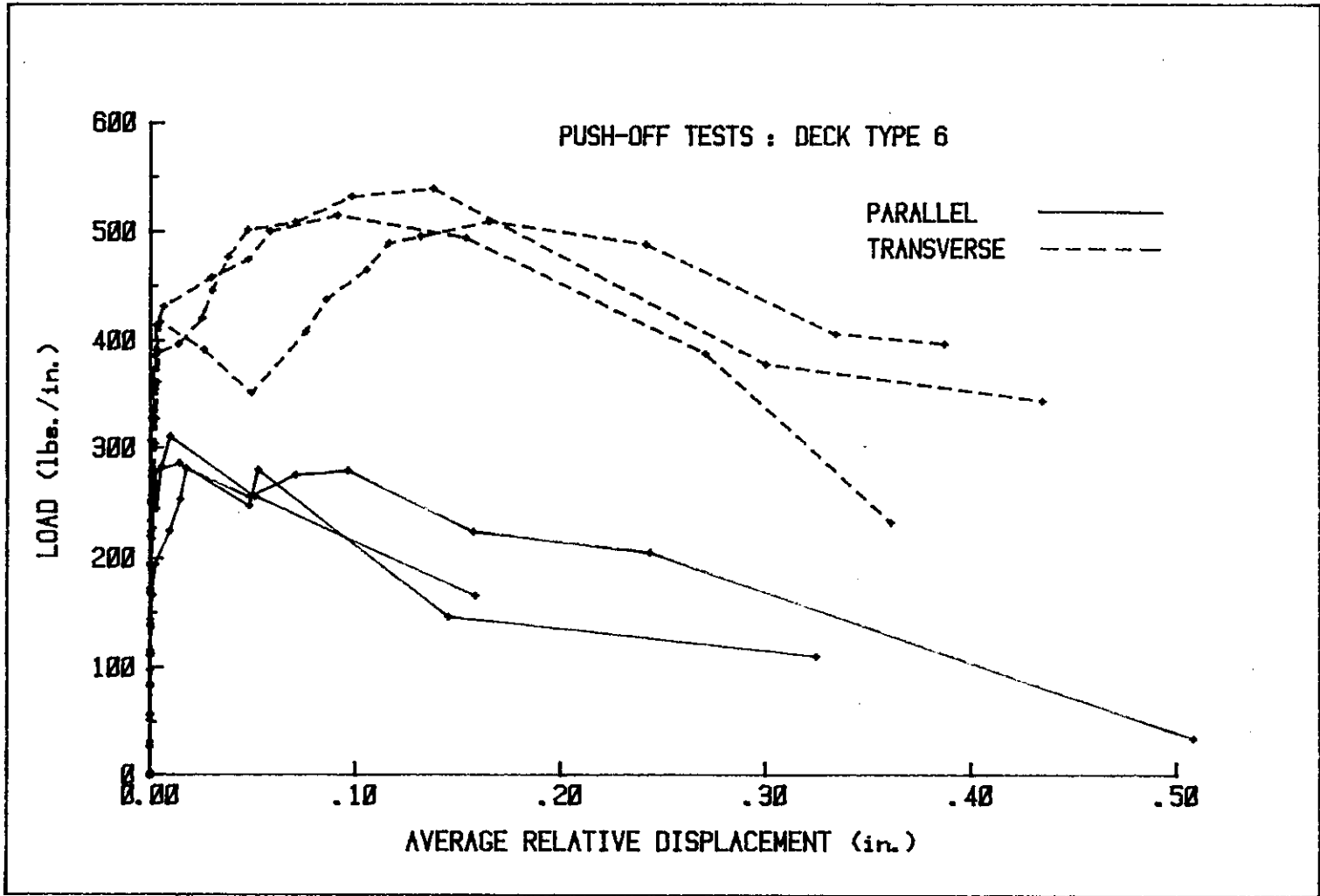


Figure 31. Push-off test results for Deck Type 6

All seven specimens were used for obtaining initial stiffness values. All specimens, except P-5-5, were used for obtaining ultimate load values for Deck Type 6. Specimen P-5-5 was not included because of the effects of the superimposed vertical load.

3.5.3.4. Deck Type 7 Seven push-off specimens were tested to determine the shear transfer mechanism properties of Deck Type 7. Figure 32 shows load-displacement curves for Deck Type 7 push-off tests. Failure of the shear transfer mechanism was by interfacial slip in the parallel direction and corbel failure in the transverse direction (see Figure 30b). The same type of corbel failure was observed on full-scale Slabs 15 and 16.

Deck Type 7 tests were also used to observe the effects of specimen size, and thickness of concrete. Specimens P-6-3 and P-6-4 and Specimens P-6-5 and P-6-7 were similar, except for the length of specimen. No significant difference in behavior was noted in the parallel specimens, however, for the transverse specimens, the shorter specimen had a 15 percent lower ultimate load (on a per length of specimen basis). This difference was thought to be due to the fact that Specimen P-6-5 had four full down corrugations and Specimen P-6-7 had only two full down corrugations, even though the ratio of the specimen lengths (which the ultimate load figure was based upon) was 5:3.

Specimens P-6-2 and P-6-6 were similar to Specimens P-6-4 and P-6-5, except the concrete thickness was 4 in. rather than 7 in. The superimposed vertical load of 37 psf was approximately equal to 3 in. of concrete, so that both sets had the same total weight. In the

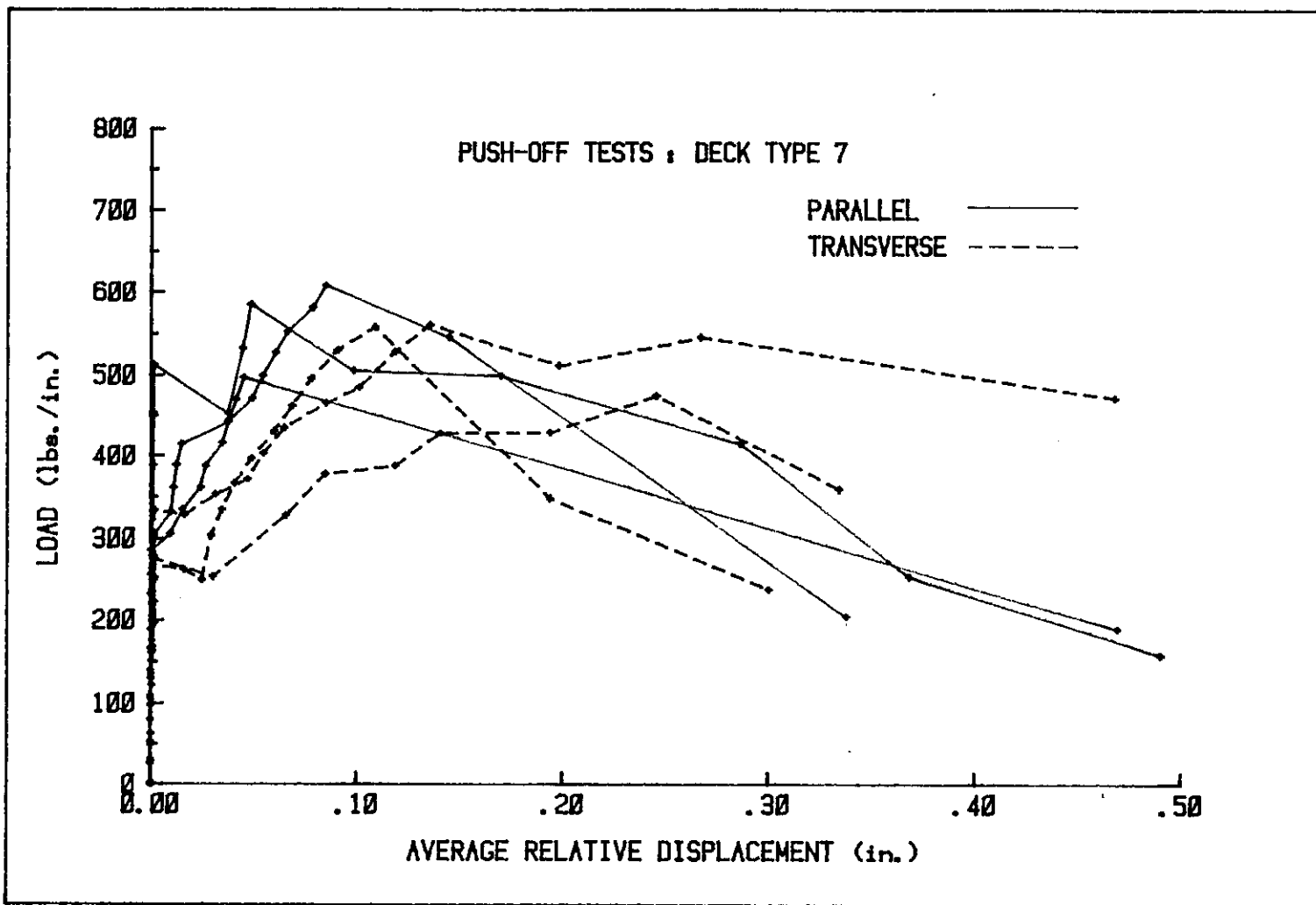


Figure 32. Push-off test results for Deck Type 7

transverse direction, surface cracking occurred only on the thinner specimen, but the strength was unchanged. In the parallel direction, cracking occurred only on the thinner specimen, and the ultimate load was reduced by 32 percent. This comparison shows that if concrete cover on the push-off specimen is too small, diagonal tension failure may occur before the shear transfer mechanism capacity is reached (see related discussion in Section 4.2.1).

Specimens P-6-1 and P-6-4 were similar, except that P-6-1 was line welded on the push end rather than spot welded because of the small lip on this edge of the deck. The same technique was used on one edge of the full-scale slab. Results showed Specimen P-6-1 to have a lower capacity, but more testing would be necessary to confirm this finding. The visible separation distance at test completion for this deck type averaged 19 in.

All seven tests were used for obtaining initial stiffness values. All specimens, except P-6-2, were used for obtaining ultimate load values. Since failure in the transverse direction was by corbel failure, it was assumed that the strength of shear transfer mechanism in this direction was proportional to $\sqrt{f_c}$ (see Section 4.2.2).

3.5.3.5. Deck Type 8 Five push-off tests (two parallel and three transverse) were conducted with Deck Type 8. Figure 33 shows load-displacement curves for this deck type. Note the increase in interfacial stiffness after a large initial slip. This characteristic was thought to be due to the shape of the embossments (see Figure 16). Failure of the shear transfer mechanism was by interfacial slip both

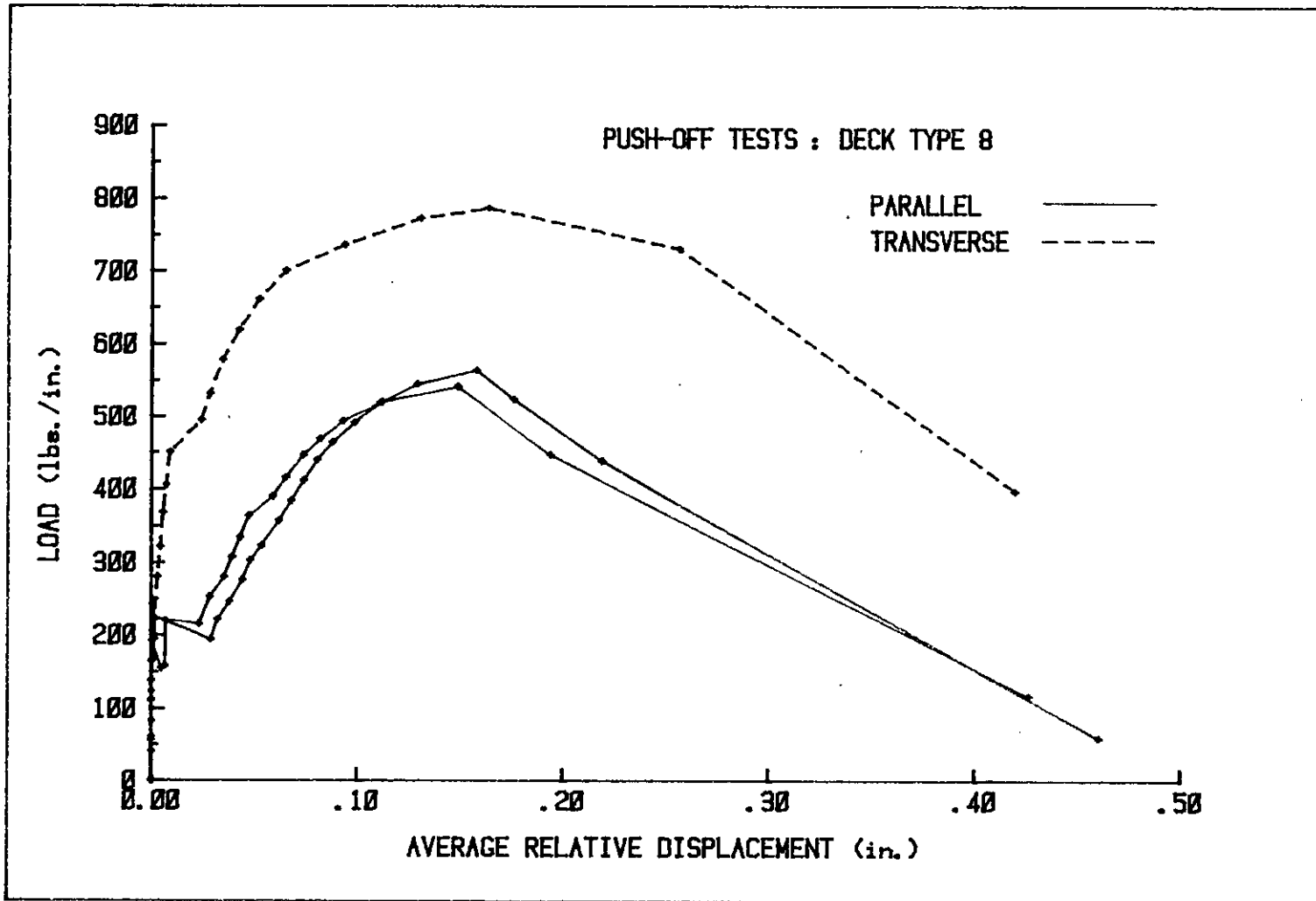


Figure 33. Push-off test results for Deck Type 8

parallel and transverse to the corrugations.

Specimens P-9-4 and P-9-5, which were 6 ft. wide, were used to see whether increasing specimen width would affect behavior. In neither of the specimens did any relative movement between the concrete and the steel deck occur beyond 36 in. from the push end; thus, it was assumed that 36 in. wide push-off specimens were sufficient for determining interfacial behavior, at least for the deck types tested for this project.

Specimen P-9-4 was also given a superimposed vertical load of 200 psf. Note that the failure mode was changed and the ultimate load reduced by 21 percent compared to Specimen P-9-5. This failure (and the resulting reduction in capacity) was thought to be due to a combination of stresses in the concrete within the region where bond between concrete and steel had been broken due to the in-plane loads. This failure mode should be investigated for slabs with a short span distance. Visible separation distance at test completion averaged 23 in.

All specimens, except P-9-4, were used in obtaining initial stiffness values. All specimens, except P-9-4 and P-9-3, were used in obtaining ultimate load values. Specimen P-9-4 was not included because of vertical load effects. Specimen P-9-3 was not included because of localized bearing failure at the point of load application.

3.5.3.6. Deck Type 9 Two elemental push-off tests (one parallel and one transverse) were conducted with Deck Type 9. Figure 34 shows load-displacement curves for Deck Type 9. Failure of the shear

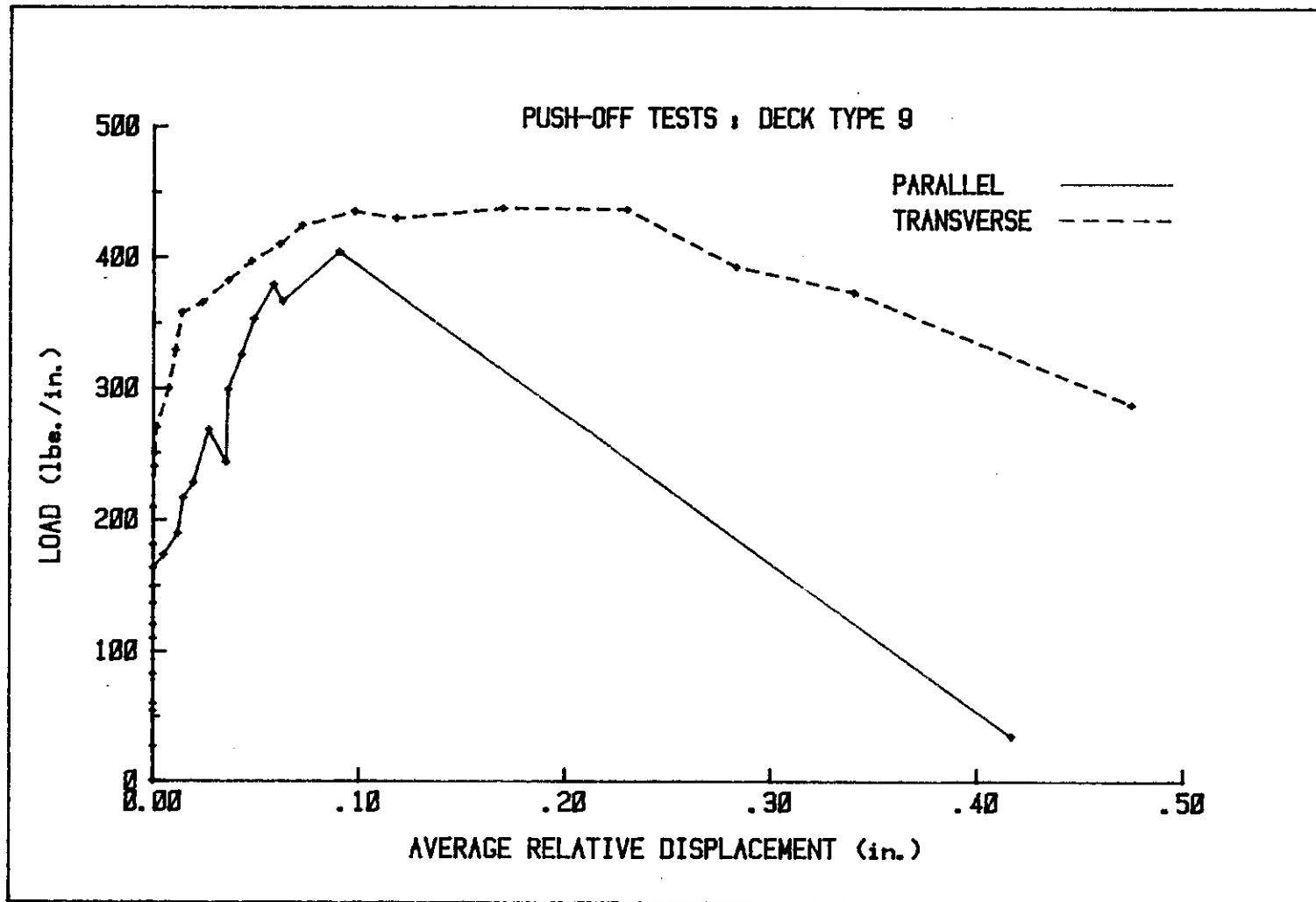


Figure 34. Push-off test results for Deck Type 9

transfer mechanism was by interfacial slip in both the parallel and transverse directions. Visible separation distance at test completion averaged 18 in.

3.5.3.7. Deck Type 2 Seven elemental push-off tests (four parallel and three transverse) were conducted with Deck Type 2. Figure 35 shows load-displacement curves for Deck Type 2. Note the large difference in ultimate capacity between the transverse and parallel directions for this deck type. Failure of the shear transfer mechanism was by interfacial slip in both the parallel and transverse directions. Interfacial slip in the transverse direction was mainly due to the concrete overriding the steel deck, since the very stiff deck geometry allowed very little cell deformation.

Deck Type 2 tests were also used to examine the effects of a superimposed vertical load, cyclic loading, and the size of specimen. In the parallel direction (comparing Specimens P-7-1 and P-7-2), the superimposed vertical load of 122 psf increased capacity by 24 percent. In the transverse direction (comparing Specimens P-7-4 and P-7-5), the superimposed vertical load seemed to have little effect.

Specimens P-7-3 and P-7-6 were subjected to one-half reversed cyclic loading, rather than monotonic loading as all other specimens. In the parallel direction, the strength was increased; in the transverse direction, it was decreased. More testing is needed to determine what effects the load history has on interfacial properties.

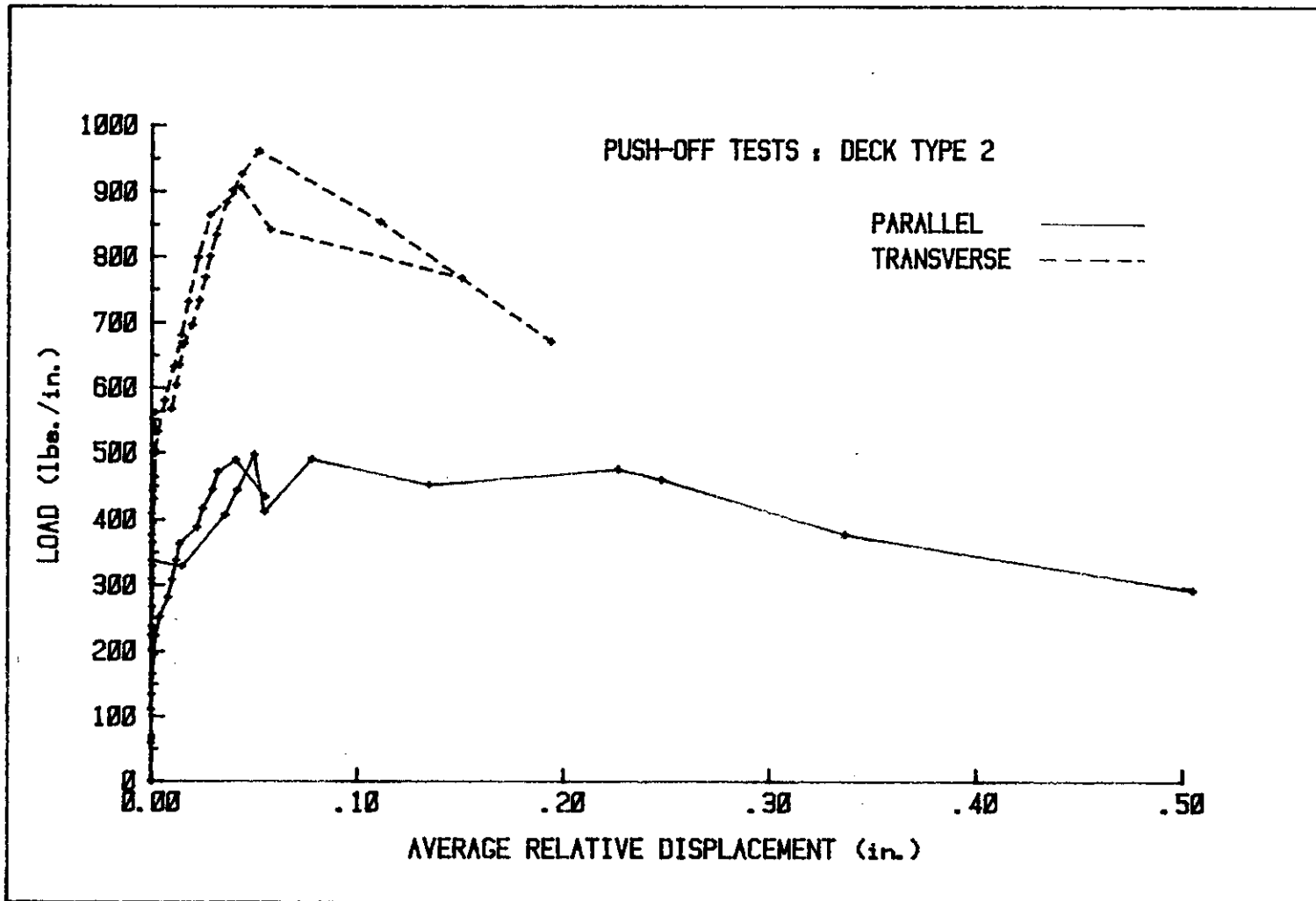


Figure 35. Push-off test results for Deck Type 2

A comparison of Specimens P-7-7 and P-7-1 showed that specimen length did not significantly affect behavior. The visible post-test separation distance averaged 27 in. for this deck type.

All seven tests were used in obtaining initial stiffness values. Tests P-7-2, P-7-3, and P-7-6 were not included in obtaining ultimate load values because of the unverified effects of cyclic loading and the superimposed vertical load effect.

3.5.3.8. Deck Type 4 Four elemental push-off tests (two parallel and two transverse) were performed using Deck Type 4. Figure 36 shows load-displacement curves for Deck Type 4. Failure of the shear transfer mechanism was by a combination of interfacial slip and concrete shearing in the down corrugations, in both the parallel and transverse directions (see Figure 37a). Note that specimens with this failure mode were very stiff prior to ultimate, and also that parallel and transverse specimens behaved quite similarly.

Each specimen was separated along the full 36 in. width of the specimen at test completion. All four tests were used in obtaining stiffness and ultimate load values. The ultimate load in both the parallel and transverse directions was considered to be proportional to $\sqrt{f_c}$, since failure occurred when concrete shear strength was overcome. To be completely correct, the ultimate strength equation for this deck type should contain both a term which is proportional to $\sqrt{f_c}$ (part of strength due to sheared concrete) and a term which is not proportional to $\sqrt{f_c}$ (part of strength due to deck concrete

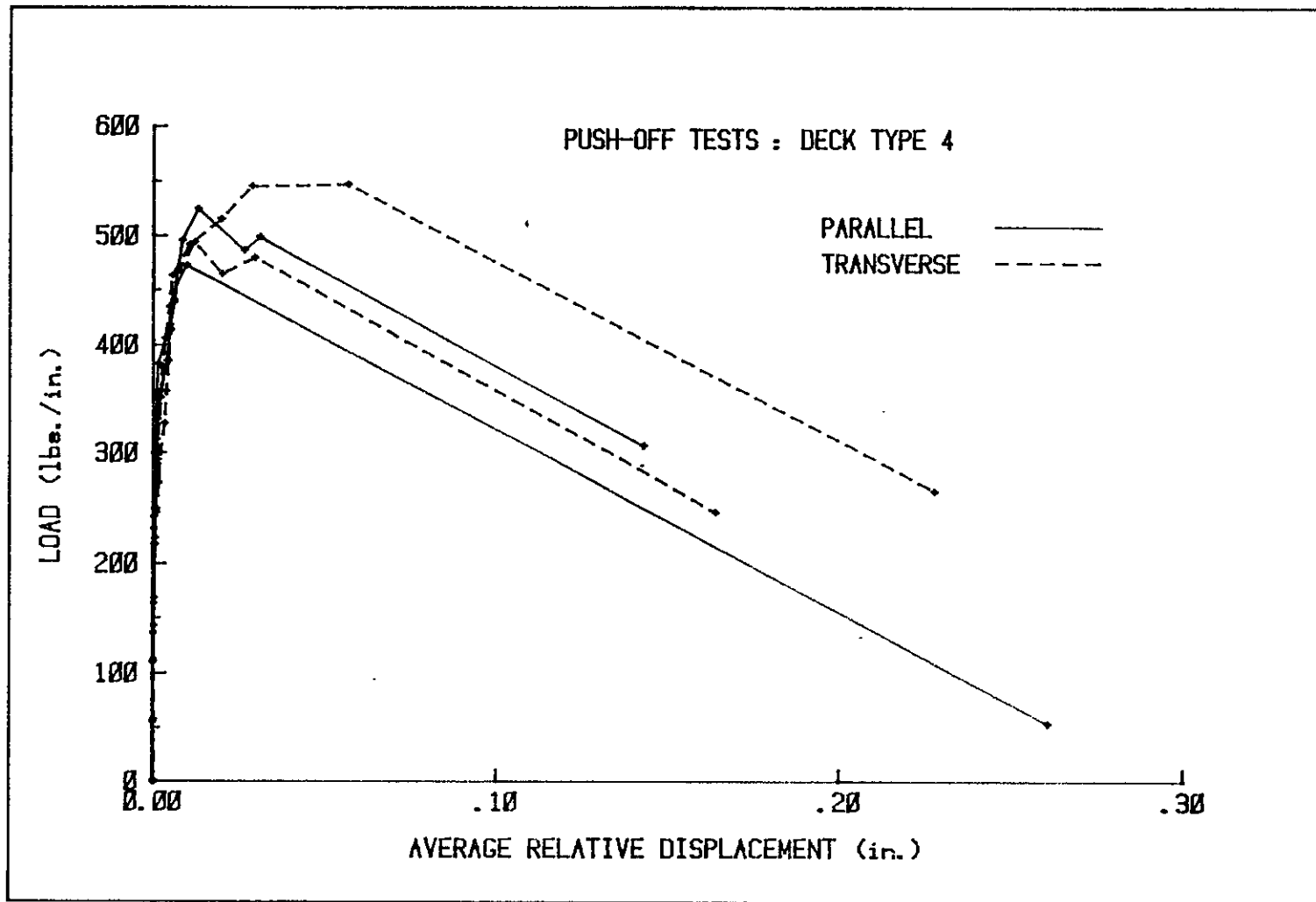


Figure 36. Push-off test results for Deck Type 4

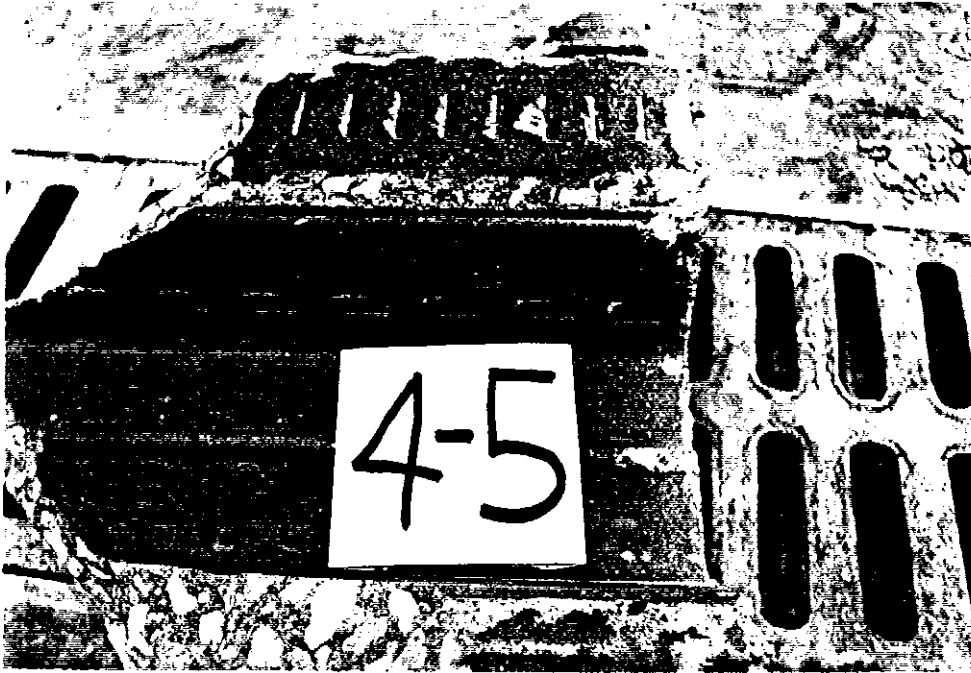


Figure 37a. Combined concrete shear and interfacial slip failure for Deck Type 4



Figure 37b. Typical weld failure

interference). However, not enough data was available to perform the necessary regressions. Comparison with results of Reference [15] (see Section 3.5.4), showed that the single term strength equation works reasonably well. This is probably true because the concrete fails at a small relative displacement, at which very little deck-to-concrete friction has been developed.

3.5.3.9. Weld tests Four elemental push-off tests (Tests P-4-7, P-10-1, P-10-2, P-10-3) were designed specifically to determine behavior and effects of the arc spot weld connections. Each specimen had two arc spot welds connecting the steel deck to the edge beam, except P-10-2, which had four, one in each down corrugation. Mig weld settings were 43 (amperage) - 9 (wire feed) for all 16 gage deck, and 33 - 6 for the 22 gage deck.

Specimens P-4-7 and P-10-1 failed by tearing of the sheet metal around the weld (Failure Mode 3.a.2). This failure mode is pictured on Figure 37b. The 11/16 in. diameter welds of P-4-7 had an ultimate capacity of 8.42 KIPS/weld. The 13/16 in. diameter welds of P-10-1 had an ultimate capacity of 9.09 KIPS/weld. Figure 38 shows the load-displacement curves for these two tests. The AISI equations (Eq. 2-2 to 2-5) predict ultimate loads of 4.49 KIPS/weld and 5.38 KIPS/weld, respectively, thus, these equations are quite conservative. Two simple tension tests (see Figure 39) on welds similar to those on Specimen P-10-1 yielded an average strength of 8.10 KIPS/weld. Results of these tests suggest that concrete directly covering arc spot welds increases their capacity by a small (12 percent)

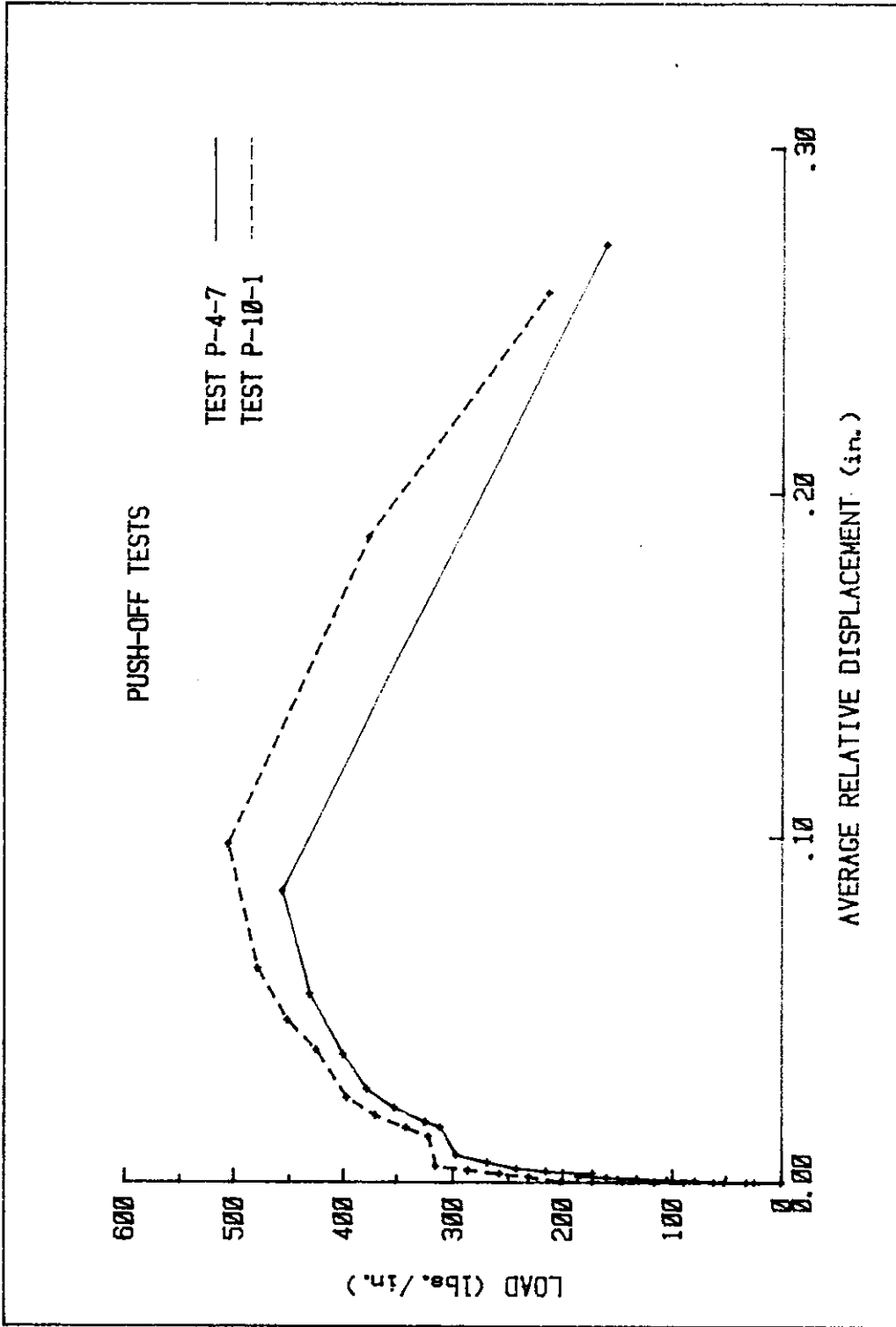


Figure 38. Push-off test results for weld failure

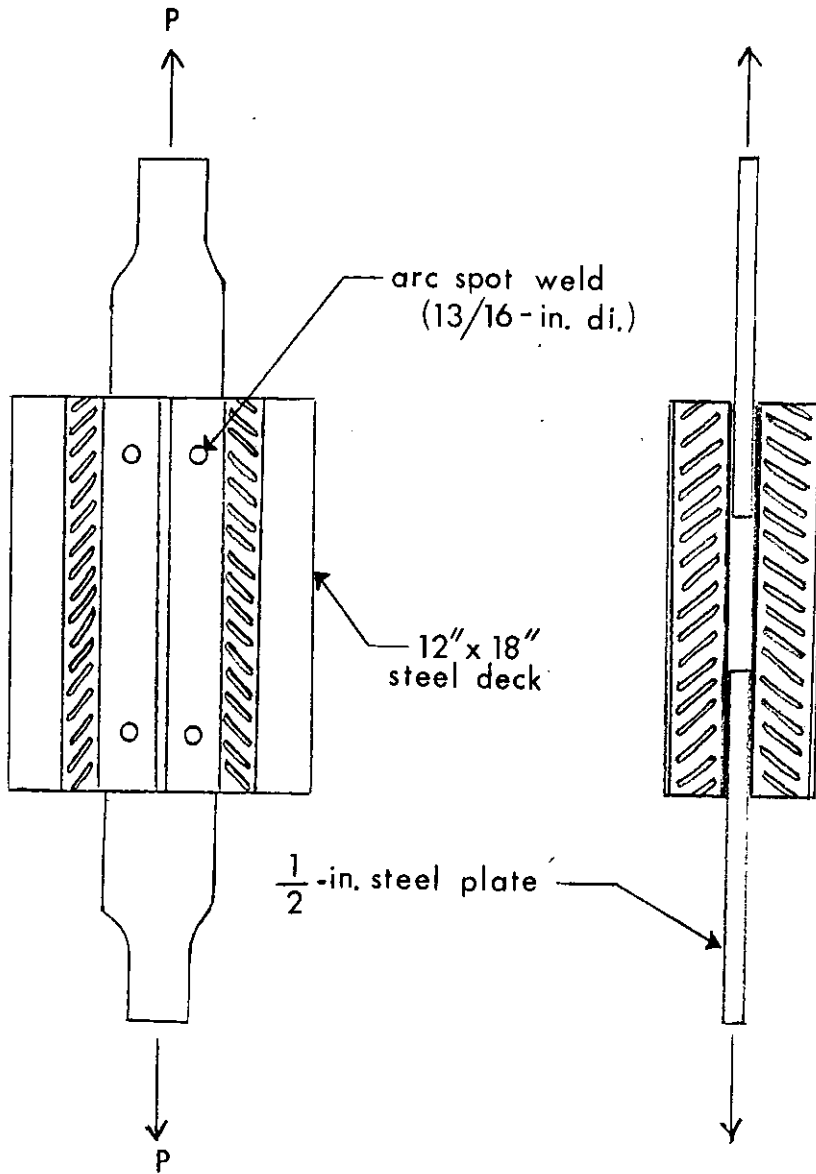


Figure 39. Arc spot weld tension test

amount.

The failure mode for Specimens P-10-2 and P-10-3 was failure of the shear transfer mechanism (Failure Modes 2.a.1 and 2.b.1). The ultimate capacity of these two tests was compared with the average capacity of that deck type with 12 welds, to determine if the number of welds affected the shear transfer mechanism capacity. Specimen P-10-2 had an 8 percent lower capacity than the average for Deck Type 5 transverse. Specimen P-10-3 had no change in capacity from the average for Deck Type 5B parallel. Thus, it was determined that the number and spacing of the welds does not significantly affect the shear transfer mechanism capacity, at least for the deck types tested.

Although the ultimate capacity was not affected by the number of welds (unless by failure of the welds themselves), the initial stiffness was affected, since the flexibility between the edge beam and the concrete includes both connection and interfacial flexibilities. Deck Type 5 (loaded parallel to the corrugations) showed a decrease in initial stiffness of 45 percent when changed from 12 welds to two welds. Deck Type 5 (loaded transverse to the corrugations) showed a decreased stiffness of 19 percent when changed from 12 welds to four welds. And Deck Type 5B (loaded parallel to the corrugations) showed a decreased stiffness of 17 percent when changed from 12 welds to two welds. Thus, it is important that a push-off specimen be constructed using the same weld procedure and spacing as the full-scale slab if results are to be used to predict the slab's initial stiffness.

3.5.4. Summary of test results

Review of the load-displacement curves for each of the push-off tests showed that all deck types tested had some similar characteristics. Initially, each had a very stiff region, in which little or no displacement occurred until chemical adhesion plus static friction resistive forces could be overcome. After significant slip occurred, the shear transfer device continued to carry increasing load, by mechanical interference with the corrugations in the transverse direction, and by frictional forces due to deck warpage and mechanical interference with embossments in the parallel direction. The load at ultimate and displacement at ultimate varied considerably with deck type. Post-ultimate ductility also varied with deck type and direction.

Some specimens were difficult to test at large displacements, as the specimen began to twist about two horizontal axes, the loaded and diagonal corner moving downward, the other two corners moving upward, so that the specimen's displaced shape was similar to a hyperbolic paraboloid. This problem was most evident on the transverse specimens of the stiffer deck types. Pre-ultimate results were thought not to be significantly affected by this phenomenon, however, large displacement testing was limited on a few specimens.

For each of the deck types tested, the shear transfer behavior and failure mechanism observed on the push-off test matched that which occurred on the full-scale slab. For example, Deck Type 5 loaded transverse to the corrugations was characterized by deck fold-over,

diagonal cracks at the seams, and interfacial slip (Failure Mode 2.b.1) on both push-off tests and full-scale slab tests. Deck Type 7 loaded transverse to the corrugations underwent corbel failure (Failure Mode 2.b.3) on both push-off and full-scale tests. These types of similarities were noted for each of the deck types.

Push-off test results (see Table 11) were also useful for identifying general trends in shear transfer mechanism behavior. In general, the thicker the deck, the greater the capacity of the shear transfer mechanism in both the parallel and transverse directions. The initial stiffness was also greater for the thicker deck types, but was also affected by the type of embossments. The relative displacement at ultimate load and the energy input at ultimate load (which give some indication of the ductility of the system) both seemed to vary with the geometry of the deck profile and type of embossments. A more complete parametric investigation is given in Section 4.2.2.

By averaging those tests designated in Section 3.5.3, the initial stiffness (to be derived from the area under the load-displacement curve at 0.003 in., see Section 4.2.3.2) and the ultimate capacity of the shear transfer mechanism were determined for each deck type, in each direction, and are shown in Table 12. The values for Deck Type 1 were determined from the pushout tests conducted with the previous project [15]. The shear transfer mechanism capacity of Deck Type 1 was thought to be proportional to $\sqrt{f_c}$, since it had the same geometry and failure mode as Deck Type 4.

Table 12. Push-off test results by deck type

Deck type	Ultimate strength (lbs./in.)		Energy input @ .003 in. (lb.-in./in.)	
	Q_{ppo} parallel	Q_{tpo} transverse	parallel	transverse
1 ^a	$\frac{\sqrt{F_c}}{\sqrt{2950}}$ 468	$\frac{\sqrt{F_c}}{\sqrt{6250}}$ 454	0.66	0.39
2	493	933	0.73	1.35
3	_b	_b	_b	_b
4	$\frac{\sqrt{F_c}}{\sqrt{2583}}$ 499	$\frac{\sqrt{F_c}}{\sqrt{2583}}$ 520	0.96	0.87
5	625	627	1.01	0.93
5B	211	326	0.58	0.63
6	293	521	0.67	0.93
7	563	$\frac{\sqrt{F_c}}{\sqrt{4019}}$ 531	0.87	0.76
8	554	786	0.57	0.66
9	404	437	0.50	0.78

^aDetermined from Ref. [15] pushout tests.

^bNo elemental tests performed.

The average shear transfer mechanism capacities of Deck Type 2 and Deck Type 4 (determined from the push-off tests) were compared with those of the previous project pushout tests (see Table 5). For Deck Type 2, parallel and transverse, and Deck Type 4, parallel and transverse, the differences were 16, 4, 3, and 7 percent, respectively.

4. ANALYTICAL INVESTIGATION

This section discusses methods for predicting the stiffnesses and ultimate strengths of steel deck reinforced concrete diaphragms. First, a short review of previously developed methods is presented. The next subsection discusses how the elemental tests were used in the analysis. The third subsection gives further explanation of the predictive methods and proposed modifications thereto. A final subsection compares predicted and analytical results.

4.1. Background and Previous Techniques

The edge zone concept for analyzing composite diaphragm slabs was developed at Iowa State University, and is discussed in Reference [15]. This concept states that the strength and stiffness of composite diaphragm slabs is highly dependent upon the capacity of the steel deck to transfer forces to the concrete. It also states that the major portion of this transfer of forces occurs within a relatively narrow band around the perimeter of the slab, called the edge zone. In other words, the edge zone is the distance in from the edge in which there is a significant horizontal force transfer occurring between the steel deck and the concrete.

There is much experimental evidence to support this concept, including measured slips and steel deck strains as reported in Section 3.1.5. Plate theory also supports this concept as presented in Reference [15] and Section 4.3.1 of this report.

Also determined in Reference [15] was an idealized force transfer distribution occurring between the edge beams and the composite slab. These force distributions were determined using a general purpose computer program (SAP6), in which the edge beams were connected to the composite slab using 1-dimensional spring elements (assumed stiffness of 30 KIPS/in./in.). The composite slab was idealized as a thick plate using 3-dimensional, 20-node, isoparametric solids. Figure 40 shows the idealized force distribution if the edge springs are in the linear elastic range. Figure 41 shows the idealized distribution for edge springs strained into a perfectly plastic range. These idealized edge distributions, along with geometry and statics, were used to develop predictive equations for the strength and stiffness of the edge zone. Further explanation and application of this technique is presented in Section 4.3.

4.2. Interpretation and Application of Elemental Push-off Tests

The elemental push-off test was chosen as the elemental test on which to base predictive equations for the diaphragm edge zone stiffness and ultimate strength (if controlled by Failure Mode 2 or 3) because its behavior best modeled that occurring in the full-scale slab. Also, this method of testing was most easily applied to the edge zone theory, since the push-off specimen could be thought of as a segment of the slab along any of the slab's edges, which would include the edge zone (see Figure 42).

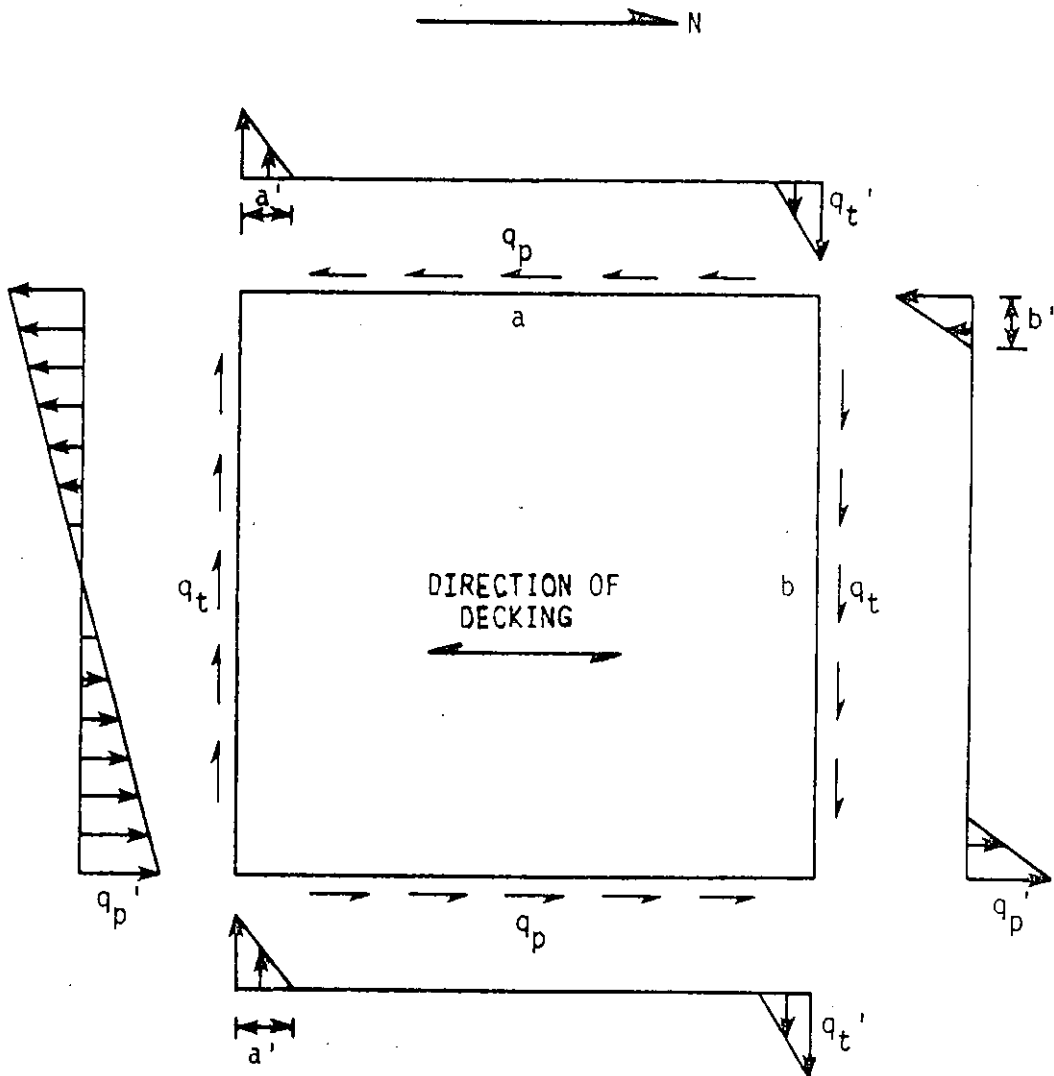


Figure 40. Idealized edge force distribution in elastic range [15]

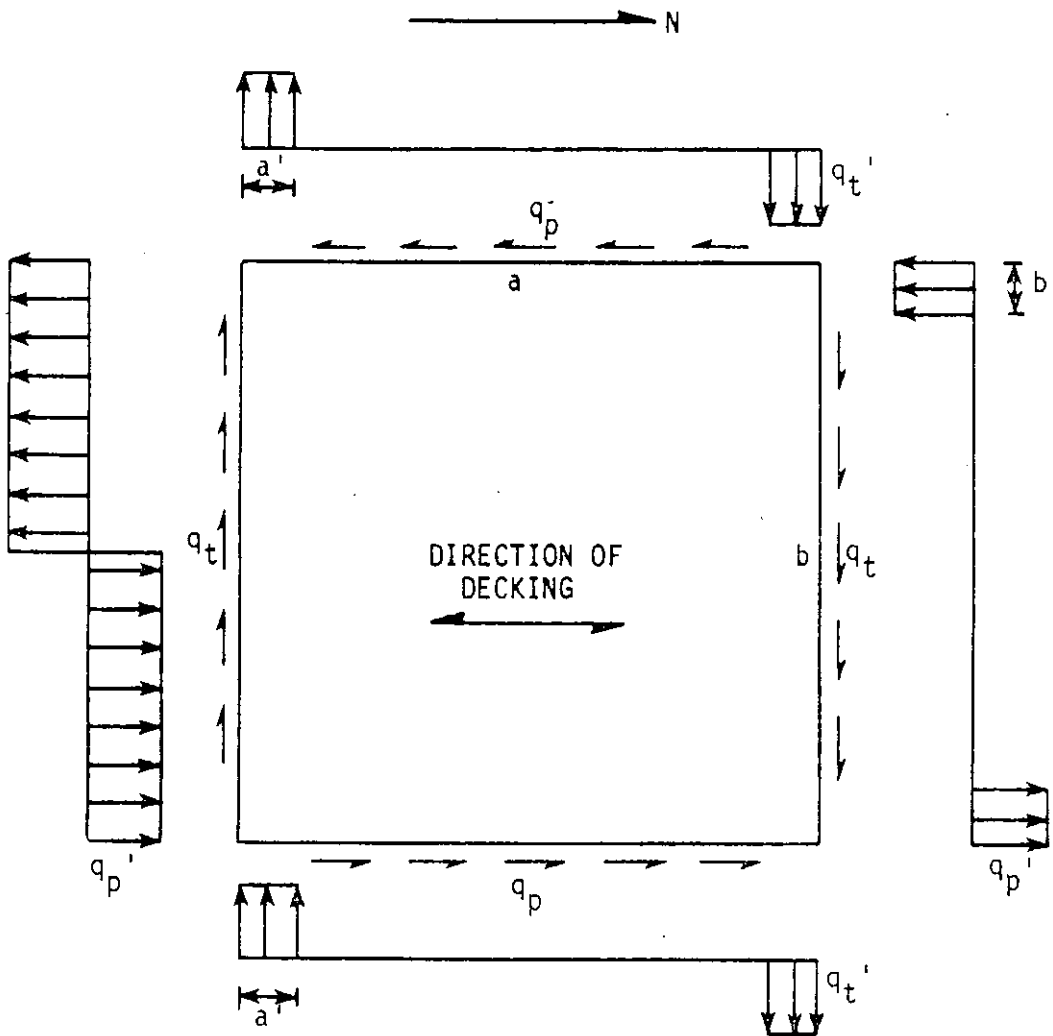


Figure 41. Idealized edge force distribution in plastic range [15]

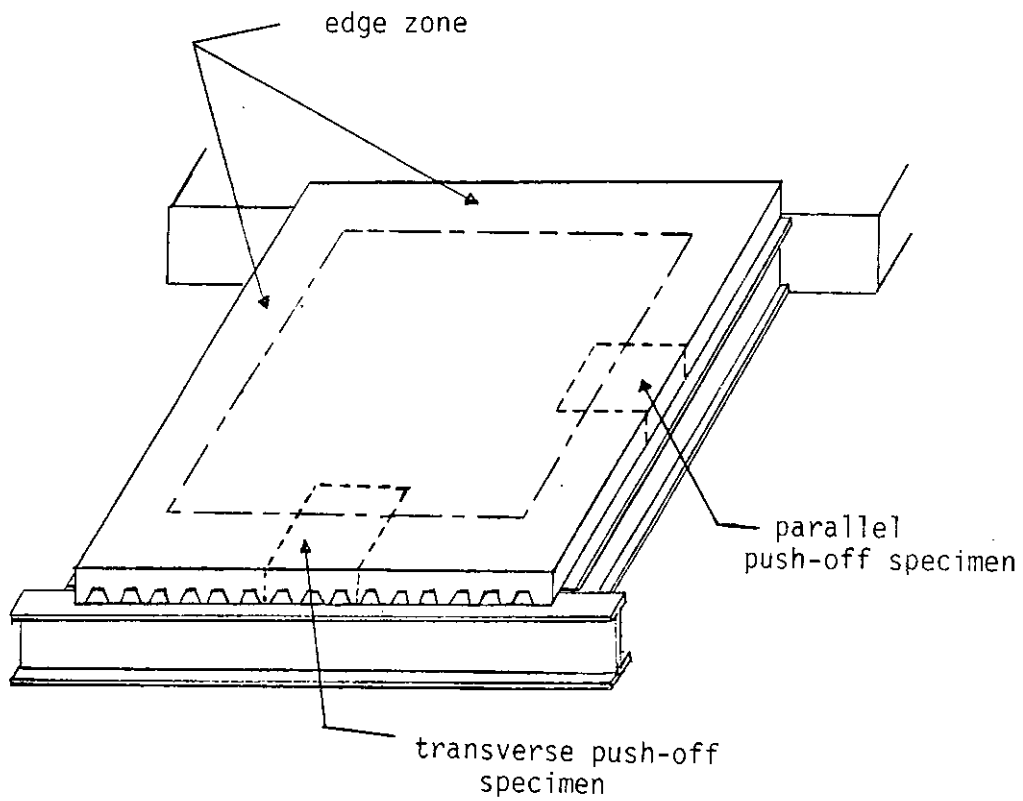


Figure 42. Relationship of edge zone to push-off specimens

4.2.1. Failure modes

The purpose of the elemental tests was to determine the capacity of the steel deck's shear transfer device to transfer force to the concrete within the edge zone. The method of load application forced this type of behavior by placing equal and opposite forces on the steel edge beam and the concrete at the edge of the push-off specimen. In each specimen, the type of shear transfer mechanism failure that occurred (interfacial slip, concrete shear, or corbel) matched that occurring in the full-scale slab.

On several of the push-off specimens, diagonal tension failure occurred simultaneously with interfacial failure. Results showed that this type of failure did not occur until interfacial capacity had been exceeded, except if a very thin concrete cover was used. For this reason, it is suggested that any following push-off tests be constructed with a 4 in. to 5 in. concrete cover. Diagonal tension was likely to occur after interfacial capacity had been exceeded, because at this point the concrete section was similar to an unreinforced concrete beam.

4.2.2. Parametric investigation

Examination of Table 12 shows that the single most important variable affecting behavior and capacity of the deck-concrete interface was the deck type itself. Comparison of results of Deck Type 5 and Deck Type 5B showed that the deck thickness was very important to this difference, with the thicker deck having a higher

shear transfer capacity. Comparison of Deck Type 5 to Deck Type 2 and Deck Type 5 to Deck Type 8 showed that deck geometry and frequency and type of embossments also significantly affected the interfacial capacity.

As discussed in Section 3.5.3, limited parametric studies were also made within various deck type specimens. Those specimens which failed in interfacial slip were not significantly affected by the concrete strength. However, more variation was noticed between specimens constructed at different times, than those constructed simultaneously, suggesting that the coefficient of friction between the deck and concrete might be slightly affected by the specific concrete mix and conditions of placement.

The strength of those specimens with concrete shear or corbel failure was assumed to be proportional to $\sqrt{f_c'}$. This is consistent with the A.C.I. Code [26], which says that the shear strength of concrete is proportional to $\sqrt{f_c'}$. As stated in Section 3.5.3.8, this approximation is not completely correct, since part of the strength is due to interference between the steel deck and concrete, the capacity of which is not proportional to $\sqrt{f_c'}$. The approximation yields good results for concrete shear failure, because only a small amount of deck-to-concrete friction has been mobilized at the small relative displacement at which the concrete fails. The approximation yields good results for corbel failure, because only a small amount of the strength is due to interference between the steel deck and concrete.

The location of seam did not have any effect on push-off specimens tested, however, placement of a steel deck seam within the edge zone could conceivably cause premature failure of that edge zone if the seam welds failed. In fact, post-ultimate behavior in both push-off and full-scale tests included failure of seam welds within the edge zone.

The superimposed vertical load of 122 psf caused an increase in capacity ranging from 77 to 126 pounds per inch in each parallel specimen tested. In the transverse direction, the superimposed vertical load seemed to have little effect, except for Specimen P-9-4, in which the capacity was reduced due to the combined in-plane and vertical load.

4.2.3. Relationship to full-scale slab

4.2.3.1. Finite element analysis A finite element analysis of the push-off test was performed using a general purpose finite element program (ANSYS). The boundary conditions were then changed to those of a full-scale slab segment as suggested in Figure 42, and the analysis rerun to compare the interfacial force distribution in the push-off test to that in the edge zone of the full-scale slab. A 2-dimensional model was used, since the intent was to study only the horizontal shear transfer, and since it was assumed that out-of-plane behavior would not affect the in-plane force distribution.

The concrete slab was modeled by 24 isotropic, 4-node isoparametric, plane stress elements. The steel deck was modeled

by 24 orthotropic, 4-node isoparametric, plane stress elements equivalent plane stress properties. Four material properties necessary to define the steel deck orthotropic elements: modulus of elasticity parallel to the corrugations, effective modulus of elasticity transverse to the corrugations, one of the poisson's ratios (the other one can be calculated), and the effective shear modulus. Each of these equivalent properties was determined according to the procedure outlined in Reference [27]. Each of the properties was given as a function of deck geometry, with the effective shear modulus being the most involved, since it depends on what degree the deck geometry is restrained from warping. The equivalent steel deck properties used for the finite element analysis were: 33000 ksi for the parallel elastic modulus, 33 ksi for the transverse elastic modulus, 0.3 for the parallel to transverse poisson's ratio, 0.0003 for the transverse to parallel poisson's ratio, and an effective shear modulus ranging from 500 ksi to 7345 ksi. The above properties were for a trapezoidal, noncellular deck. All isoparametric elements included incompatible displacement shapes.

At each node point, the concrete and steel deck elements were connected by two 1-dimensional lengthless springs, one in the x-direction, and one in the y-direction. These spring elements had nonlinear capabilities, and were used to model the shear transfer mechanism of the system. The steel edge beam was also incorporated into the analysis, and was rigidly attached to one edge of the steel deck. Models were run with the steel deck corrugations oriented both

parallel and transverse to the direction of the applied load.

Figure 43a shows the basic element and node layout.

To model the push-off test, equal and opposite forces were applied to the steel edge beam and to the concrete at one corner of the specimen. The only displacement boundary conditions imposed were those necessary to prevent rigid body motion. Boundary conditions for modeling the full-scale slab segment included applying the force at all nodes along the length of the edge beam, restraining the displacement of the edge beam in the direction perpendicular to the load, and restraining all displacements at the edge of the specimen opposite that of the steel edge beam. These restraints were thought to model an interior point of the slab, where no relative movement between the steel deck and concrete occurred.

The load-displacement curve given to the interfacial springs is shown in Figure 43b (see Section 4.3.1.2 for the effects of different load-displacement curves). The stiffness of each interfacial spring was calculated using a contributory area approach. Since each steel deck and concrete element (as shown in Figure 43a) was 6 in. x 9 in., 54 square inches of interface was assigned to each central node, 27 square inches to each edge node, and 13.5 square inches to each corner node.

Results showed that the steel deck stresses and interfacial spring forces within the edge zone were very similar with each set of boundary conditions, however, the concrete stresses were radically different. Thus, assuming that the state of stress in the concrete does

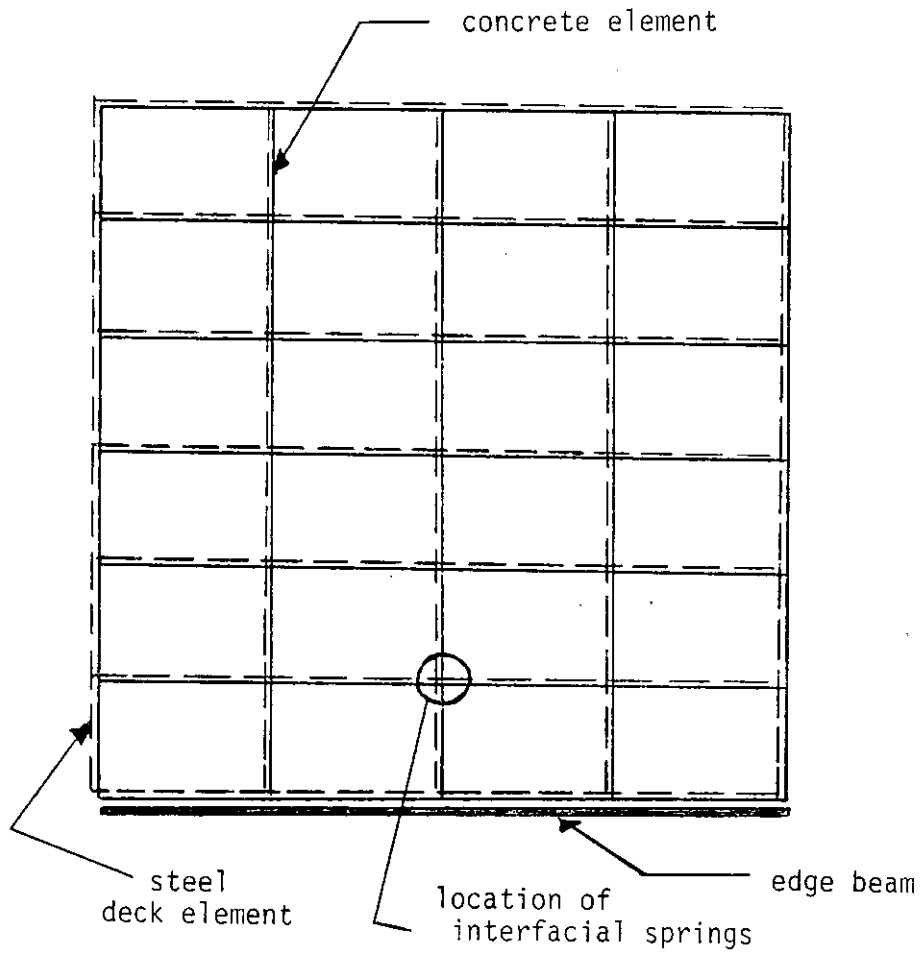


Figure 43a. Finite element node and element locations

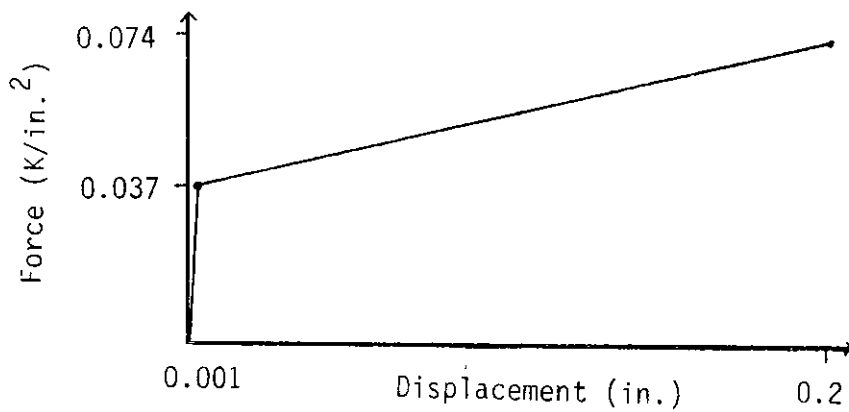


Figure 43b. Finite element interfacial spring load-displacement curve

not significantly affect interfacial behavior, the push-off test would be a good model for directly measuring shear transfer behavior. Typical finite element results are shown in Figure 44. These results are for the load applied parallel to the deck corrugations, with applied loads of 222 lbs./in. and 667 lbs./in. Notice the very similar interfacial force distribution with each set of boundary conditions, and also how the edge zone "grows" with increasing applied force. Results also showed that the interfacial force distribution was very similar with either parallel or transverse deck orientation.

4.2.3.2. Stiffness The initial flexibility of the edge zone is composed of two separate displacements: displacement between the edge beams and the steel deck, and displacement between the steel deck and the concrete. Measurements on the push-off tests included both of these displacements, thus the initial edge zone flexibility or stiffness was determined directly from the push-off tests, in a per inch of specimen length basis.

Examination of Figures 26, 27, and 31 to 36 shows that no initial linear elastic range existed for most of the push-off specimens, thus an energy equivalent elastic stiffness was used for initial stiffness calculations. The equivalent stiffness was found by equating the area under the actual load-displacement curve up to a displacement of 0.003 in., to that of a linear elastic curve to the same displacement. The equivalent stiffness (K_{eq}) is

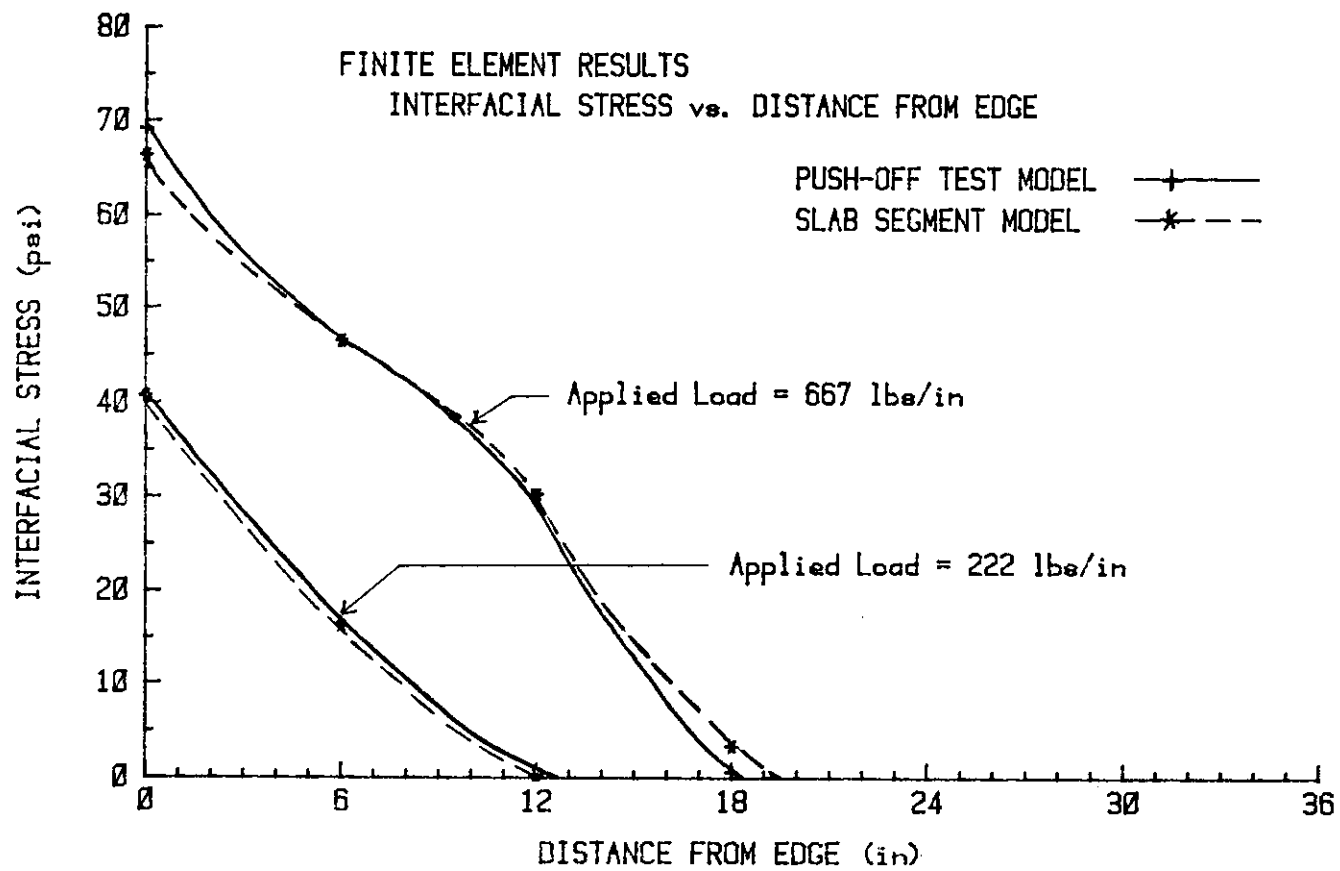


Figure 44. Typical finite element results

$$K_{eq} = \frac{2(A_{\Delta})}{\Delta^2} \quad (4-1)$$

where A_{Δ} = area under load-displacement curve to displacement

Δ

$\Delta = 0.003$ in.

A displacement of 0.003 in. was chosen because the measured slip on the full-scale slabs was typically 0.003 in. or smaller at the initial load point. The average area under the load-displacement curve up to 0.003 in. for each deck type is given in Table 12.

4.2.3.3. Ultimate load The ultimate edge zone capacity was also determined from the push-off tests. If edge zone capacity was controlled by connection failure (weld failure), then the ultimate strength of the push-off specimen (per unit length) was the same as the corresponding full-scale slab edge zone strength (per unit length), since in both cases, 100 percent of the force applied at the edge was transferred through the welds.

If the capacity was controlled by failure of the shear transfer mechanism, then values from the push-off test could not be applied uncorrected to the full-scale slab edge zone. In the push-off test, 100 percent of the applied load was transferred between the steel deck and the concrete by means of the shear transfer mechanism. In the full-scale slab, the shear force in the slab was carried compositely by the concrete and the steel deck, thus, the amount of

shear force ultimately carried by the steel deck remained in the steel deck, rather than being transferred by the shear transfer mechanism. Then, since less than 100 percent of the force applied to the edge of the full-scale slab was carried by the shear transfer mechanism, it had a higher capacity for applied load than the push-off test.

The increase in strength was equal to the shear force carried by the steel deck. According to Luttrell [4], the shear flexibility of a corrugated steel deck which is restrained from warping is given by the expression

$$\Delta_s = \frac{Va}{b} \cdot \frac{1}{G_s t_s} \cdot \frac{s}{d} \quad (4-2)$$

where

V = applied load

a = length perpendicular to applied load

b = length parallel to applied load

G_s = shear modulus of deck = 11300 ksi

t_s = thickness of deck sheeting

d = corrugation spacing

s = total length of steel sheeting (perimeter) per corrugation.

A similar expression was given by Davies and Fisher [13]. For a composite slab, the restraint preventing deck profile warpage is provided by the concrete. Then, equating the shear displacement in

the concrete and steel deck, the ratio of force (per applied force per unit length) carried by the shear transfer mechanism in the push-off test to that carried by the shear transfer mechanism of the full-scale slab edge zone is given by

$$C_{po} = \frac{t_s (d/s) n_s + t_c}{t_c} \quad (4-3)$$

where

C_{po} = push-off test correction factor

n_s = shear modulus ratio, steel deck to concrete

t_c = average thickness of concrete.

Then, the ultimate edge zone strength of the slab (if capacity is limited by failure of the shear transfer mechanism) is

$$Q = C_{po} Q_{po} \quad (4-4)$$

where

Q_{po} = push-off test capacity

Q = slab edge zone capacity.

The C_{po} correction factor was verified using the previously described finite element model. Using a deck thickness of 0.06 in., a d/s ratio of 0.65, a concrete shear modulus of 1300 ksi, and a concrete thickness of 4 in., the calculated C_{po} was 1.085. The ratio of force transferred in the finite element push-off model to that transferred in the finite element slab segment model was 1.080.

The C_{po} push-off test correction factor varied from 1.04 with Deck Type 1, Slab 1, to 1.18 with Deck Type 4, Slab 9.

4.3. Proposed Predictive Method

The proposed predictive methods which follow are based on the edge zone concept developed in Reference [15]. Several modifications and extensions are outlined; however, the basic development is the same.

4.3.1. Edge zone distance

The edge zone distance is defined as the distance in from the edge of the slab in which there is shear force transfer taking place between the steel deck and the concrete slab. Previously [15], the edge zone distances were assumed to equal $a/12$ for edge zones parallel to the applied load and $b/12$ for edge zones perpendicular to the applied load. However, theory, experimental evidence, and finite element analysis show that this distance varies with deck type, and also increases as the load applied to the edge zone is increased.

4.3.1.1. Theoretical solution A theoretical prediction of the edge zone distance was formulated assuming that the steel deck along any edge of the diaphragm is continuously, elastically connected to the concrete slab, that the steel deck only deforms in shear, and that the deformation of the concrete within the edge zone is negligible compared to that of the steel deck. Figure 45 shows a slice of the model used for the theoretical solution. A concentrated force was applied at the edge of the deck, to model the force transmitted from the edge beams through the welds.

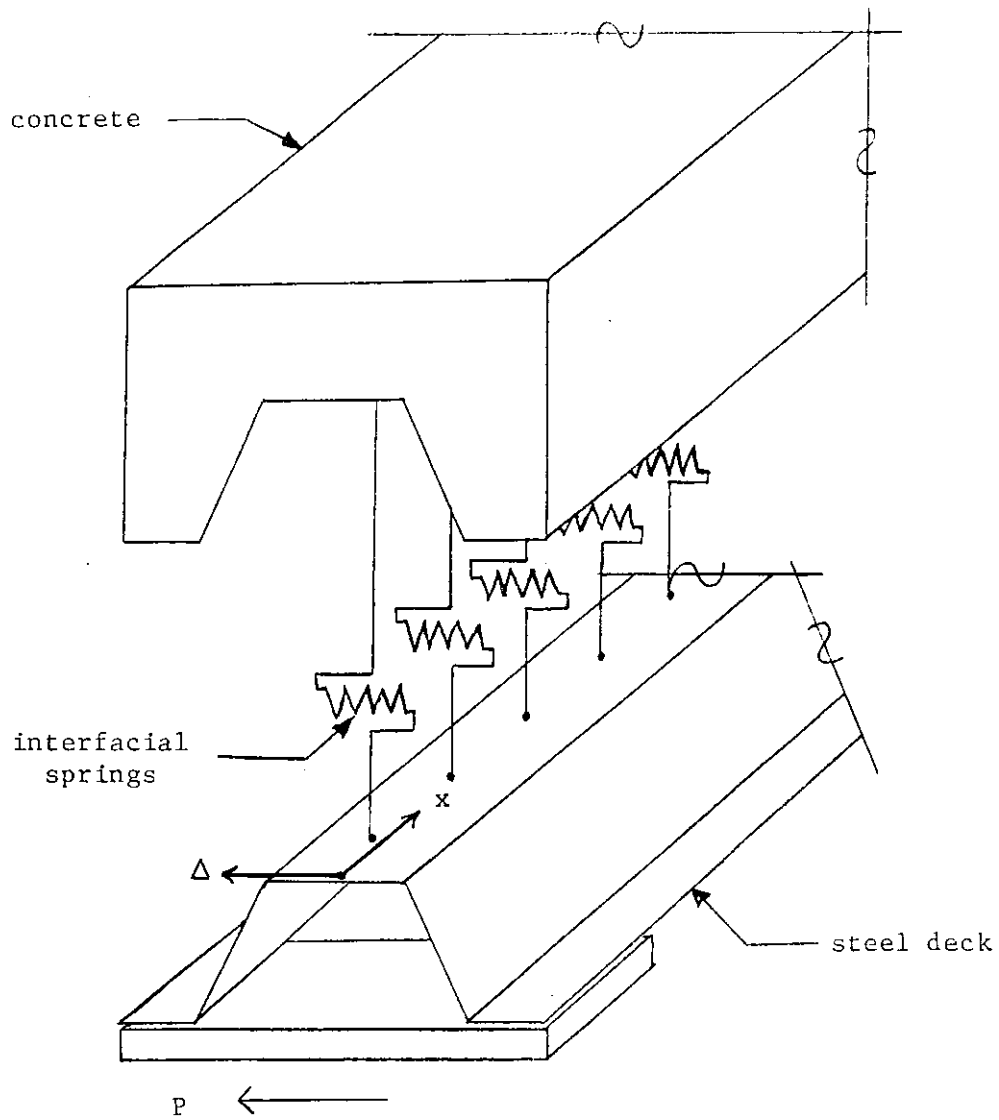


Figure 45. Model for theoretical edge zone development

For a shear deformation ($d\Delta$) on any segment of deck length, dx ,

$$d\Delta = \frac{V_1 f}{G_s A} dx \quad (4-5)$$

where

V_1 = shear force in the deck

f = shear flexibility shape factor

G_s = deck shear modulus

A = cross-sectional area of deck.

If the continuous springs have a stiffness K , then the shear (V_1) at any distance x is

$$V_1 = -P + \int_0^x K\Delta dx . \quad (4-6)$$

Substituting Eq. (4-6) into Eq. (4-5) and differentiating with respect to x , yields the controlling differential equation:

$$\Delta'' - B^2 \Delta = 0 \quad (4-7)$$

where

$$B = \sqrt{\frac{fK}{G_s A}} .$$

The general solution to this differential equation is

$$\Delta = c_1 e^{Bx} + c_2 e^{-Bx} \quad (4-8)$$

where c_1 and c_2 are constants which can be found from the boundary conditions. The two boundary conditions used were

$$\Delta(\infty) = 0$$

$$P = K \int_0^{\infty} \Delta dx . \quad (4-9)$$

From the first $c_1 = 0$, and from the second $c_2 = PB/K$, so that

$$\Delta = \frac{PBe^{-Bx}}{K} . \quad (4-10)$$

At this point, the edge zone was defined as that distance from the edge within which 95 percent of the force had been transferred.

Using Equation (4-9),

$$0.95 P = K \int_0^{a'} \frac{PBe^{-Bx}}{K} dx .$$

Solving for the edge zone distance (a' or b'),

$$a' = 3 \sqrt{\frac{G_s A}{fK}} . \quad (4-11)$$

Putting Eq. (4-11) in a per length of edge basis and letting

$G_{eff} = G_s/f$, yields

$$a' = 3 \sqrt{\frac{G_{eff} t_s}{K}} \quad (4-12)$$

where K is the stiffness of the shear transfer mechanism in KIPS/in.²/in. and G_{eff} is the effective shear modulus of the steel deck in the edge zone. This G_{eff} will be much smaller than the shear modulus of

Eq. (4-2), since the deck within the edge zone is not completely restrained from warping, as the deck in the center of the slab is. Equation (4-12) predicts that the edge zone distance will increase with increasing deck shear stiffness, and will decrease with increasing shear transfer stiffness.

Unfortunately, determining the G_{eff} and the K to use in Eq. (4-12) is not a simple matter. There is not general agreement in the literature on how to calculate G_{eff} near the edge. Using the method of References [22] and [27], for trapezoidal geometry, the G_{eff} (near the edge) ranges from approximately 300 ksi to 1100 ksi, depending on connector spacing. The equivalent K at failure, determined from the push-off test results ranges from 0.5 KIPS/in.²/in. to 5.0 KIPS/in.²/in. Then, for noncellular trapezoidal deck, ranging in thickness from 0.035 in. to 0.062 in., the possible range of edge zone distances at failure (using Eq. (4-12)) is from 4.0 in. to 35 in. This distance would be reduced by a small amount if the effect of flexural deformations had been included.

4.3.1.2. Experimental evidence Experimental evidence from both the full-scale tests and the elemental push-off tests support the concept of a varying width edge zone. Slip measurements such as shown in Figure 18 and deck strain measurement as shown in Figure 19 show the edge zone on the full-scale test propagating inward as cyclic displacements were increased.

On the push-off tests, an approximation of the edge zone distance at failure was determined by measuring the visible separation distance between the concrete and steel deck at test completion (as reported in Section 3.5.3). The greater the shear stiffness of the deck, the wider the edge zone seemed to be. Figure 46 shows the average measured separation distance for each deck type plotted against $t_s d/s$ (which according to Eq. (4-2) is proportional to the shear stiffness of the deck). The ratio d/s was taken equal to 1.0 for the cellular deck. A curvilinear regression through the eight data points of Figure 46 yielded

$$b' = 115 (t_s d/s)^{0.50} . \quad (4-13)$$

It was assumed that a' was equal to b' , based on the finite element results of Section 4.2.3.1. This rough estimate of edge zone distance at failure is only valid for deck types with thicknesses between 0.03 in. and 0.12 in., heights between 1.5 in. and 3.0 in., trapezoidal cell geometry, and embossments as the major shear transfer device. Note that both Eq. (4-12) (which is completely theoretical) and Eq. (4-13) (which is completely empirical) show the edge zone distance to be proportional to the square root of the deck shear stiffness.

4.3.1.3. Finite element model The same finite element model described in Section 4.2.3.1 was used to study the effects of various parameters on the edge zone distance. Both the shear stiffness of

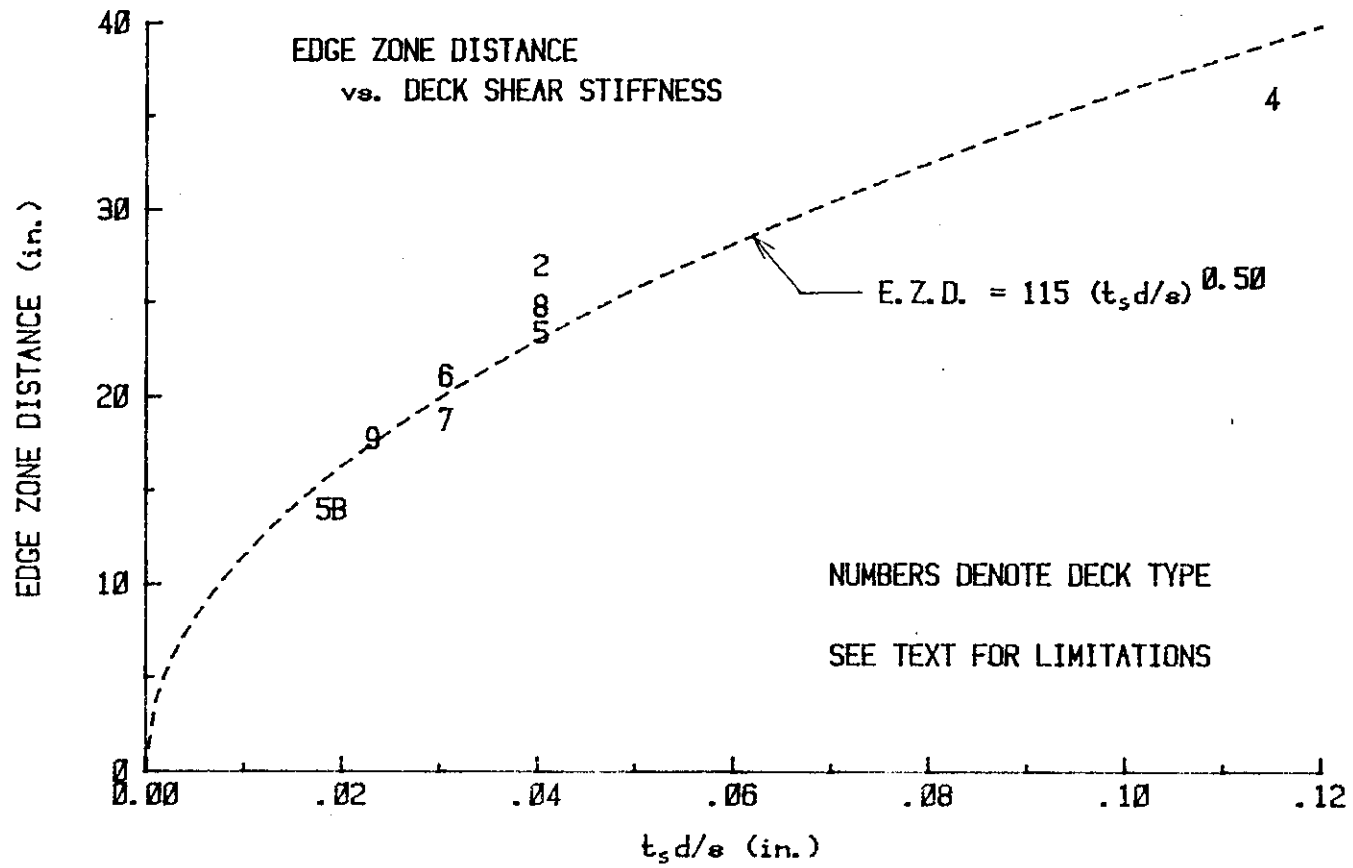


Figure 46. Experimentally measured edge zone distances

the deck, and the stiffness of the shear transfer mechanism were varied, to study the effect of each variable. For comparison purposes, the effective edge zone distance in the following discussion was again considered to be that distance from the edge at which 95 percent of the force had been transferred.

Two general trends were verified. First, increasing the shear stiffness of the deck increased the edge zone distance. For example, with G_{eff} equal to 500 ksi, with linear elastic interfacial springs set to 1.0 KIPS/in.²/in., and with deck thickness set at 0.02 in., 0.06 in., and 0.12 in., the effective edge zone distances were 10.0 in., 15.0 in., and 18.5 in., respectively. These edge zone distances vary a small amount from those predicted by Eq. (4-12), because of the relatively coarse finite element mesh used, and the resulting interpolation necessary to calculate the effective edge zone distance.

Secondly, the edge zone distance increased as the stiffness of the interfacial shear transfer device decreased. For example, with G_{eff} equal to 500 ksi, with the deck thickness set to 0.06 in., and with linear elastic interfacial springs set at 1.0 KIPS/in.²/in. and 0.5 KIPS/in.²/in., the effective edge zone distances were 15.0 in. and 18.0 in., respectively. This characteristic was also shown with nonlinear interfacial springs, as the equivalent stiffness of the interfacial springs (shear transfer device) decreased in the nonlinear range, the edge zone distance increased (see Figure 44).

4.3.2. Stiffness

In calculating the initial stiffness of the composite diaphragm slab, the in-plane deflection was considered to be composed of several components:

$$\Delta_{\text{tot}} = \Delta_{\text{b}} + \Delta_{\text{s}} + \Delta_{\text{z}} + \Delta_{\text{f}} \quad (4-14)$$

where

Δ_{tot} = total deflection

Δ_{b} = bending deflection of composite system

Δ_{s} = shear deflection of composite system

Δ_{z} = deflection due to edge zone deformation

Δ_{f} = deflection due to axial flexibility of edge
beam framing connections.

For bending, the cantilevered slab was considered to behave as a plate girder, with the composite slab acting as the web of the girder, and the edge beams acting as the flanges. The bending deflection (Δ_{b}) at the end of the girder (as given in Reference [15]) is

$$\Delta_{\text{b}} = \frac{V a^3}{3(E_{\text{c}} I_{\text{c}} + E_{\text{b}} I_{\text{b}})} = \frac{V}{K_{\text{b}}} \quad (4-15)$$

where

a = length of the cantilever beam

E_{c} = concrete modulus of elasticity

I_{c} = moment of inertia of composite web

E_b = edge beam modulus of elasticity

I_b = moment of inertia of edge beams about girder
neutral axis.

The thickness used in computing the moment of inertia of the composite web is the average concrete thickness plus $n = E_s/E_c$ times the effective steel deck thickness. For deck oriented perpendicular to the applied load, the effective steel deck thickness for bending is A_s/b , where A_s is the total steel deck cross-sectional area. For deck oriented parallel to the applied load, the effective steel deck thickness should be taken as zero (since the deck effective modulus of elasticity transverse to the corrugations is so small). If relatively deep edge beams are used, some judgement is necessary in determining what percentage of the edge beams is effective in bending, due to a shear lag problem. Design guides published by the H. H. Robertson Company [28], suggest using only the top flange of the edge beam as effective. For calculations in this report, the depth of edge beam effective for bending was determined by guidelines set forth in Reference [29]. For a span to flange width ratio of 3.75, the percentage of flange width effective is 86 percent (for a cantilever beam). Thus, assuming the upper 86 percent of the edge beams to be effective, the effective cross-sectional area of each edge beam is 15.0 square inches. This area of steel was used in computing the moment of inertia of the edge beams.

The shear deflection, Δ_s , is given by

$$\Delta_s = \frac{V a}{b(G_s t_s d/s + G_c t_c)} = \frac{V}{K_s} \quad (4-16)$$

where

a = length of cantilever beam

b = depth of cantilever beam

G_s = shear modulus of steel deck = 11300 ksi

t_s = thickness of deck

d/s = previously defined corrugated deck shear coefficient

G_c = shear modulus of concrete

t_c = average concrete thickness.

This equation assumes that only the web of the plate girder is effective against shear, and that the shear stiffness of the corrugated deck is as given in Eq. (4-2).

Previously [15], the deflection due to the deformation of the edge zone was based on the idealized force distribution shown in Figure 40. However, this force distribution does not take into account the axial deformation of the edge beams which occurs when the edge zone is very stiff, as it initially is. Figure 47 shows the edge zone force distribution including axial flexibility of the edge beams. These force distributions were developed by assuming a rigid slab, and a continuous linear elastic spring connecting the slab and the edge beams. The resulting forces on a typical beam segment are shown

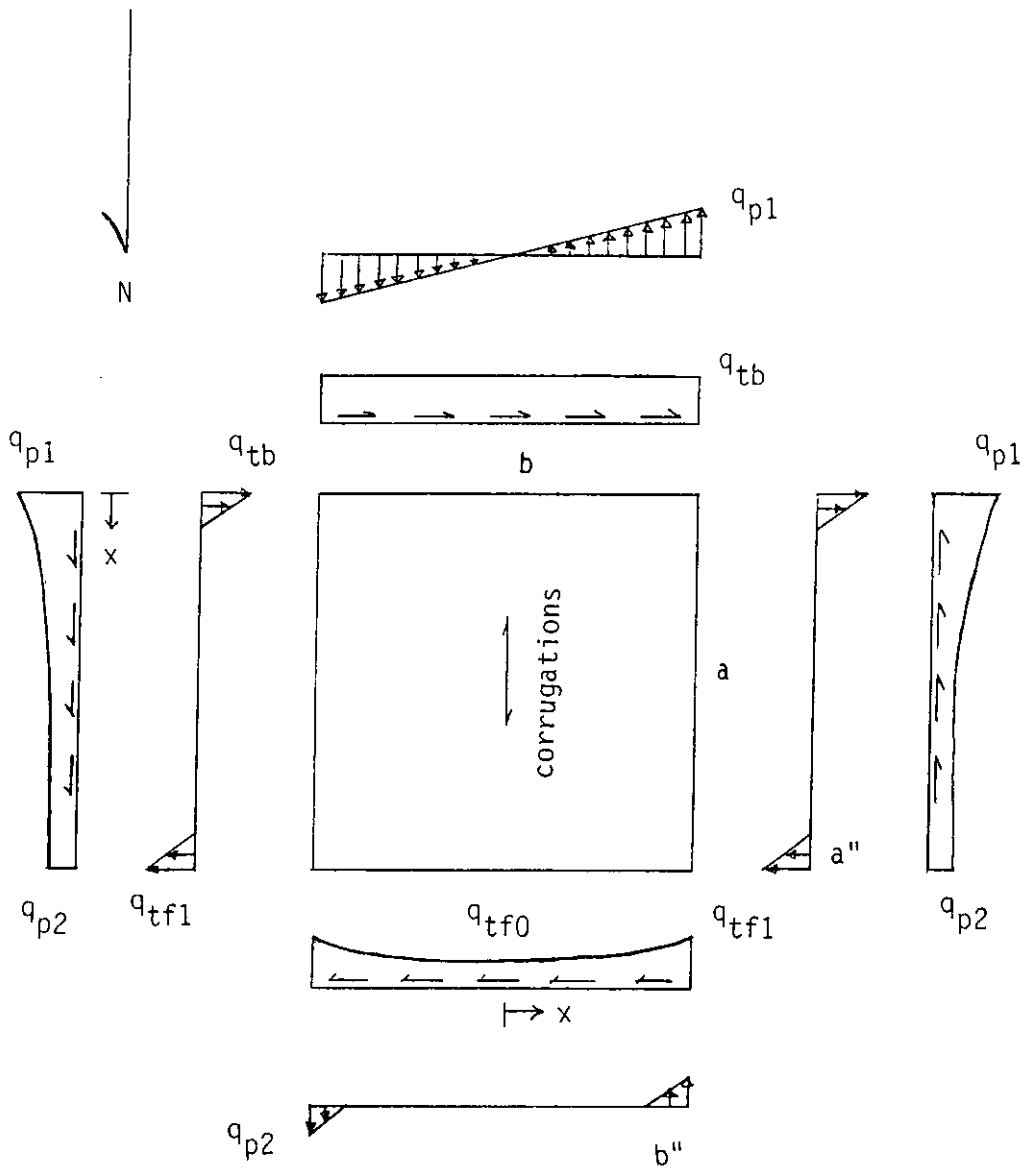


Figure 47. Initial edge force distribution

in Figure 48. Δ represents the edge zone displacement, and σ is the axial stress in the edge beam.

Summing forces in the x-direction yields

$$\int_x^{x+dx} K \Delta(x) dx = A_b (\sigma(x+dx) - \sigma(x)) \quad (4-17)$$

or using derivative notation,

$$K \Delta(x) = A_b \sigma'(x) . \quad (4-18)$$

Since the slab is assumed rigid, the change in edge zone displacement, $\Delta'(x)$, must be equal to the axial strain in the edge beam, thus,

$$\Delta'(x) = \frac{\sigma(x)}{E_b} \quad (4-19)$$

and

$$\Delta''(x) = \frac{\sigma'(x)}{E_b} . \quad (4-20)$$

Substituting into Eq. (4-18) yields the controlling differential equation

$$\Delta''(x) - \frac{K}{E_b A_b} \Delta(x) = 0 . \quad (4-21)$$

This equation was solved separately for a side beam and for the front moving beam, since each has a different set of boundary conditions. The resulting edge zone displacements can be linearly related to the edge forces by the following definitions:

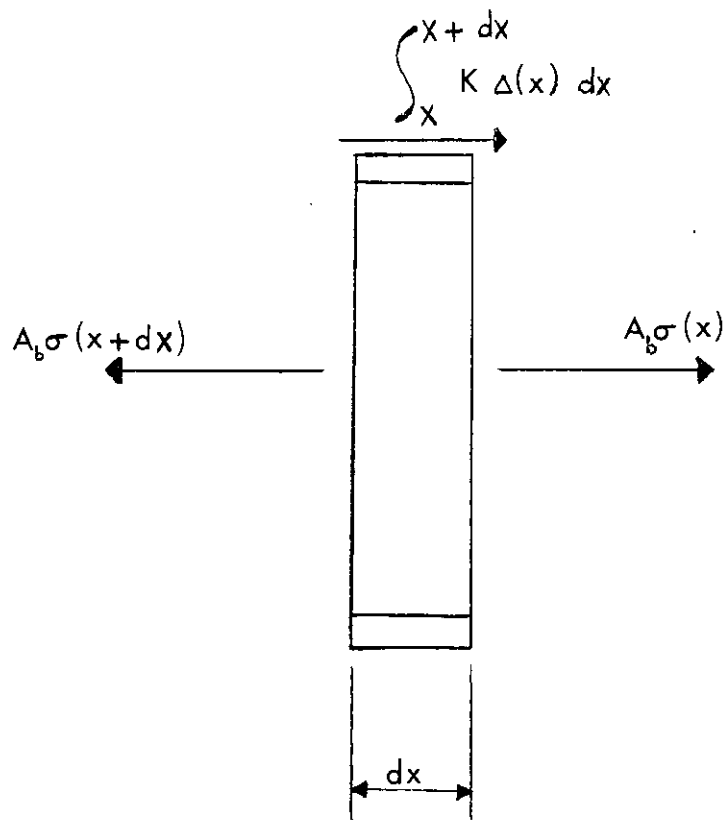


Figure 48. Horizontal forces on typical edge beam segment

$$q_{tf0} = K_t \Delta_{tf0} = \text{edge force at center of front beam}$$

$$q_{tb} = K_t \Delta_{tb} = \text{edge force along abuttment}$$

$$q_{tf1} = K_t \Delta_{tf1} = \text{edge force at end of front beam} \quad (4-22)$$

$$q_{p1} = K_p \Delta_{p1} = \text{edge force at fixed end of side beam}$$

$$q_{p2} = K_p \Delta_{p2} = \text{edge force at free end of side beam}$$

where K_t and K_p are the equivalent edge zone spring stiffnesses, in a direction transverse and parallel to the corrugations, respectively.

For the front moving beam with the origin at the center, the boundary conditions are

$$\sigma(o) = 0$$

$$\Delta(o) = \Delta_{tf0} \quad (4-23)$$

Using these boundary conditions to solve Eq. (4-21), and also using the linear transformations of Eq. (4-22), the edge force along the length of the front moving beam is

$$q_{tf}(x) = q_{tf0} \cosh(g_t x) \quad (4-24)$$

where

$$g_t = \sqrt{\frac{K_t}{E_b A_b}} \cdot$$

Substitution into Eq. (4-24) shows that

$$q_{tf1} = q_{tf0} \cosh (g_t b/2) . \quad (4-25)$$

Note that as K_t approaches zero, the term $\cosh (g_t x)$ approaches 1.0, and the force distribution becomes constant along the length of the beam.

Procedure for a side beam is similar. With the origin at the abutment, the boundary conditions are

$$\sigma(a) = 0$$

$$\Delta(0) = \Delta_{p1} . \quad (4-26)$$

The first of these boundary conditions assumes that the axial force at the free end of the side beam is negligible compared to that at the fixed end. Using these boundary conditions to solve Eq. (4-21), and also using the linear transformations of Eq. (4-22), the edge force distribution along the length of the side beam is

$$q_p(x) = q_{p1} \operatorname{sech} (g_p a) \cosh (g_p (x-a)) \quad (4-27)$$

where

$$g_p = \sqrt{\frac{K_p}{E_b A_b}} .$$

The relationship between the edge forces at each end of the beam are found by substituting into Eq. (4-27), so that

$$q_{p2} = q_{p1} \operatorname{sech} (g_p a) . \quad (4-28)$$

Again, the force distribution becomes constant along the length as K_p approaches zero. A 2-dimensional finite element model of a side beam connected to a rigid slab by a series of connecting (edge zone) springs yielded a force distribution in very close agreement with Eq. (4-27). Also, examination of strains in the edge beams at initial load points, indicated that the force transfer occurring near the fixed end, was considerably greater than that at the free end, as indicated by Eq. (4-27).

The average edge forces (found by integrating along the length and then dividing by the length) for the front moving beam (q_{tfav}) and for the side beam (q_{pav}) are given by

$$q_{tfav} = \frac{2 q_{tf0}}{b g_t} \sinh \left(\frac{g_t b}{2} \right) \quad (4-29)$$

$$q_{pav} = \frac{q_{p1}}{a g_p} \tanh (g_p a) . \quad (4-30)$$

Also, by definition, let

$$r_1 = \frac{\Delta_{p1}}{\Delta_{pav}} = \frac{q_{p1}}{q_{pav}} = g_p a \coth (g_p a) \quad (4-31)$$

$$r_2 = \frac{\Delta_{p2}}{\Delta_{pav}} = \frac{q_{p2}}{q_{pav}} = g_p a \operatorname{csch} (g_p a) \quad (4-32)$$

$$r_3 = \frac{\Delta_{tfl}}{\Delta_{tfav}} = \frac{q_{tfl}}{q_{tfav}} = g_t \frac{b}{2} \operatorname{coth} (g_t \frac{b}{2}) . \quad (4-33)$$

Resultant forces on edge beams and abutment will be as shown in Figure 49. The total edge zone deflection can be determined in a manner similar to that given in Reference [15], by a combination of geometry and statics.

Summing forces on the front moving beams yields

$$V = q_{tfav} (b + \frac{r_3 a''}{3a} (3a - a'')) - q_{tb} (\frac{a''^2}{3a}) . \quad (4-34)$$

The relationship between q_{tfav} and q_{tb} can be found by summation of forces on the south reaction block, or on the concrete slab as

$$r_4 = \frac{\Delta_{tb}}{\Delta_{tfav}} = \frac{q_{tb}}{q_{tfav}} = \frac{b + r_3 a''}{b + a''} . \quad (4-35)$$

Then by substituting for q_{tb} and letting $\ell_t'' = a''[r_3(3a - a'') - a''r_4]/3a$ Eq. (4-34) becomes

$$V = q_{tfav} (b + \ell_t'') . \quad (4-36)$$

Similarly, by summation of moments on the south reaction block

$$V = q_{pav} [\frac{r_1 b^2}{6a} + b + \frac{r_2 b''}{6a} (3b - 2b'')] \quad (4-37)$$

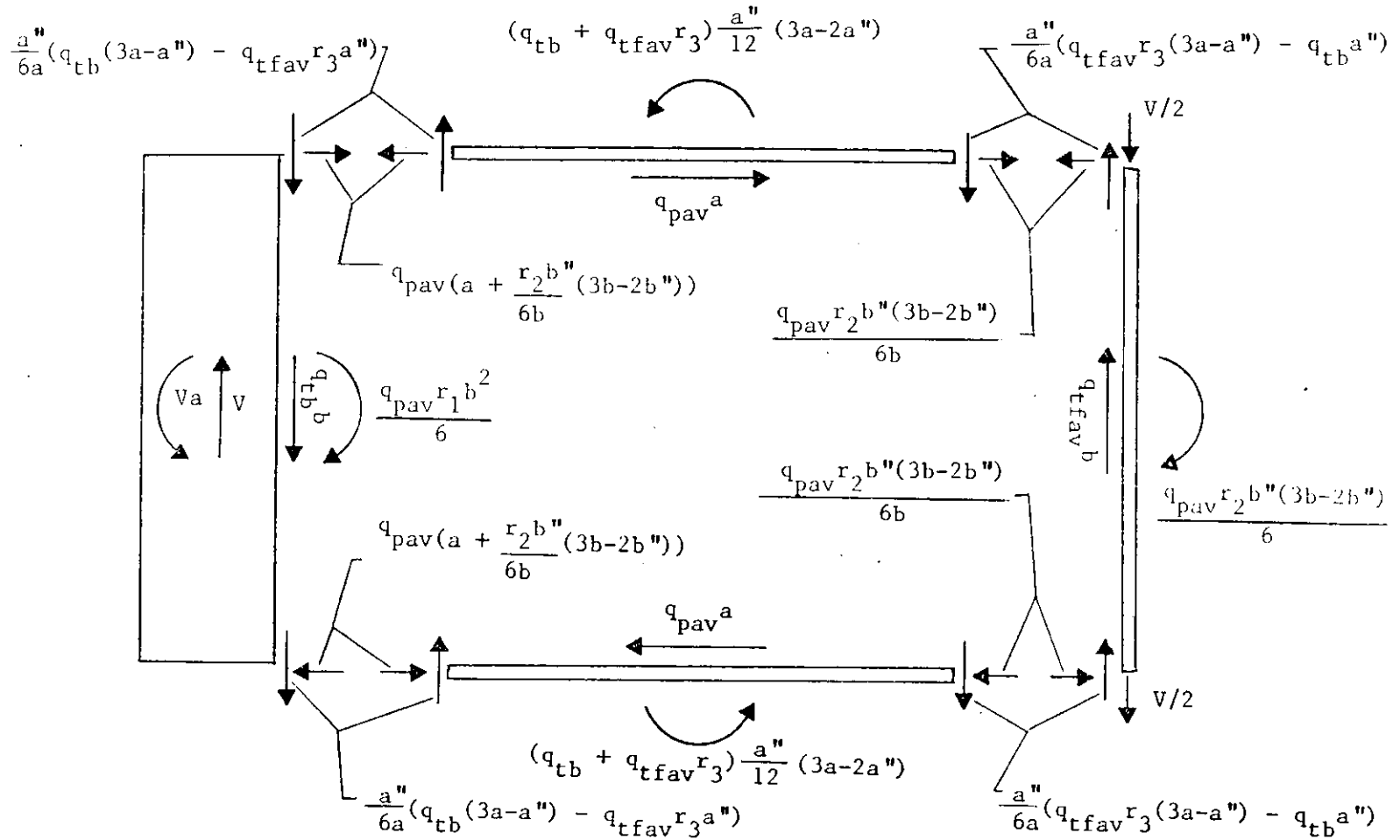


Figure 49. Framing member forces (initial)

or letting $\ell_p'' = (r_1 b^2 + r_2 3bb'' - r_2 2b''^2)/6a$,

$$V = q_{pav} (b + \ell_p'') . \quad (4-38)$$

Figure 50 shows the geometrical relationships between Δ_{tfl} , Δ_{tb} , Δ_{pl} , and Δ_z . For clarity, the total edge zone displacement, Δ_z , is broken down into that due to transverse edge zone displacement (Figure 50a) and parallel edge zone displacement (Figure 50b). Addition of the two contributions yields the relationship

$$\Delta_z = \Delta_{tfl} + \Delta_{tb} + \frac{2a}{b} \Delta_{pl} . \quad (4-39)$$

Substituting from Eqs. (4-31), (4-33), and (4-35),

$$\Delta_z = r_4 \Delta_{tfav} + r_3 \Delta_{tfav} + \frac{2a}{b} r_1 \Delta_{pav} . \quad (4-40)$$

Substituting from Eqs. (4-36) and (4-38), and also using Eq. (4-22) relationships

$$\frac{\Delta_z}{V} = \frac{r_4 + r_3}{K_t (B + \ell_t'')} + \frac{2ar_1}{K_p b (b + \ell_p'')} \quad (4-41)$$

or the total edge zone stiffness (K_z) is

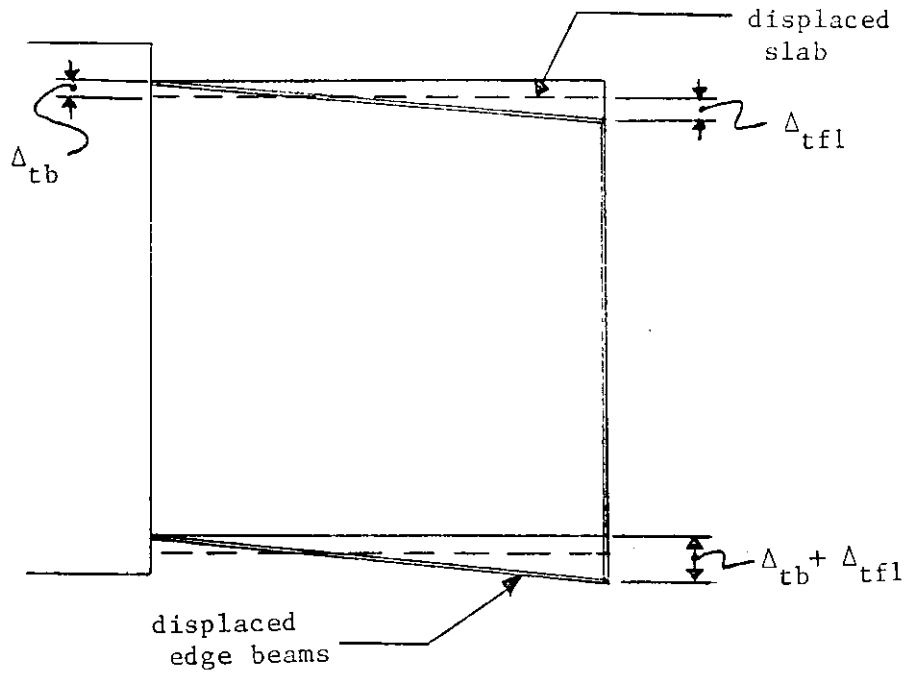


Figure 50a. Transverse edge zone displacement

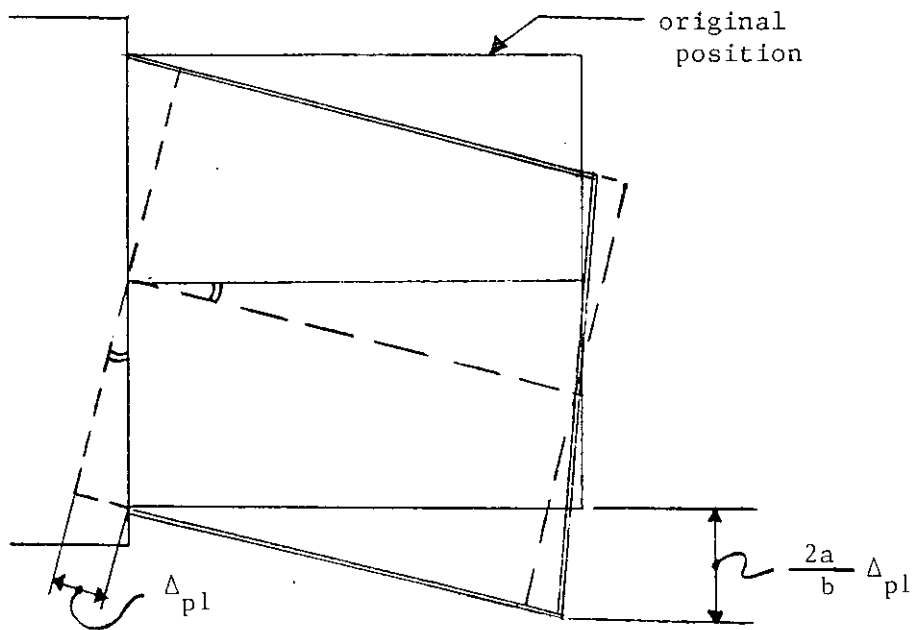


Figure 50b. Parallel edge zone displacement

$$K_z = \frac{1}{\frac{r_4 + r_3}{K_t (b+l_t'')} + \frac{2ar_1}{K_p b(b+l_p'')}} \quad (4-42)$$

Note that as the basic edge zone stiffnesses K_t and K_p become small compared to the edge beam axial stiffness, Eq. (4-42) reduces to the expression for edge zone stiffness given in Reference [15],

$$K_z = \frac{1}{\frac{2}{K_t (b+l_t)} + \frac{2a}{K_p b(b+l_p)}} \quad (4-43)$$

The final component of initial diaphragm flexibility (Δ_f) is due to the flexibility of the edge beam abutment connections, in a direction parallel to the edge beams. This flexibility is a possible source of in-plane diaphragm displacement in any test frame or building, but will vary with frame and connection type. This displacement will not cause any additional strain in the composite slab, as a small rigid body rotation is the source of the additional flexibility. The displacement at the location of the edge beam to abutment connection (Δ_c) is related geometrically to the resulting diaphragm displacement by

$$\Delta_f = \frac{2a}{b} \Delta_c \quad (4-44)$$

Measurements on Slabs 18, 19, and 20 each showed this component of the initial stiffness ($K_f = V/\Delta_f$) to be approximately 10000 KIPS/in.

An equation for the initial stiffness of the composite diaphragm can be developed based on Eq. (4-14). Substituting for the individual deflections gives

$$\frac{V}{K_{\text{tot}}} = \frac{V}{K_b} + \frac{V}{K_s} + \frac{V}{K_z} + \frac{V}{K_f} \quad (4-45)$$

where

- K_{tot} = total composite diaphragm stiffness
- K_b = bending stiffness of composite girder
- K_s = shear stiffness of composite girder
- K_z = edge zone stiffness
- K_f = frame connection stiffness.

Solving for the total initial stiffness of the composite diaphragm system (K_{tot}) yields

$$K_{\text{tot}} = \frac{1}{\frac{1}{K_b} + \frac{1}{K_s} + \frac{1}{K_z} + \frac{1}{K_f}} \quad (4-46)$$

4.3.3. Ultimate load

The ultimate load capacity of steel deck reinforced concrete slabs will be limited by one of three things: the shear strength of the composite slab, the strength of the deck's shear transfer mechanism, or the strength of the edge fasteners (see Table 3). Two possible methods for predicting failure in the second category, and

one method each for predicting failure in the first and third categories, are discussed individually in the following subsections.

4.3.3.1. Composite slab: diagonal tension failure The ultimate strength based on the shear failure of the concrete can be computed based on the shear wall equation from the American Concrete Institute (ACI) Code 318-83 [26]. Reference [15] also used this equation for predicting the diagonal tension capacity. ACI Equation 11-33 is based on the assumptions that the shear distribution across the section is parabolic, that the tensile strength of the concrete is $4 \sqrt{f_c'}$, and that the effective depth of the wall is 80 percent of the length. The first assumption is no longer valid in the case of the diaphragm slab with edge beams, since the shear distribution in the web (slab) of the composite girder is approximately constant. The tensile strength of concrete is still assumed to be $4 \sqrt{f_c'}$. The diaphragm slab equivalent length (effective depth) is the total length minus two times the effective edge zone distance, which can be taken conservatively as 80 percent of the length. Thus, $0.8b$ is again used as the effective length, although for a different reason. Considering these modifications, ACI Equation 11-33 becomes

$$V = 4 \sqrt{f_c'} t_e (0.8 b) \quad (4-47)$$

where

$$t_e = t_c + n_s (d/s) t_s$$

t_c = average concrete thickness

n_s = ratio of G_s/G_c

d/s = ratio for corrugated steel deck effective thickness
in shear

t_s = steel deck thickness.

This development assumes that both the concrete and the steel deck are carrying a portion of the shear force when diagonal tension occurs.

4.3.3.2. Shear transfer mechanism failure: edge zone distance

method The development of the shear transfer mechanism capacity, based on the edge zone distance method is similar to that given in Reference [15], with a couple modifications. The assumed force distribution at ultimate is shown in Figure 41. The corresponding forces on the framing members are shown in Figure 51. Summing forces on the north framing beam gives

$$V = q_t b + \frac{2a' q_t'}{a} (a - a') \quad (4-48)$$

or letting $\ell_t' = 2a' - 2a'^2/a$,

$$V = q_t b + q_t' \ell_t' \quad (4-49)$$

Summing moments on the south reaction block gives

$$V = q_p b + \frac{q_p' b^2}{4a} + \frac{b' q_p'}{a} (b - b') \quad (4-50)$$

or letting $\ell_p' = (b^2 + 4bb' - 4b'^2)/4a$,

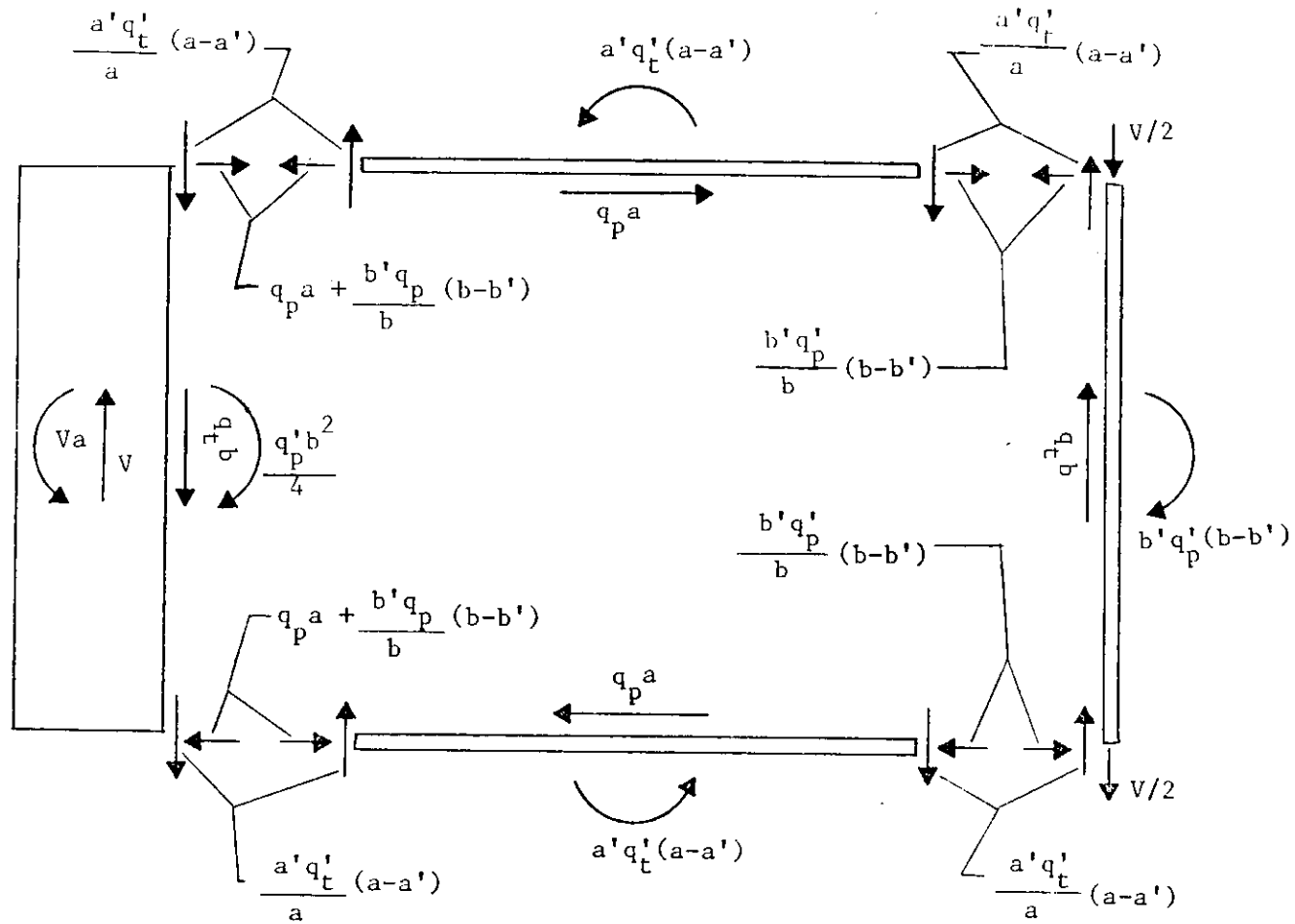


Figure 51. Framing member forces at ultimate (Method 1) [15]

$$V = q_p b + q_p' \ell_p' . \quad (4-51)$$

Eqs. (4-48) to (4-51) are the same as those used in Reference [15].

At ultimate load, the maximum values of q_t and q_t' were taken as $C_{po} Q_{tpo}$, where Q_{tpo} was the push-off test ultimate strength in the transverse direction. Similarly, the maximum values of q_p and q_p' were taken as $C_{po} Q_{ppo}$, where Q_{ppo} was the push-off test ultimate strength in the parallel direction. This is slightly different than the method given in Reference [15], which increased q_p' by a frictional factor μq_t . However, there is no evidence which suggests that an interaction between q_p' and q_t will cause an increased q_p' capacity; thus, this factor is not used. Also, the a' and b' distances used were as determined in Section 4.3.1.1.

Substituting from Eqs. (4-49) and (4-51), the shear transfer mechanism capacity (V) becomes

$$V = \text{minimum} \begin{cases} C_{po} Q_{tpo} (b + \ell_t') \\ C_{po} Q_{ppo} (b + \ell_p') \end{cases} \quad (4-52)$$

4.3.3.3. Shear transfer mechanism failure: beam on elastic foundation method Beam on elastic foundation method is an alternate method to that discussed in Section 4.3.3.2 for computing the shear transfer mechanism capacity of a composite diaphragm slab. The basic edge force distribution is the same as shown in Figure 41, except rather than assuming a distance a' and b' , and the shape of the force

distribution for the q_p' and q_t' forces, the transverse force at the end of each edge beam is computed directly. These forces are computed by assuming the edge beam to act as a beam on elastic foundation, with the deck-concrete shear transfer mechanism providing the elastic foundation forces. The resulting forces on the edge members are shown in Figure 52. W_t is the perpendicular force at the end of a side beam, W_p is the perpendicular force at each end of the front moving beam.

In order to determine the proper boundary conditions for the beams, the failure mechanisms for a shear transfer failure were determined. For transverse shear transfer failure (Figure 53), the steel deck and edge beam displacement relative to the concrete resembles a free-ended cantilever beam. For parallel shear transfer failure (Figure 54), the displacement of the steel deck and edge beam relative to the concrete is like a guided cantilever beam, since the front moving beam is continuous and connected to the loading apparatus at each end. Note that cycling tends to increase the parallel edge zone distance b' .

From these failure mechanisms, the boundary conditions used for W_t were semi-infinite beam, one end free; and for W_p , were semi-infinite beam one end guided. For the cellular deck, the boundary conditions for both W_t and W_p were semi-infinite beam, one end guided, because of the angular rigidity at the corners of the slab provided by the pan. Semi-infinite beams were used, since the width of the edge zone was considerably less than one-half the diaphragm

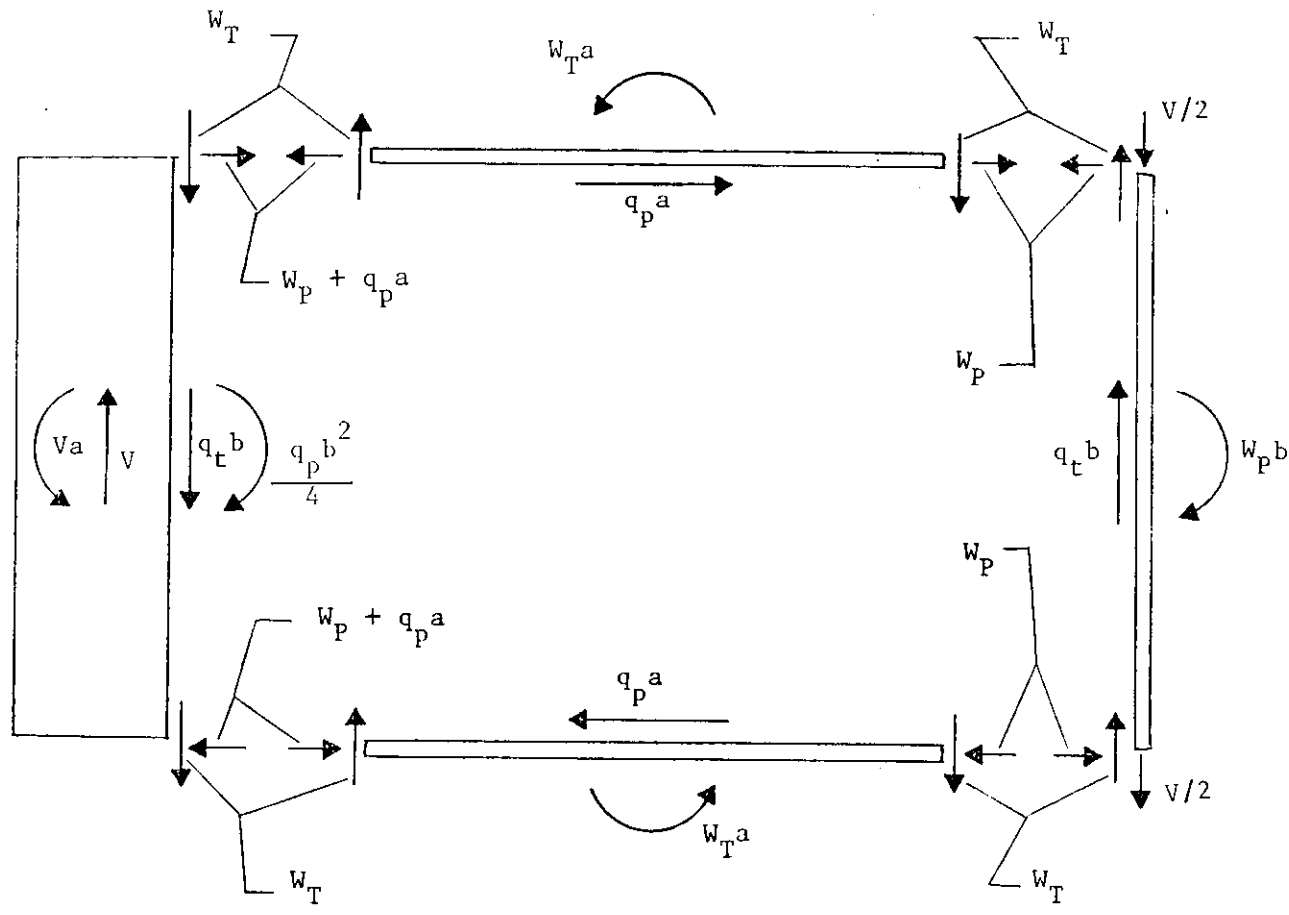
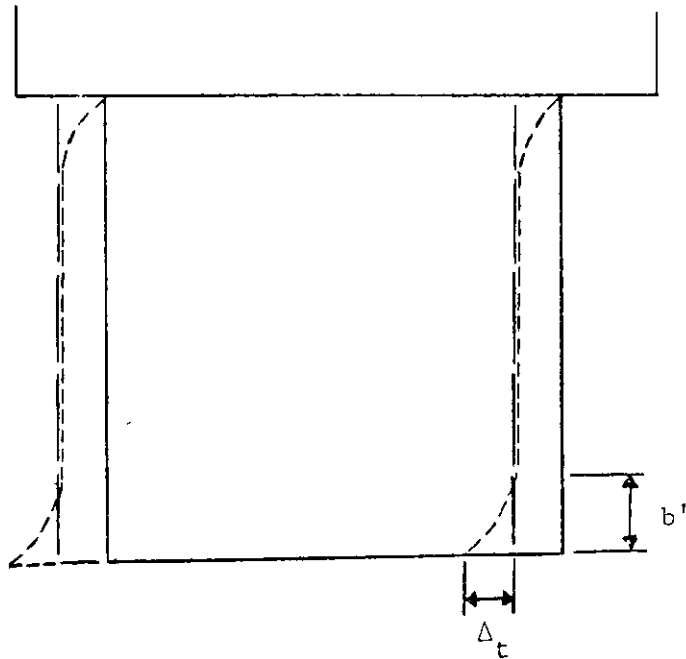


Figure 52. Framing member forces at ultimate (Method 2)



- original position
- - - - displaced concrete slab
- · · · displaced steel deck

Figure 53. Failure mechanism for transverse shear transfer failure (Failure Mode 2.b)

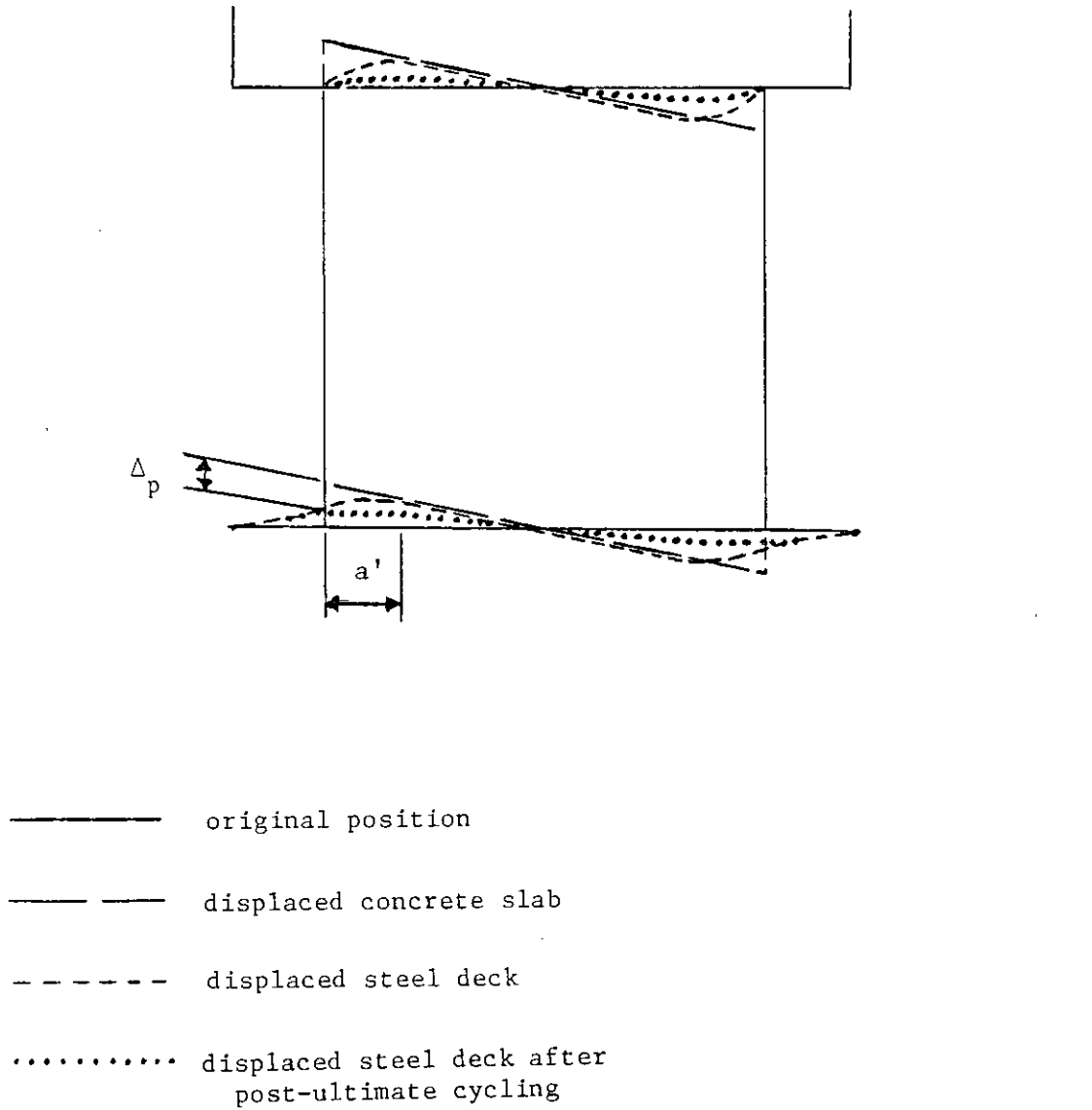


Figure 54. Failure mechanism for parallel shear transfer failure (Failure Mode 2.a)

length or width.

From Reference [29] (with some rearrangement), for a semi-infinite beam on elastic foundation, end free, force at end (W_{tpo}),

$$W_{tpo} = \Delta \frac{1}{\sqrt{2}} K^{3/4} (E_b I_b)^{1/4} \quad (4-53)$$

and for a semi-infinite beam on elastic foundation, end guided, force at end (W_{ppo}),

$$W_{ppo} = \Delta \sqrt{2} K^{3/4} (E_b I_b)^{1/4} \quad (4-54)$$

where

Δ = relative displacement at failure (from push-off test)

K = equivalent push-off test stiffness at failure

$$= 2 A_f / \Delta^2$$

E_b = framing beams elasticity modulus

I_b = framing beam vertical axis moment of inertia

A_f = area under push-off test load-displacement curve at failure.

W_{tpo} and W_{ppo} for each deck type were determined by finding the average $\Delta \cdot K^{3/4}$ for that deck type from the push-off tests.

From Figure 52, summing forces on the north moving beam yields

$$V = Q_t b + 2 W_t \quad (4-55)$$

and summing moments on the south reaction block,

$$V = Q_p \left(\frac{b^2}{4a} + b \right) + \frac{b}{a} W_p . \quad (4-56)$$

At ultimate, Q_p was taken as $C_{po} Q_{ppo}$, Q_t as $C_{po} Q_{tpo}$, W_p as $C_{po} W_{ppo}$, and W_t as $C_{po} W_{tpo}$. All four values taken from the push-off tests (Q_{ppo} , Q_{tpo} , W_{ppo} , W_{tpo}) were also corrected for differences in concrete strength where applicable, as given in Table 12.

The ultimate shear transfer mechanism capacity of the slab is the minimum of Eqs. (4-55) and (4-56). Advantages of this method over that of Section 4.3.3.2 include not having to make estimates of the a' and b' distances, and also that it includes the effect of the edge beam size on shear transfer mechanism capacity. The $\Delta \cdot K^{3/4}$ factor, used for determining the W_p and W_t forces, was reasonably consistent among push-off tests of similar deck type and direction.

4.3.3.4. Edge connection failure The composite diaphragm slab capacity due to edge connection failure was computed using the same edge force distribution used for computing the shear transfer mechanism capacity, given in Figure 41. Similar to Reference [15], two perpendicular forces (F_1 , F_2) were considered to act on each corner connection at ultimate

$$F_1 = \frac{a q_t}{n_a}$$

$$F_2 = \frac{b q_p}{n_b} \quad (4-57)$$

where

n_a = number of connections in length a

n_b = number of connections in length b.

Failure will occur when the ultimate connection capacity (Q_u)

$$Q_u = \sqrt{(F_1)^2 + (F_2)^2} \quad (4-58)$$

Again, letting $q_p' = q_p$ and $q_t' = q_t$, and using Eqs. (4-49) and (4-51), the slab capacity (V) is

$$V = \frac{Q_u}{\left[\left(\frac{a}{n_a (b + \ell_t')} \right)^2 + \left(\frac{b}{n_b (b + \ell_p')} \right)^2 \right]^{0.5}} \quad (4-59)$$

Some judgement is necessary in determining what ultimate strength (Q_u) should be used for the arc spot welds, since AISI equations (Eqs. 2-2 to 2-5) do not correspond well with actual welds tested for this project (welds tested had a higher strength than that predicted by the AISI equations). However, use of the AISI weld equations should yield conservative estimates of the slab capacity (V). Equation (4-59) is not valid for stud connections, since stud capacity may depend on edge distance and cover. Also, the ℓ_t' and ℓ_p' terms will be different since the edge zone distances (a' and b') will change if studs are used.

4.4. Comparison of Experimental and Analytical Results

The purpose of the analytical work completed was to develop equations to predict the initial stiffness and ultimate capacity of steel deck reinforced concrete slabs. This section discusses application of the equations developed in Section 4.3, and compares the predictions of these equations with actual slab test results.

4.4.1. Initial stiffness

The experimental stiffness, the stiffness predicted by Eq. (4-46), and the stiffness predicted by Reference [15] equations, for Slabs 1 to 20 are shown in Table 13.

The values used for Eq. (4-46) calculations were as follows. K_b and K_s were calculated using Eqs. (4-15) and (4-16), and the slab properties shown in Tables 1 and 6. K_z was calculated using Eq. (4-42). K_p and K_t for use in Eq. (4-42) were determined using Eq. (4-1). For Slab 4, K_p and K_t were simply reversed since the steel deck was oriented in the other direction. Also for use in Eq. (4-42), the effective area of the edge beams was as determined in Section 4.3.2. It was assumed that a'' and b'' were approximately 12 in. at the initial load point for all deck types tested. This 12 in. assumption was based on the finite element results of Section 4.2.3.1. This distance would actually vary slightly with the deck type, but was assumed constant since it would be difficult to determine, and since the value of K_z calculated was not very sensitive to the choice of a'' and b'' anyway. K_f was set to 10000 KIPS/in. for all slabs. No

Table 13. Comparison of analytical and experimental results for initial stiffness

Slab number	K (experimental) (KIPS/in.)	K (Eq. 4-46) (KIPS/in.)	K (Ref. 15) (KIPS/in.)
1	1800	- ^a	3000
2	2000	- ^a	2900
3 ^b	1600	1500	1600
4 ^b	1300	1400	1500
5	1700	1500	1400
6	2600	2100	1900
7	1500	- ^c	- ^c
8	1100	- ^a	1100
9	1900	1900	1600
10	1700	1700	1800
11	1600	1600	1600
12	1800	1700	1800
13	1900	1900	1600
14	1900	2000	2100
15	1300	1400	1400
16	1300	1400	1400
17	2200	2100	1800
18	1700	1700	1700
19	1300	1500	900
20	1300	1500	900

^aNo push-off tests with studs.

^bValues taken from Ref. [15] pushout tests.

^cNo push-off tests with Deck Type 3.

values were calculated for Slabs 1, 2, and 8, since no push-off tests with studs were conducted. No value for Slab 7 was calculated, since no push-off tests were conducted with Deck Type 3.

There was reasonably close agreement between analytical and experimental stiffnesses for all 16 slabs for which Eq. (4-46) calculations were made. Note that in most cases, Eq. (4-46) yielded better results than the method of Reference [15]. The author also feels that the proposed method for calculating initial stiffness, more accurately represents actual slab behavior. Both predictive methods worked equally well for slabs with and without a superimposed vertical load.

4.4.2. Ultimate load

Table 14 lists the experimental ultimate loads and the predicted ultimate loads based on the equations developed in Section 4.3.3. The proposed predictive method involved calculations for three possible failure modes (diagonal tension, shear transfer mechanism, and edge connection) with the lowest calculated value being the controlling failure mode. Two possible methods for determining the shear transfer mechanism capacity were discussed, and results of both are given in Table 14. No push-off tests with studs or with Deck Type 3 were performed; thus, tabulations for Slabs 1, 2, 7, and 8 are not complete. The AISI equations (Eqs. 2-2 to 2-5) were used for predicting the ultimate strength of an arc spot weld for use in predicting Failure Mode 3, even though these equations were known to be

19	147	<u>138</u>	147	169	284
20	94.6	<u>153</u>	<u>96.7</u>	<u>115</u>	96 ^e

^aSolid underlined is controlling mode with Method 1 for Mode 2; dashed underlined is controlling mode with Method 2 for Mode 2.

^bNo push-off specimens with studs.

^cNo push-off specimens with Deck Type 3.

^dDoes not include superimposed vertical load effect.

^eDid not control because of low estimate of weld strength.

quite conservative.

The proposed equations yielded good results for predicting diagonal tension failure, although slightly conservative in most cases. Both methods for predicting the shear transfer mechanism capacity yielded fairly reasonable results. This failure mode seems to be more erratic, due to the highly variable frictional and adhesional characteristics involved. Neither predictive method was consistently better than the other as compared to experimental results. Edge connection failure did not control on any of the slabs for which calculations were completed; thus, Eq. (4-59) could not be tested, although formulation was consistent with that of Eq. (4-52).

The predictive equations developed did not take into account the effects of the superimposed vertical load (if any). However, all predictive equations were conservative for those slabs with a design vertical load superimposed (Slabs 12, 13, 14, 16, 17, 18). This may not be true of slabs with a different aspect ratio.

A comparison was also made of predicted ultimate load by the proposed method (using Eq. 4-52 for Failure Mode 2), the predicted ultimate load by the Reference [15] method (using push-off strengths given in Table 12), and the experimental results. This comparison is shown in Table 15. The proposed method yields slightly better results, predicting the ultimate load more closely on 12 of the 18 slabs. The proposed method also has the advantage of predicting the correct failure mode more often. If shear transfer failure parallel (Failure Mode 2.a) and shear transfer failure transverse (Failure

Table 15. Comparison of predictive methods for ultimate load

Slab number	Experimental (KIPS)	Proposed method (KIPS)	Ref. 15 method (KIPS)
1	168	174	182
2	186	173	181
3	97.8	78.9	76
4	87.7	88.7	106
5	116	106	115
6	147	127	146
7	137	_a	_a
8	54.4	_b	_b
9	220	199	156
10	161	144	130
11	95.0	75.3	87
12	180	148	130
13	250	213	167
14	208	144	130
15	103	104	92
16	124	105	94
17	146	127	146
18	161	140	130
19	147	138	147
20	94.6	96.7	90

^aNo push-off tests with Deck Type 3.

^bNo push-off tests with studs.

Mode 2.b) are considered two separate failure modes, the proposed method predicts the correct failure mode on 17 of 18 slabs, whereas the Reference [15] equations predict the correct failure mode on only 11 of 18 slabs.

5. SUMMARY AND CONCLUSIONS

5.1. Summary

Four different elemental testing apparatuses for composite diaphragm slabs were designed and constructed. The main function of these elemental tests was to determine properties of the shear transfer mechanism between the steel deck and the concrete slab.

Four elemental cantilever tests were performed. Failure of these specimens was not that of the shear transfer mechanism; thus, it was discontinued. Eight elemental friction tests were performed. The elemental friction test seemed to be a good measure of initial adhesion, but did not model the behavior occurring in the full-scale slab. Six elemental shear tests were performed. The elemental shear test seemed to be a good model of the shear transfer occurring in the composite slab, however, results were not readily adaptable to present analytical techniques.

Fifty-five elemental push-off tests were performed. The elemental push-off test most accurately modeled the shear transfer mechanism behavior of the full-scale slab. The push-off test was used to determine the properties of the various deck types, as well as effects of certain other parameters.

Eleven full-scale composite slabs (Slabs 10 to 20) were also tested in conjunction with this project. These eleven slabs, along with Slabs 1 to 9, were used as the basis for evaluating the performance of the elemental tests.

Predictive equations were developed for the initial stiffness and ultimate capacity of the composite diaphragm slab, based on slab properties and results of the elemental push-off tests. These predictive equations were based on the edge zone concept developed in Reference [15]. Modifications to the previous method include:

- 1) including edge beam axial flexibility in the initial edge zone stiffness,
- 2) slight modifications in the bending and shear flexibility calculations,
- 3) a corrected diagonal tension equation,
- 4) two methods for computing the shear transfer mechanism capacity,
- 5) a variable edge zone distance, and
- 6) a simplified edge connection failure equation.

All force distributions assumed were verified using finite element analysis. Finally, predicted results were compared to actual experimental results of the full-scale composite slabs.

5.2. Conclusions

The following conclusions were based on the results of the study summarized above.

- 1) The elemental friction test and elemental cantilever test did not provide the necessary shear transfer mechanism behavior.

- 2) The elemental shear test and elemental push-off test both provide information on the shear transfer mechanism. The elemental push-off test yields information most readily adaptable to the present analytical technique.

3) Push-off test results were reasonably consistent, and their behavior matched that occurring in the full-scale slab.

4) The shear force distribution in the push-off test is very similar to that in the full-scale slab, and can be directly related.

5) It is important that the diaphragm slab be connected to edge beams on all four sides to avoid a flexural failure of the composite slab.

6) The defined edge zone distance varies with the deck type and also with the amount of applied load.

7) The thickness and geometry of the steel deck were the most important variables in determining the shear transfer mechanism capacity.

8) The type and number of embossments may significantly affect the interfacial capacity.

9) Concrete strength did not significantly affect shear transfer mechanism capacity, unless the failure mechanism involved shearing of the concrete.

10) A superimposed vertical load consistently increased interfacial capacity on the parallel push-off tests, but did not significantly affect the transverse push-off tests.

11) The number and spacing of weld connections does not significantly affect interfacial behavior.

12) AISI equations for arc spot weld capacity may be quite conservative.

13) Concrete directly covering arc spot welds does not significantly affect their capacity.

14) The edge zone concept and proposed predictive equations (Eqs. 4-46 and 4-52) seem to effectively represent slab behavior, however, more modifications may be necessary to incorporate other pertinent variables.

5.3. Recommendations for Continued Study

1) Experimentally determine effects of load-history on interfacial behavior and capacity.

2) Conduct push-off tests with a varying number of studs, to determine what effect studs have on interfacial behavior.

3) Experimentally determine effects of different test frame configurations, adjacent spans, and deck orientation on composite slab behavior.

4) Apply a superimposed vertical load on a shorter span composite diaphragm slab, to define a possible new combined failure mode.

5) Experimentally investigate possible localized failure conditions for the composite slab.

6) Experimentally determine whether steel edge beams will act compositely with steel deck reinforced floor slab, if arc spot weld connections rather than stud connections are used.

7) Analytically and/or experimentally determine the edge force distribution after diagonal cracking has occurred in the slab.

8) Complete a 3-dimensional finite element analysis to determine what effect out-of-plane displacements have on the in-plane behavior of the shear transfer mechanism within the edge zone.

9) Develop empirical equations for predicting conservative push-off capacities, based only on deck thickness, depth of embossments, and corrugation geometry.

6. REFERENCES

1. Nilson, A. H. "Shear Diaphragms of Light Gage Steel." Journal of the Structural Division, ASCE 86, No. ST11 (November 1960), 111-140.
2. Department of the Army, Navy, and the Air Force. Seismic Design of Buildings. Army TM5-809-10. Washington, D.C.: U.S. Government Printing Office, April, 1973.
3. Nilson, A. H. "Diaphragm Action of Light Gage Steel Construction." AISI Regional Technical Paper, 1960.
4. Luttrell, L. D. "Structural Performance of Light Gage Steel Diaphragms." Research Report 319. Department of Structural Engineering, Cornell University, Ithaca, N.Y., August 1965.
5. Apparo, T. V. "Tests on Light Gage Steel Diaphragms." Research Report 328. Department of Structural Engineering, Cornell University, Ithaca, N.Y., December 1966.
6. American Iron and Steel Institute. Design of Light Gage Steel Diaphragms. Washington, D.C.: AISI, 1967.
7. Easley, J. T. "Buckling Formulas for Corrugated Metal Shear Diaphragms." Journal of the Structural Division, ASCE 101, No. ST7 (July 1975), 1403-1417.
8. Steel Deck Institute. Diaphragm Design Manual. St. Louis, MO: The Steel Deck Institute, 1981.
9. Bryan, E. R. and El-Dakhakni, W. M. "Shear Flexibility and Strength of Corrugated Decks." Journal of the Structural Division, ASCE 94, No. ST11 (November 1968), 2549-2580.
10. Davies, J. M. and Lawson, R. M. "The Shear Flexibility of Corrugated Steel Sheeting." Third International Specialty Conference on Cold-Formed Steel Structures, University of Missouri-Rolla, November 24-25, 1975.
11. Davies, J. M. and Bryan, E. R. Manual of Stressed Skin Diaphragm Design. New York: John Wiley and Sons, Inc., 1982.
12. Arnold, V. E., Greimann, L. F. and Porter, M. L. "Pilot Tests of Composite Floor Diaphragms." Progress Report ERI-79011. Engineering Research Institute, Iowa State University, Ames, Iowa, September 1978.

13. Davies, J. M. and Fisher, J. "The Diaphragm Action of Composite Slabs." Proceedings of the Institute of Civil Engineers (England), Part 2, No. 67 (December 1979), 891-906.
14. Brangwin, D. J. "Interfacial Shear of Composite Floor Diaphragms." Unpublished Master's Thesis. Iowa State University, Ames, Iowa, 1979.
15. Porter, M. L. and Greimann, L. F. "Seismic Resistance of Composite Floor Diaphragms." Final Report ERI-80133. Engineering Research Institute, Iowa State University, Ames, Iowa, May 1980.
16. Porter, M. L., Ekberg, C. E., Jr., Greimann, L. F. and Elleby, H. A. "Shear-Bond Analysis of Steel-Deck-Reinforced Slabs." Journal of the Structural Division, ASCE 102, No. ST12, (December 1976), 2255-2268.
17. Porter, M. L. and Ekberg, C. E., Jr. "Behavior of Steel-Deck-Reinforced Slabs." Journal of the Structural Division, ASCE 103, No. ST3 (March 1977), 663-677.
18. American Iron and Steel Institute. Commentary on the September 3, 1980 Edition of the Specification for the Design of Cold-Formed Steel Structural Members. Washington, D.C.: AISI, 1983.
19. Slutter, R. G. "Tests of Lightweight Concrete Pushout Specimens Containing Stud Shear Connectors and Metal Deck Form." Report No. 200.66.438.1. Fritz Engineering Laboratory, Lehigh University, May 1980.
20. Krupicka, G. L. "The Behavior and Analysis of Steel-Deck-Reinforced Concrete Slabs with End Span Studs." Unpublished Master's Thesis. Iowa State University, Ames, Iowa, 1979.
21. American Iron and Steel Institute. Specification for the Design of Cold-Formed Steel Members. Washington, D.C.: AISI, 1983.
22. Hussain, M. I. and Libove, C. "Stiffness Tests of Trapezoidally Corrugated Shear Webs." Journal of the Structural Division, ASCE 103, No. ST5 (May 1977), 971-987.
23. Porter, M. L. "Investigation of Light Gage Steel Forms as Reinforcement for Concrete Slabs." Unpublished Master's Thesis. Iowa State University, Ames, Iowa, 1968.
24. Neilsen, M. K. "Effects of Gravity Load on Composite Floor Diaphragm Behavior." Unpublished Master's Thesis. Iowa State University, Ames, Iowa, 1984.

25. American Society for Testing and Materials. Diagonal Tension in Masonry Assemblages. ASTM E 519-81. Philadelphia, PA: ASTM, 1976.
26. American Concrete Institute. Building Code Requirements for Reinforced Concrete. ACI Standard 318-83. Detroit, MI: ACI, 1983.
27. Nilson, A. H. and Atrek, E. "Non-linear Finite Element Analysis of Light Gage Steel Shear Diaphragms." Report No. 363. Department of Structural Engineering, Cornell University, Ithaca, N.Y., September 1976.
28. Q-Floor/Taproute Systems: Technical Data Guide. H. H. Robertson Co., Pittsburgh, PA, 1982.
29. Roark, R. J. and Young, W. C. Formulas for Stress and Strain. New York: McGraw Hill, 1975.

7. ACKNOWLEDGMENTS

This research was conducted with funds made available by the National Science Foundation and supported by the Engineering Research Institute of Iowa State University. The steel deck was provided by Vulcraft, a division of Nucor Corporation; Wheeling Corrugating Company, a division of Wheeling-Pittsburgh Steel Corporation; Mac-Fab Products, Inc.; Bowman Construction Products; and H. H. Robertson Company.

The author wishes to acknowledge the invaluable assistance of faculty members Dr. Max L. Porter and Dr. Lowell F. Greimann. The author also acknowledges the help of an excellent working partner, Michael K. Neilsen. Also making large contributions to the experimental work were lab technician Doug Wood, graduate student Sam Easterling, and several hourly employees including Doug Johnson, Doug Kuhel, Mark Geisler, Tim Dedic, Shawn French, and Glenn Hunter.

The author is also very thankful for continuous support of his wife, Rhonda, through long hours and late nights at various stages of this investigation.